Enhancing CMIP6 Climate Predictions Through Machine Learning

M.Tech. Thesis

By

MAHEEP DEV ARUN

(2302104013)

DEPARTMENT OF CIVIL ENGINEERING
INDIAN INSTITUTE OF TECHNOLOGY INDORE
May 2025

Enhancing CMIP6 Climate Predictions Through Machine Learning

A THESIS

Submitted in partial fulfillment of the
requirements for the award of the degree
of
Master of Technology

in

Water, Climate, and Sustainability

By

MAHEEP DEV ARUN

(2302104013)

DEPARTMENT OF CIVIL ENGINEERING
INDIAN INSTITUTE OF TECHNOLOGY INDORE
May 2025

INDIAN INSTITUTE OF TECHNOLOGY INDORE

CANDIDATE'S DECLARATION

I hereby certify that the work which is being presented in the thesis entitled **Enhancing CMIP6 Climate Predictions Through Machine Learning** in the partial fulfillment of the requirements for the award of the degree of **Master of Technology** in **Water, Climate, and Sustainability** and submitted in the **Department of Civil Engineering, Indian Institute of Technology Indore**, is an authentic record of my own work carried out during the time period from **July 2023** to **May 2025** under the supervision of Prof. Manish Kumar Goyal, Department of Civil Engineering, Indian Institute of Technology Indore.

The matter presented in this thesis has not been submitted by me for the award of any other degree of this or any other institute.

maheep
29/05/25

Signature of the student with date
Maheep Dev Arun

This is to certify that the above statement made by the candidate is correct to the best of my/our knowledge.

Manish

Signature of the Supervisor of
M.Tech. dated 2nd June 2025
Prof. Manish Kumar Goyal

Maheep Dev Arun has successfully given his/her M.Tech. Oral Examination held on **24 May 2025**.

Manish

Signature(s) of Supervisor(s) of M.Tech. Thesis
Date: 2nd June 2025

Convener, DPGC
Date:

ACKNOWLEDGEMENT

I want to show gratitude to my supervisor, Prof. Manish Kumar Goyal, whose wisdom, guidance, encouragement, and unwavering belief in my potential have been the pillars of this research journey. His deep knowledge, patience, and thoughtful critiques not only shaped this thesis but also transformed me into a better researcher. His mentorship extended beyond academics, filling me with the courage to experiment and the perseverance to overcome obstacles. For that, I will always be grateful. My heartfelt gratitude goes to my incredible lab mates and seniors, whose friendship and intellectual companionship made this journey enriching and enjoyable. From brainstorming sessions in difficult times to troubleshooting unforeseen obstacles I faced, their support was a constant source of strength. A special note of thanks to my Water, Climate, and Sustainability batchmates; their unwavering support and encouragement carried me through the toughest phases of this academic pursuit. Their belief in me, even when mine wavered, reminded me why perseverance matters. This milestone is theirs as much as it is mine. Finally, I acknowledge the countless researchers and authors whose pioneering work laid the foundation for this study. Standing on the shoulders of giants, I have been able to see further, and for that, I am profoundly thankful. This accomplishment is not mine alone, with the guidance, support, and kindness of everyone who stood by me. To each of you, I extend my deepest appreciation.

Maheep Dev Arun

2302104013

Abstract

This study examines how machine learning (ML) approaches can be applied to enhance the performance of CMIP6 multi-model ensembles (MME) for climate projections across ten vulnerable locations in India. The research evaluates traditional MME methods (simple mean) alongside ML models—Long Short-Term Memory (LSTM), Artificial Neural Networks (ANN), and Support Vector Regression (SVR) to predict precipitation (PCP), maximum and minimum temperature (TMAX and TMIN) under both scenarios SSP245 and SSP585. Key findings include performance improvement of ML models consistently outperforming traditional MME, with LSTM achieving the highest R^2 values (e.g., 0.85 for precipitation in Location 3 under SSP245) and reduced RMSE and MAE. SVR and ANN also showed significant improvements, particularly in capturing extreme events and seasonal trends. Temperature Projections show that all methods performed well for temperature variables, with minor variations, as temperature trends exhibit less variability over time. Trend Analysis shows that the MME-mean revealed statistically significant increasing trends in all locations, while LSTM displayed high variability, and ANN provided more stable projections. SVR was less reliable for long-term trend detection. Entropy Analysis: Variability indices (SVI_{AE} and SVI_{ME}) indicated that SVR and MME-mean exhibited higher variability, whereas LSTM and ANN produced more consistent results, especially at annual scales. The study concludes that ML-augmented ensembles, particularly LSTM, enhance the accuracy of climate projections, offering valuable insights for climate resilience planning in vulnerable regions. However, traditional MME remains robust for consensus-based trend analysis. These findings contribute to optimizing climate model ensembles for improved decision-making in adaptation strategies.

Keywords: Climate Change, Extreme Events, Machine Learning, Climate Variability

Table of Contents

List of Tables

List of Figures

List of Abbreviations

GCMs: General Circulation Models

SSP: Shared Socioeconomic Pathways

NEX-GDDP-CMIP6: NASA Earth Exchange Global Daily Downscaled Projections

IMD: India Meteorological Department

PCP: Precipitation

TMAX: Maximum Temperature

TMIN: Minimum Temperature

QM: Quantile Mapping

EQM: Empirical Quantile Mapping

ML: Machine Learning

LSTM: Long-short Term Memory

ANN: Artificial Neural Network

SVR: Support Vector Machine

RMSE: Root Mean Square Error

MAE: Mean Absolute Error

KGE: Kling Gupta's Efficiency

SVI: Standard Variability Index

AE: Apportionment Entropy

ME: Marginal Entropy

MME: Multi-Model Ensemble

MME-ML: Multi-Model Ensemble – Machine Learning

GCMs: General Circulation Models

Chapter 1

Introduction

Climate change projections rely heavily on Global Climate Models (GCMs), particularly those from the Coupled Model Intercomparison Project Phase 6 (CMIP6), due to their ability to simulate future climate scenarios under various emission scenarios (Semenov et al., 2024; S. Zhang & Chen, 2021). GCMs of CMIP6 provide a comprehensive framework for understanding climate dynamics by integrating improved spatial resolutions, advanced physical processes, and diverse socioeconomic scenarios, such as the Shared Socioeconomic Pathways (SSPs) (Bian et al., 2023; Peng et al., 2023). These models are indispensable for downscaling climate data to local scales, enabling detailed assessments of temperature, precipitation, and extreme weather events, which are critical for impact studies and adaptation planning (Almazroui et al., 2021; Hirabayashi et al., 2021). Despite their coarse resolution, CMIP6 GCMs have demonstrated enhanced performance in replicating historical climate patterns and projecting future changes, though uncertainties remain, specifically in regional precipitation and temperature variability (Bayar et al., 2023; Wu et al., 2024). The role of CMIP6 GCMs is further underscored by their utility in hydrological, agricultural, and ecological impact assessments, making them a cornerstone of modern climate science (Anil & Anand Raj, 2022). Thus, understanding the strengths and weaknesses of these models is essential for refining climate projections and informing policy decisions aimed at mitigation and adaptation. The CMIP6 multi-model ensemble (MME) is a cornerstone for climate projections, yet it faces significant challenges, including biases, uncertainty, and inter-model spread, which complicate the interpretation and reliability of its outputs. Biases in CMIP6 models vary by geographical location and magnitude, leading to potential inaccuracies in projections, particularly for variables like precipitation and temperature (Y. H. Kim et al., 2020; Knutti et al., 2010). For example, systematic cold biases in high-latitude regions and dry biases in tropical and subtropical areas persist across models, undermining confidence in regional climate predictions (Y. H. Kim et al., 2020; Osso et al., 2023). Uncertainty arises from multiple sources, such as the small number of models, unclear distribution in parameter space, and unrepresented extreme behaviors, which collectively limit the ensemble's ability to capture the full range of plausible climate futures (Knutti et al., 2010; Lehner et al., 2020). Additionally, inter-model spread reflects structural differences in model responses, often independent of present-day conditions, further exacerbating uncertainty (Sanderson & Knutti, 2012; Y. Zhang

et al., 2023). This spread is particularly pronounced in projections of regional events, such as the North Atlantic Oscillation and polar warming, where model disagreements dominate the total uncertainty (McKenna & Maycock, 2021; Y. Zhang et al., 2023). Addressing these challenges is critical for refining climate projections and informing robust adaptation strategies, especially in climate-sensitive regions (Tyagi et al., 2024). (Das et al., 2024; Moradkhani et al., 2024) explore challenges in-depth, offering insights into mitigating biases, quantifying uncertainty, and reducing inter-model spread to enhance the utility of CMIP6 MME for climate research and policy.

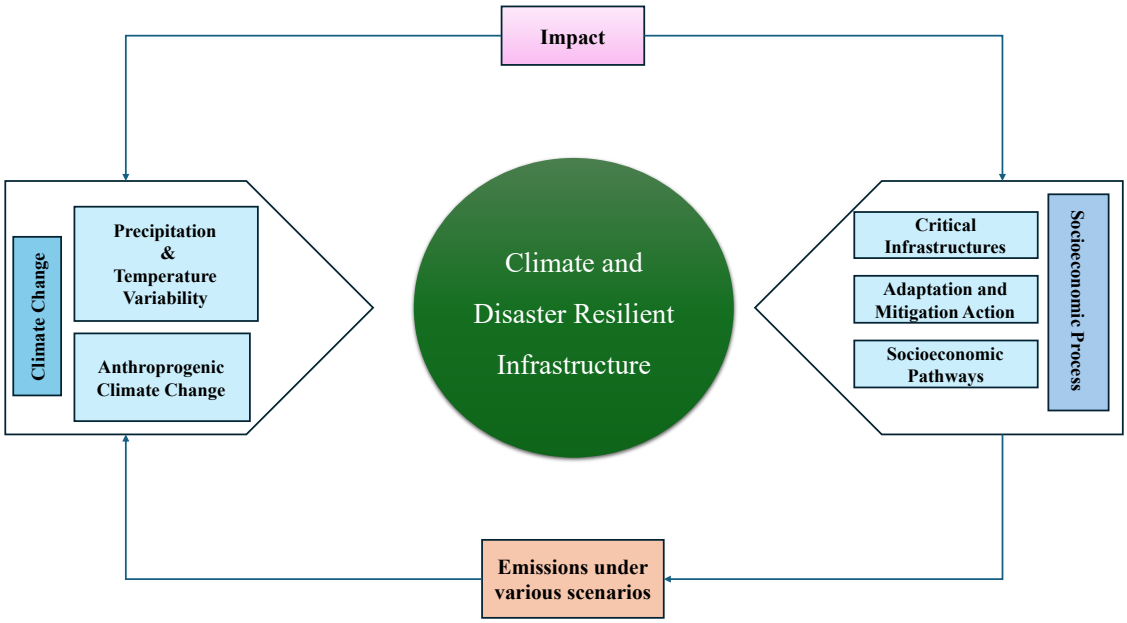

Figure 1 Overview of the study

1.1 Biases in GCMs

Bias correction is a critical step in climate modeling, as GCMs regularly exhibit systematic biases due to simplifications in physical processes, coarse spatial resolutions, and inadequate representation of regional climate features. These biases can significantly undermine the reliability of climate projections, particularly for variables like precipitation and temperature, which are essential for impact assessments in water resources, agriculture, and disaster management (Jose et al., 2022). To address these limitations, various bias correction techniques have been developed so that GCM outputs can be aligned with observed data, ensuring more accurate and actionable climate information. Quantile mapping (QM) is a widely used method to match the statistical transformations of the cumulative distribution functions (CDFs) of modeled and observed data (Grillakis et al., 2013; Robertson et al., 2023). While effective, QM

can alter the climate change signal, particularly for precipitation (Pierce et al., 2015). Advanced versions of bias correction techniques like quantile delta mapping (QDM) and scaled distribution mapping (SDM) preserve trends and raw climate signals, respectively, offering improved performance for temperature and precipitation corrections (Frei et al., 2022; Li & Li, 2023). For multivariate applications, methods such as multivariate bias correction account for inter-variable dependencies, enhancing the physical consistency of corrected outputs (Y. Kim et al., 2023). Recent innovations include machine learning-based approaches, such as generalized regression neural networks (GRNNs) for temperature bias correction (Dutta & Bhattacharjya, 2022) and deep learning pathways for precipitation (W. Gao et al., 2024) Additionally, wavelet-based techniques like continuous wavelet bias correction (CWBC) address biases in both magnitude and frequency, proves effectiveness of variables like sea surface temperature (Kusumastuti et al., 2022). Despite these advancements, challenges persist, such as overcorrection in methods like Bias Correction and Spatial Disaggregation (BCSD), which can distort climate signals (Chandel et al., 2024). The Multi-Model Ensemble (MME) technique has become a cornerstone in climate projections, offering a robust approach to uncertainties inherent in individual General Circulation Models (GCMs). However, despite its widespread adoption, significant challenges persist in enhancing the reliability of MME outputs. Current MME methods often suffer from overconfidence, where ensemble spreads underestimate true forecast uncertainties, leading to biased projections (J. Zhu et al., 2013). For instance, simple model averaging approaches can dilute fine-scale spatial information and introduce biases from low-resolution models, compromising the accuracy of regional climate predictions (Vrac et al., 2024). Additionally, traditional techniques like k-means clustering tend to favor high-density areas in climate variable distribution, failing to fully capture variability, particularly in extreme events (Cannon, 2015). Further limitations arise from the structural uncertainties in GCMs, such as parameterization errors and imperfect initial conditions, which are not adequately sampled in conventional ensembles (Yokohata et al., 2012). Studies highlight that while MMEs broadly improve reliability, they often exhibit overdispersion or underdispersion, depending on the geographic area and climate variable (Exbrayat et al., 2018; Yokohata et al., 2012). For example, precipitation projections in semi-arid regions remain highly uncertain due to model inconsistencies and insufficient observational constraints (Exbrayat et al., 2018). Moreover, methods like Bayesian Model Averaging (BMA) and Reliability Ensemble Averaging (REA) have shown promise but require refinement to address spatial inconsistencies and multi-variable dependencies (Guan et al., 2022). These approaches aim to enhance ensemble reliability by integrating performance-based weighting,

nonparametric distributions, and automated downscaling. Nevertheless, the need for further improvement persists, particularly in optimizing model selection, reducing inter-model dependencies, and incorporating diverse error metrics (Ganguly & Arya, 2023; Talukder et al., 2025). This study seeks to build on these advancements by developing a more robust MME framework that addresses these limitations, ultimately improving the reliability of climate projections for decision-making and risk assessment. Traditional multi-model ensembling techniques, such as simple mean and weighted mean, are foundational approaches in ML that aim to improve predictive performance by combining the outputs of multiple models. The simple mean method aggregates predictions by averaging them equally across all models, assuming each model contributes uniformly to the final output (Ren et al., 2016). In contrast, the weighted mean assigns varying weights to predictions of each model based on their respective performance, thereby allowing more accurate models to exert greater influence on the ensemble's results (Ali et al., 2015; J. Zhu et al., 2013). These techniques are particularly effective in addressing the bias-variance trade-off, leveraging the strengths of diverse models to improve overall accuracy and performance (Dong et al., 2020; Ren et al., 2016). Similarly, (J. Zhu et al., 2013) introduced a weighted mean model for operational risk assessment, highlighting its practicality over complex methods that require extensive historical data. Despite their advantages, traditional ensembling techniques may lack the flexibility and adaptability offered by advanced methods like bagging, boosting, and stacking, which dynamically optimize model combinations (Rane et al., 2024; Tang et al., 2024). Nevertheless, simple and weighted mean approaches remain integral to ensemble learning, providing a baseline for understanding and developing more sophisticated strategies. This research explores the efficacy of traditional ensembling techniques in contemporary applications, examining their strengths, limitations, and potential enhancements in the context of evolving ML models. By synthesizing insights from prior studies (Ali et al., 2015; Dong et al., 2020; Ren et al., 2016), we aim to bridge the gap between foundational methods and modern advancements, offering a comprehensive perspective on their role in predictive modeling. The comparison between traditional CMIP6 MME and emerging ML-based ensembles has gained significant attention in climate science due to their respective strengths and limitations. CMIP6 MMEs, which integrate simulations from multiple GCMs, have been widely used for climate projections, offering a robust framework for assessing uncertainties (Eyring et al., 2016). However, they are computationally expensive and often exhibit biases in representing complex climate processes (Reichstein et al., 2019). In contrast, ML-based ensembles leverage data-driven approaches to improve predictive accuracy, reduce computational costs, and enhance

the representation of nonlinear climate dynamics (Rasp & Thuerey, 2021). Recent studies suggest that hybrid approaches combining CMIP6 and ML techniques may outperform standalone methods, particularly in regional climate projections (Labe & Barnes, 2022).

1.2 Screening of GCMs

Despite these advancements, a systematic comparison of their performance, uncertainty quantification, and scalability remains underexplored. This study aims to evaluate CMIP6 MME against ML-based ensembles in terms of predictive skill, bias correction, and extreme event representation, contributing to the ongoing discourse on optimizing climate projection methodologies. The evaluation of multi-model ensemble performances is critical in ensuring robust and reliable predictions across various domains, from climate science to financial forecasting. Performance metrics such as R^2, Root Mean Square Error (RMSE), Mean Absolute Error (MAE), and Kling-Gupta Efficiency (KGE) are widely employed to find model, precision, and generalizability (Chai & Draxler, 2014a; Plevris et al., 2022). R^2 measures the proportion of variance explained by the model, providing insights into its explanatory power, while RMSE and MAE quantify prediction errors, with RMSE penalizing larger errors more heavily due to its sensitivity to outliers (Hodson, 2022; Willmott, 2005a). MAE, on the other hand, offers a more intuitive interpretation of average error magnitude, making it suitable for applications where error distributions deviate from normality (Brassington, 2017). The KGE metric, which integrates correlation, bias, and variability, is particularly valuable for evaluating hydrological and environmental models, as it addresses the improvement upon traditional metrics by balancing key performance factors (Botchkarev, 2019; Correndo et al., 2022). Recent literature emphasizes the importance of selecting appropriate metrics tailored to the specific nature of the data and the purpose of the study. For instance, RMSE is optimal for Gaussian errors, whereas MAE is preferred for Laplacian distributions (Chai & Draxler, 2014a). However, reliance on a single metric can be misleading, as each captures distinct facets of model performance. A multi-metric approach, combining R^2, RMSE, MAE, and KGE, is increasingly advocated to deliver a comprehensive assessment of ensemble models (Plevris et al., 2022). Despite advancements, challenges persist in metric selection, particularly in contexts with imbalanced data or varying risk appetites, where traditional metrics may fail to align with practical outcomes (Dessain, 2023; Tunkel & Herbold, 2022). The purpose of this study is to address the gaps by systematically evaluating multi-model ensemble performances using a suite of metrics, thereby enhancing the interpretability and applicability of ensemble

predictions in diverse fields. By integrating theoretical insights with empirical validation, this research aims to contribute to ongoing discourse on optimal metric selection and ensemble model evaluation.

1.3 Integration of Machine Learning

The integration of ML with ensembles of GCMs has emerged as a transformative approach to improve the accuracy and reliability of climate projections. Traditional GCMs, while foundational for climate research, often suffer from uncertainties due to coarse spatial resolutions, structural biases, and computational limitations (MA & Stratonovitch, 2010; Rampal et al., 2024). ML techniques, such as convolutional neural networks (CNNs), random forests (RF), and long short-term memory (LSTM) networks, address these challenges by improving downscaling, parameterization, and ensemble weighting (González-Abad & Baño-Medina, 2023; Sun et al., 2023). For instance, ML-based multi-model ensembles (MMEs) have demonstrated superior performance in simulating precipitation and temperature extremes compared to conventional arithmetic mean ensembles, with methods like Extreme Gradient Boosting (XGBR) and Random Forest Regressor (RFR) outperforming other techniques in diverse geo-climatic regions (Shetty et al., 2023). The implications of ML-enhanced GCM ensembles for climate change impact assessment are profound. By reducing uncertainties and improving spatial-temporal resolution, these models provide more reliable projections of future climate scenarios, such as temperature rises under SSP245 and SSP585 pathways (Shetty et al., 2023). For example, deep learning frameworks like CNNs have achieved higher skill scores (e.g., Taylor Skill Score of 0.98) in reproducing local-scale precipitation patterns, enabling better risk assessments for extreme weather events (Sun et al., 2023). Additionally, ML algorithms facilitate the quantification of uncertainty through techniques like Bayesian Model Averaging (BMA), which outperforms simple ensemble means in capturing climate variability (Talukder et al., 2025). Such advancements are essential for informing adaptation strategies in vulnerable sectors, like agriculture and water resource management, where precise climate projections are essential for mitigating the impacts of global warming (Bojer et al., 2024; Krishnamoorthy & Sistla, 2023). In summary, ML not only refines the predictive capabilities of GCM ensembles but also strengthens their utility in climate change impact assessments by addressing key limitations of traditional methods. The following sections explore these advancements in detail, highlighting their methodological innovations and practical applications.

Chapter 2

Study Area

The present study focuses on ten different locations across India, selected for their vulnerability to climate extremes such as floods, heatwaves, and droughts. These locations are 10 km stretch of National Highways, surrounded by agricultural fields, water bodies, factories, and other critical infrastructures, making them critical to study in the context of increasing climate variability. These locations are L1, L2, L3… and L10. For each location, a 10 km stretch has been identified for detailed climate impact analysis. The study examines key variables, including PCP, TMAX, and TMIN, using historical data to project future climate conditions.

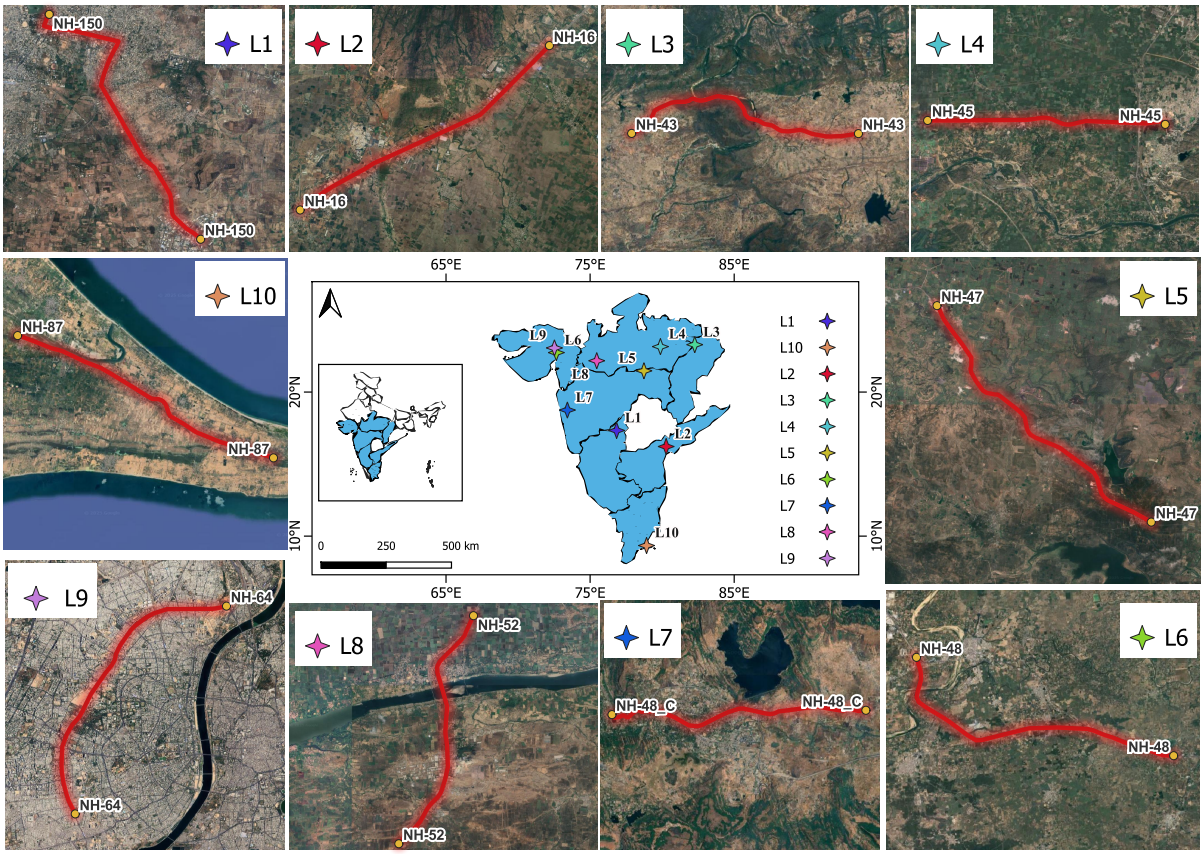

Figure 2 Location Map of the National Highways considered in this study

Location 1 is situated in Karnataka, around a 10 km stretch of NH 150 from Kalaburagi to Yadgiri, crosses through an area dotted with lakes and rivers, including the Bhima River, and is prone to flooding due to the hilly terrain. The region experiences an average annual rainfall of 838 mm and temperatures ranging from 39.1°C to 17.1°C.

Figure 3 Satellite Image of Location 1

Location 2 is located in Andhra Pradesh and covers a 10 km segment on National Highway 16 from Guntur to Chilakaluripet. This stretch passes through hilly terrain, causing stormwater to flow towards low-lying areas, often leading to flooding naturally. The region, which hosts many textile industries, educational institutions, and hospitals, receives an average annual rainfall of 966 mm, with temperatures ranging between 33.96°C and 25.13°C.

Figure 4 Satellite Image of Location 2

Location 3 is situated in Chhattisgarh, a 10 km section on National Highway 43 between Manendragarh and Ambikapur has been selected. This area is characterized by its proximity to the Hasdeo River, Aaruni Dam, and various waterfalls, making it particularly flood-prone. The

annual rainfall here is approximately 1130 mm, with average maximum and minimum temperatures of 30°C and 17.6°C, respectively.

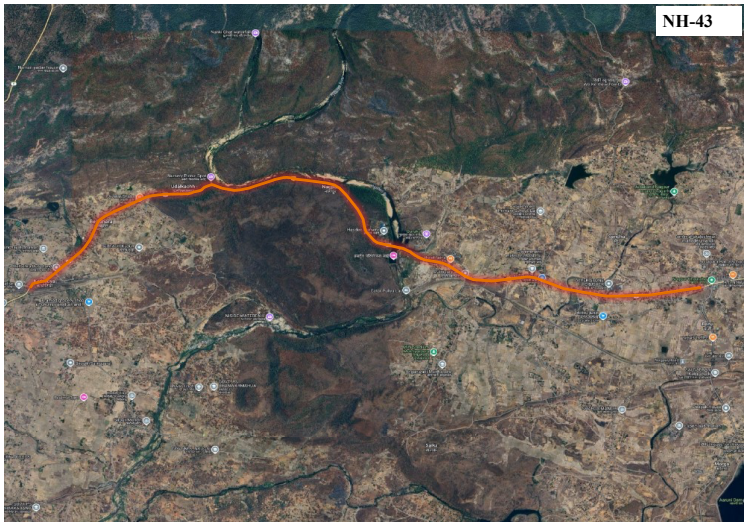

Figure 5 Satellite Image of Location 3

Further north, Location 4 is located in Madhya Pradesh and includes a 10 km stretch on National Highway 45 from Shahpura to Jabalpur, where the Narmada River and several lakes define the local landscape. Prone to both flooding and seismic activity (Seismic Zone III), this region experiences an annual rainfall of 1280 mm, with temperatures ranging from 32.1°C to 18.3°C.

Figure 6 Satellite Image of Location 4

Location 5 is located in Maharashtra, around National Highway 47, which covers a segment from Betul to Saoner, an area surrounded by dams such as Umri, Kolar, and Nanda. This region,

also vulnerable to floods, has a recorded average rainfall of 1060.2 mm, and temperatures fluctuate between 45°C and 12°C.

Figure 7 Satellite Image of Location 5

Location 6 is another section of 10 km stretch from Lonavala to Khandala around National Highway 48, a popular tourist destination in Maharashtra. Known for its waterfalls and scenic viewpoints, the area has been severely affected by flooding in recent years, receiving an average annual rainfall of 4223 mm, with temperatures ranging from 34°C to 11°C.

Figure 8 Satellite Image of Location 6

Location 7 is in Gujarat, a 10 km stretch of National Highway 48 from Himatnagar to Vadodara, which passes through an industrial zone and intersects with major state highways. This region experiences an annual rainfall of 749 mm, with temperatures varying from 40°C to 14°C.

Figure 9 Satellite Image of Location 7

Location 8 is another segment of National Hiway 52 in Madhya Pradesh that runs from Dewas to Sendhwa, an area marked by both industrial and agricultural activities. The Narmada River, which flows through this region, contributes to its vulnerability to floods. The area sees an average rainfall of 833.6 mm and temperatures ranging between 44°C and 10°C.

Figure 10 Satellite Image of Location 8

Similarly, Location 9 in Gujarat, which covers the stretch around National Highway 64 from Ahmedabad to Nadiad, runs through a dense urban area. The region's rainfall averages 749 mm annually, and temperatures range from 40°C to 14°C.

Figure 11 Satellite image of Location 9

Further south, Location 10 in Tamil Nadu, marked on National Highway 87 between Ramanathapuram and Mandapam, runs close to the coastline, making it particularly vulnerable to both floods and cyclones. The region receives an average annual precipitation of 821 mm, with temperatures ranging from 40°C to 21°C. Lastly, This comprehensive study of these 10 km stretches along various highways highlights the critical climate-related challenges these key transport routes face. The combination of geographical features and climate extremes makes these highways particularly vulnerable, warranting detailed analysis for better climate resilience planning.

Figure 12 Satellite Image of Location 10

Chapter 3

Datasets and Methodology

In this study, data is collected from mainly two sources, i.e., India Meteorological Department (IMD) for observed data of precipitation and temperature, and CMIP6 is collected from NEX-GDDP-CMIP6 for both historical values and future predictions, respectively. This study employed 13 bias-corrected and downscaled GCMs to a resolution of 0.25° for daily PCP, TMAX, and TMIN data under SSP-245 and SSP-585 scenarios. Due to high daily variability, data was aggregated monthly, and EQM was applied to bias-correct GCM outputs using IMD-observed data for improved accuracy in climate projections. For the ensemble of these GCMs, ML techniques (LSTM, ANN, and SVR) have also been incorporated to improve future predictions, and trend analysis is also performed to understand the future patterns in PCP, TMAX, and TMIN.

3.1 Observational Gridded Data

IMD dataset provides daily gridded rainfall with a high spatial resolution of 0.25°. The IMD dataset provides a more accurate and higher-resolution representation of rainfall over India than the existing datasets due to its denser rain gauge stations network and robust interpolation method (Pai et al., 2014). IMD also provides daily temperature data for India at a spatial resolution of (1° × 1°), particularly to analyze climate extremes like heatwaves and cold waves. The data set used temperature observations from 395 quality-controlled stations across India. It includes daily TMAX and TMIN recorded by the IMD and covers from 1951 to 2023. The dataset was compared with the global temperature dataset developed by the University of Delaware, showing a strong correlation (0.8) between the two, confirming the accuracy of the IMD data(Srivastava et al., 2009).

3.2 Climate Model Simulations

NEX-GDDP-CMIP6 offers 0.25° resolution, bias-corrected climate projections based on the outputs of CMIP6 GCMs. The CMIP6 GCMs were developed in support of the Sixth Assessment Report of the Intergovernmental Panel on Climate Change (IPCC AR6), which supports climate change studies. It is designed to assist climate scientists in conducting local and regional climate change studies. The dataset covers daily climate data from 1950 to 2100. All climate projection models provide daily average variables spanning from 1950 to 2014

("retrospective simulation") and from 2015 to 2100 ("prospective simulation"). The dataset is derived from 35 GCM models and uses four Scenarios SSP126, SSP245, SSP370, and SSP585), covering future projections (2015–2100) and each model's historical projections spanning from 1950–2014 for future climate scenarios (Thrasher et al., 2022).13 models which are selected for the study out of 35 GCMs models are mentioned in Table 1:

Table 1 List of 13 GCMs used in this study

Models No.	Model Name	Institution
1	ACCESS-CM2	CSIRO-ARCCSS, Australia
2	ACCESS-ESM1-5	CSIRO-ARCCSS, Australia
3	BCC-CSM2-MR	Beijing Climate Centre, China
4	CanESM5	Canadian Centre for Climate Modelling and Analysis (CCCMA), Canada
5	EC-Earth3-Veg-LR	The EC-Earth consortium, Europe
6	EC-Earth3	The EC-Earth consortium, Europe
7	INM-CM4-8	Institute for Numerical Mathematics, Russia
8	INM-CM5-0	Institute for Numerical Mathematics, Russia
9	MPI-ESM1-2-HR	Max Planck Institute for Meteorology Earth System, Germany
10	MPI-ESM1-2-LR	Max Planck Institute for Meteorology Earth System, Germany
11	MRI-ESM2-0	Meteorological Research Institute, Japan
12	NorESM2-LM	Norwegian Climate Centre, Norway
13	NorESM2-MM	Norwegian Climate Centre, Norway

3.3 Methodology

This study utilized 13 GCMs from the NEX-GDDP dataset. It is bias-corrected and downscaled to a spatial resolution of 0.25°, with daily values available for PCP, TMAX, and TMIN. IMD's observed data and GCMs data were downloaded for the historical period spanning 1951 to 2023, while the future data for GCMs was obtained for the period 2024 to 2100. For this study, only two SSP scenarios, SSP-245 and SSP-585, were considered to analyze climate projections and their potential impacts under intermediate and high-emission pathways, respectively. Given that daily-scale data often exhibits low correlation due to high variability, the data was aggregated to a monthly scale. To correct biases in the climate model outputs, EQM was applied to bias-correct monthly PCP, TMAX, and TMIN data generated by the 13 CMIP6 climate models, using observed data from the IMD as a reference. Quantile mapping is an effective bias correction technique that adjusts model data to align with observed data distributions by matching quantiles between the two datasets. Specifically, EQM was applied individually to each of the 10 geographic locations by first fitting the observed and modeled data distributions at quantile intervals of 1%. This interval size was selected to capture a high-resolution quantile distribution and improve mapping accuracy. To ensure the robustness of the quantile mapping results, bootstrap sampling was employed, with 10 bootstrapped samples used to estimate uncertainty, and corrections were applied only on "wet days" (days with non-zero precipitation) to avoid skewing results with dry days. Two interpolation methods, **linear** and **tricubic**, were used to ensure smooth transformations of model data between quantiles, yielding two corrected outputs for each location.

$$\mathrm{X_{corr,t}} = \mathrm{ecdf_{obs}^{-1}}(\mathrm{ecdf_{mod,t}}(\mathrm{X_{mod,t}})) \quad (1)$$

where, $X_{corr,t}$ is the corrected model PCP value on day t, $ecdf_{obs}^{-1}$ is the inverse ecdf of observed data, $ecdf_{mod,t}$ is the ecdf of model data, and $X_{mod,t}$ is the raw model precipitation value on day t. An R Package: qmap was used to perform the bias correction.

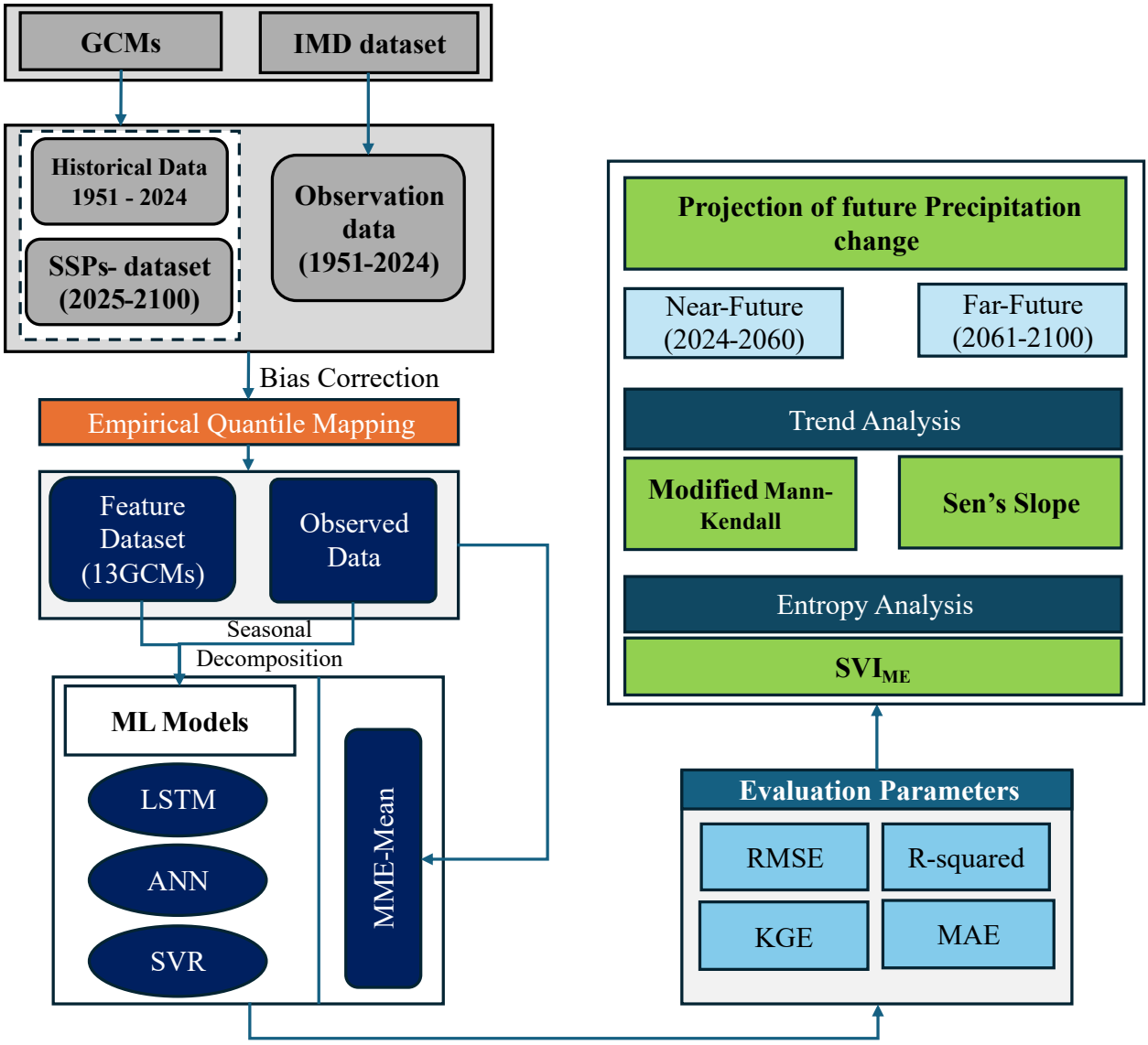

Figure 13 Flow diagram of Methodology

Following bias correction, an MME was created by calculating the mean across the 13 GCMs for PCP, TMAX, and TMIN. MME methods further reduce the uncertainties by averaging the outputs from multiple GCMs, which minimizes errors inherent to individual models.

$$\text{Mean}(t) = \frac{1}{N}\sum_{i=1}^{N} m(t) \qquad (2)$$

Where Mean(t) is the arithmetic mean of GCMs for time t, N is the total number of GCMs (13), and m(t) is the model values of nth GCM for time t. This ensemble was then compared with observed data from 2010 to 2023 to assess the MME's accuracy and reliability. ML models were applied to enhance predictive performance further. Specifically, LSTM, ANN, and SVR were used. Before model training, seasonal decomposition is used to decompose observed data into different components mentioned in equation (3) via the `Statsmodels` Time Series Analysis

(TSA) module in Python. This decomposition was intended to help the models capture seasonal peaks and other patterns present in the observed data, leading to a more accurate fit. Time series decomposition typically dissolves into the trend, seasonality, and residual (or noise). The trend component captures the long-term and underlying patterns in the data. In contrast, the seasonality component reflects short-term, regular fluctuations caused by recurring factors, such as seasonal changes or cycles. The residual component represents uncertainty in the variability that remains after removing the effects of trend and season. By isolating these components, we can observe valuable insights into the data's structure, making it easier to analyze and forecast. In this study, the decomposition approach used is **additive decomposition**; the sum of its components is shown in Equation 3:

$$S(x) = \text{Trend}(x) + \text{Seasonal}(x) + \text{Residual}(x) \quad (3)$$

This method works best when the seasonal effects do not change with the series' magnitude. The ML-based MME produced improved results when compared to the conventional MME-Mean approach, indicating that ML models were effective in capturing the details of observed climate patterns.

3.4 Long Short-Term Memory (LSTM)

LSTM networks are a type of recurrent neural network (RNN) specifically designed to model sequential data while addressing the vanishing gradient problem typically faced by standard RNNs. The provided code applies LSTMs to predict precipitation using a dataset that incorporates observed values and additional features, including trend and seasonal components derived from seasonal decomposition. The process begins with data preprocessing, where the monthly frequency is set, and the time-series is decomposed into trend and seasonal components. Missing values in these components are filled using forward and backward filling to ensure continuity. The dataset is then divided into training and testing sets based on the timeline.

Features are scaled using Standard Scaler to improve model performance and retain consistency across features. The scaled data, including both input features and the target variable, is formatted into sequences using the Time series Generator, which prepares data windows with a specified look-back period to capture temporal dependencies, particularly seasonal trends.

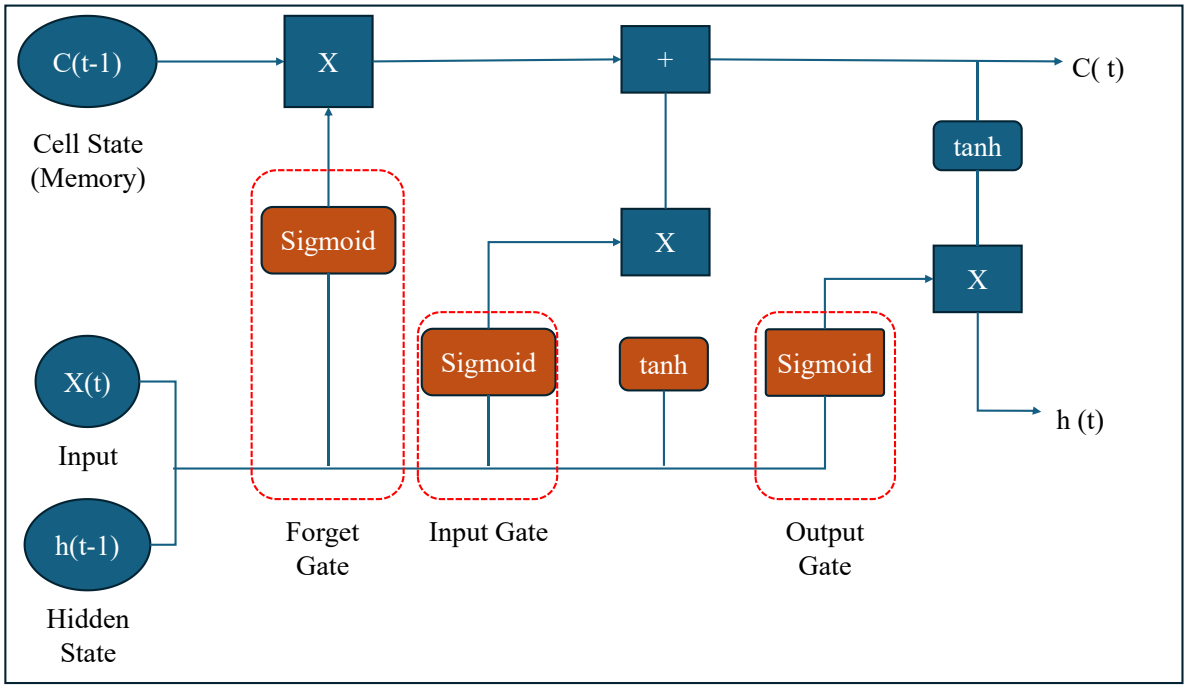

Figure 14 General Architecture of LSTM cell

Figure 14 shows that the LSTM cell is composed of several key components that enable it to capture long-term dependencies. The cell state (C_{t-1}) stores memory from the previous time step and is updated with new information using the input gate, which is activated by a tanh function. (X(t) is the current input to the LSTM cell. The hidden state (h_{t-1}) represents the output from the previous time step. The LSTM includes three gates: the forget gate, input gate, and output gate. The forget gate uses a sigmoid function to determine which parts of the previous cell state to forget, the input gate uses a sigmoid function to decide which new information to store in the cell state, and the output gate, which controls which parts of the cell state should affect the current output. The updated cell and hidden states are calculated by combining the previous values with the respective gates, allowing them to manage the long-term dependencies in sequence data efficiently. The Model architecture comprises two LSTM layers with different combinations of neurons, both using ReLU activation to capture complex nonlinear patterns. Dropout layers are added between LSTMs for regularization to reduce overfitting, and the final dense layers ensure the transformation of learned patterns into single precipitation predictions. The model uses the Adam optimizer and Mean Squared Error (MSE) loss function to optimize weights during training. Early stopping is applied to stop training when the model ceases to improve, ensuring computational efficiency and preventing overfitting. Once trained, the model predicts the testing dataset through sequences generated from the TimeseriesGenerator. These predictions are inverse-scaled to the original range for

evaluation. Model performance is assessed using the R^2 score, a metric that measures the proportion of variance in the observed data explained by the predictions. The code also generates a plot of observed versus predicted precipitation values, visualizing the model's predictive accuracy over time. This implementation highlights the LSTM's capability to handle time-dependent patterns and its effectiveness for precipitation prediction.

3.5 Artificial Neural Networks (ANN)

It is a powerful ML technique inspired by the structure and functioning of the human brain, particularly for capturing nonlinear relationships in data. The provided code demonstrates the application of an ANN for precipitation prediction, focusing on decomposing the observed data into trend, seasonal, and residual components. It utilizes an MLPRegressor, a type of feedforward ANN. The process starts with data preparation, where the observed precipitation series undergoes seasonal decomposition using an additive model, splitting it into trend, seasonal, and residual components. Missing values in these components are interpolated for smooth processing. The model defines the residuals as the target variable while using multiple precipitation features Model-1 to Model 13, along with the seasonal and trend components, as predictors. The data is split into training and testing sets based on specified date ranges, and feature normalization is performed using StandardScaler to improve ANN convergence. The ANN is structured using the MLPRegressor with different combinations of hidden layers and nodes, ReLU activation for non-linearity, the Adam optimizer for adaptive learning, and regularization (α) to prevent overfitting. Early stopping ensures efficient training by halting the process when improvement plateaus. The model predicts the residuals, which are combined with the trend and seasonal components to reconstruct the final precipitation values. Additional constraints ensure non-negative predictions. The performance metrics mentioned in Table 2 evaluate the model's performance. Visualization of observed versus predicted values over time offers insights into the model's ability to capture precipitation variability. This implementation highlights the ANN's capability for time-series prediction, its ability to handle complex relationships between features, and its reliance on residual learning to leverage the trends and seasonality inherent in precipitation data. Numerical expressions of MLP regressor are given as:

$$h = \theta(W_i . X + B_j) \quad (4)$$

Where X is the input feature, W_i represents the weight of the matrix connecting the input layer to the hidden layer, B_j represents the bias of the hidden layer, and θ is the activation function (ReLU) applied element-wise to introduce non-linearity.

3.6 Support Vector Regression (SVR)

It is a robust ML technique derived from Support Vector Machines (SVM), suitable for modeling complex nonlinear relationships in data. The provided code applies SVR for precipitation prediction, emphasizing the decomposition of observed data into trend, seasonal, and residual components to improve predictive accuracy. The process begins with preprocessing, where seasonal decomposition separates the 'Observed' time series into trend, seasonal, and residual components, enabling the SVR model to focus on residuals, which are typically less structured. Features such as precipitation indices Model-1 to Model-13, along with seasonal and trend components, serve as inputs for the model, while the target variable is the residual component. On the basis of the period, the dataset is partitioned into training and testing, and a StandardScaler ensures normalized feature distributions, which are critical for the SVR's optimal performance. This model is configured with a radial basis function (RBF) kernel to capture nonlinear patterns, with hyperparameters such as the regularization term C, kernel parameter gamma, and epsilon defining the tolerance limit for prediction errors. After the scaled data is trained, the model predicts residuals for the testing set. These residuals are combined with the trend and seasonal components to reconstruct the final predicted values, which are then clipped to non-negative values to adhere to the physical constraints of precipitation data. Model evaluation is performed using metrics such as RMSE, R^2, KGE, and MAE to assess the model's predictive capability. A plot comparing observed and predicted values over time provides a visual representation of the model's performance. The mathematical expression for SVR is be found in (Stitson et al., 1996). This implementation highlights SVR's strengths in handling nonlinear relationships, particularly when combined with techniques like seasonal decomposition. The SVR effectively models residual variability while leveraging seasonal and trend information to make accurate predictions of precipitation dynamics.

3.7 Performance Evaluation

The evaluation of machine learning models, including General Circulation Models (GCMs), relies on various evaluation metrics to assess their performance. Among these, R^2 shows how

well your independent variables explain the variation in your outcome; values close to 1 indicate greater predictive accuracy (Shiru & Chung, 2021). RMSE quantifies the average magnitude of prediction errors, penalizing larger deviations more heavily, making it useful for understanding overall model performance (Foyhirun, Chutipat et al., 2019). MAE provides a straightforward average of absolute errors, offering a clear interpretation of model accuracy without squaring deviations (Dumbre et al., 2024). KGE integrates correlation, bias, and variability into a single metric, providing a comprehensive assessment of model performance, particularly for spatial and temporal patterns (Nashwan & Shahid, 2020). These metrics are often used in combination to address different aspects of model performance, such as precision RMSE, MAE, R^2, and KGE, ensuring a robust evaluation framework for climate models and other predictive applications.

3.7.1 R-SQUARED

It is a statistical measure that evaluates a portion of the total variation in the outcome variable that is accounted for by the independent variables in a regression model, ranging from 0 to 1, where 0 means that the model explains none of the variability in the outcome variable, and 1 means a perfect fit where all variability is explained (Miles, 2005), also known as the coefficient of determination. The formula to calculate R^2 is given below in equation (5):

$$R^2 = 1 - \frac{SS_{res}}{SS_{total}} \tag{5}$$

where SS_{res} is the sum of squared residuals, and SS_{total} is the total sum of squares. However, R^2 has limitations. It can be misleading, as a high value does not always indicate a good model fit, especially if the model suffers from bias or overfitting (Onyutha, 2020). Conversely, a poor R^2 does not certainly imply a poor model, particularly in fields like social sciences, where explained variance may inherently be low (J. Gao, 2024).

3.7.2 Mean Absolute Error

It is generally used to evaluate the accuracy of predictive models, especially in regression tasks. It measures the average magnitude of errors between predicted and actual values without considering their direction, making it a robust indicator of model performance (Willmott, 2005b). The formula for MAE is given by:

$$\mathrm{MAE} = \frac{1}{n}\sum_{i=1}^{n}\left|Y_i - \widehat{Y}_i\right| \quad (6)$$

where Y_i is the actual values, $\widehat{Yi}$ denotes the predicted values, and n represents the number of observations. The minimum possible value of MAE is 0, indicating perfect prediction accuracy, while the maximum value is unbounded and depends on the scale of the data (Chai & Draxler, 2014b). In summary, MAE serves as a reliable metric for assessing model performance, with its simplicity and clarity making it a staple in fields ranging from climate science to machine learning. Its minimum value of 0 signifies perfect accuracy, while its maximum value is context-dependent, reflecting the variability in the dataset.

3.7.3 Root Mean Square (RMSE)

It is generally used to evaluate a predictive model's accuracy by measuring the differences between observed and predicted values. To calculate RMSE, Equation (7) is given below:

$$\mathrm{RMSE} = \sqrt{\frac{1}{n}\sum_{i=1}^{n}(U_i - \widehat{U}_i)^2} \quad (7)$$

where U_i represents the observed values, $\widehat{Ui}$ is the predicted value, and n represents the number of observations. RMSE aggregates the magnitudes of prediction errors into a single measure, with larger errors receiving disproportionately higher weight due to the squaring operation. It makes RMSE particularly sensitive to outliers, which can be advantageous when large errors are undesirable (Brassington, 2017; Chai & Draxler, 2014b). The minimum value of RMSE is zero, indicating perfect prediction accuracy where all predicted values match the observed values exactly. The maximum value, however, is unbounded and depends on the length of the data and the magnitude of errors. For example, in climate research, RMSE values can vary significantly based on the dataset's variability and the model's performance (Willmott, 2005b). Nonetheless, researchers often recommend using RMSE alongside other metrics like MAE to provide a comprehensive assessment of model performance (W. Zhu, 2022).

3.7.4 Killing Gupta's Efficiency (KGE)

It is generally used in hydrology to evaluate the performance of hydrological models by assessing the goodness of fit between observed and simulated data. It addresses some limitations of the Nash-Sutcliffe Efficiency (NSE) by decomposing the evaluation into three

orthogonal components: correlation, variability bias, and mean bias (Mathevet et al., 2023). It is calculated using the following equation:

$$\mathrm{KGE} = 1 - \sqrt{(\mathrm{r}-1)^2 + (\alpha-1)^2 + (\beta-1)^2} \quad (8)$$

where r represents the Pearson's correlation coefficient between observed and simulated values, R is the ratio of simulated to observed standard deviations (variability), and B represents the ratio of simulated to observed means (bias). The KGE ranges from -∞ to 1, where a value equal to 1 shows perfect agreement between observed and simulated data. Unlike the NSE, which has an inherent benchmark of 0 (corresponding to the mean flow predictor), the KGE lacks a fixed benchmark. (Knoben et al., 2019) Demonstrated that using the mean flow as a predictor results in a KGE value of approximately -0.41 rather than 0. The KGE's decomposition into correlation, variability, and bias components provides a better understanding of model performance, making it a valuable tool for hydrological applications. However, its uncertainty lacks a closed-form description, necessitating empirical methods like bootstrapping for confidence interval estimation (Vrugt & de Oliveira, 2022).

Table 2 Details of Evaluation Metrics

S. No	Performance Indicator	Equation	Range
1	Root Mean Square Error	$RMSE = \sqrt{\frac{1}{n}\sum_{i=1}^{n}(U_i - \widehat{U}_i)^2}$	0 to ∞
2	R-SQUARED	$R^2 = 1 - \frac{SS_{res}}{SS_{total}}$	0 to1
3	Killing Gupta's Efficiency	$KGE = 1 - \sqrt{(r-1)^2 + (\alpha-1)^2 + (\beta-1)^2}$	-∞ to 1
4	Mean Absolute Error	$MAE = \frac{1}{n}\sum_{i=1}^{n}\lvert Y_i - \widehat{Y}_i\rvert$	0 to ∞

3.8 Entropy

The concept of entropy, along with two entropy-based measures, marginal entropy (ME) and apportionment entropy (AE), is discussed in this section, along with the standardized variability

index (SVI) and its application in analyzing the spatiotemporal variability of rainfall. The section also explores how Mean and ML techniques contribute to understanding rainfall variability.

3.8.1 Apportionment Entropy (AE)

AE was introduced by (Maruyama et al., 2005), quantifies how the total annual rainfall P is distributed across different temporal scales (monthly or seasonal) within a given year. The probability of rainfall occurring at a particular timescale i is expressed as p_i/P. AE is computed annually for each grid location using the equation

$$AE = -\sum_{i=1}^{n_c} \frac{P_i}{P} \log_2 \frac{P_i}{P} \quad (9)$$

Where,

P = total annual rainfall,

p_i = rainfall amount for the specified timescale in that year,

nc = number of class intervals (e.g., nc = 365 for daily, 12 for monthly, 4 for seasonal).

When rainfall is uniformly distributed across all intervals (equally likely events), AE reaches its maximum value H_{max}, defined as $\log_2 nc$. The value of H_{max} depends on the timescale (e.g., $\log_2 12$ for monthly and $\log_2 4$ for seasonal). Essentially, AE captures intra-annual rainfall variability, reflecting how rainfall amounts are distributed within a year at different temporal resolutions.

3.8.2 Marginal Entropy (ME)

ME quantifies the uncertainty or average information content of a random variable X with a probability distribution P(x) as defined by (Mishra et al., 2009). This measure evaluates the entropy of a single time series, capturing its inherent randomness. For instance, when applied to a historical monthly rainfall time series at a given station, ME reflects the overall unpredictability across the entire record. Further methodological details can be found in (Mishra et al., 2009).

In this study, ME is computed for Indian rainfall data at three temporal scales: annual, seasonal, and monthly, to assess interannual variability at each scale. The mathematical formulation for ME is given by:

$$ME = -\sum_{i=1}^{n_c} \frac{r_i}{R} \log_2 \frac{r_i}{R} \quad (10)$$

where:

r_i = rainfall amount in the i-th year,

R = total rainfall over the study period (2024–2100).

The same equation (Eq. 10) can be adapted for monthly and seasonal scales by substituting r_i with rainfall values for the respective months or seasons.

3.9 Trend Analysis

3.9.1 Mann-Kendall Test

Mann and Kendall introduced this, and it is a widely used non-parametric method for detecting monotonic trends in environmental and hydrological time series data. Its popularity stems from its robustness against non-normal distributions and missing data, making it particularly useful in hydroclimatology. However, a key limitation of the traditional MK test is its assumption of serial independence, which is often violated in hydroclimatic data due to inherent autocorrelation. To address this issue, the **Modified Mann-Kendall (MMK) test** was developed by (Hamed & Rao, 1998), incorporating a variance correction factor to account for autocorrelation, thereby reducing the likelihood of false trend detection (Type I error). The MMK test has since become a standard tool in trend analysis, especially for datasets exhibiting persistence or seasonal effects. The MMK test is particularly useful in datasets where autocorrelation is present, which can affect the reliability of trend detection. Autocorrelation can lead to false trends being identified by the classical MK test. The MMK test corrects this by adjusting the variance of the test statistic, thus providing a more accurate assessment of trends in the presence of serial correlation (Sa'adi et al., 2019). Given its robustness and adaptability, the MMK test remains a critical tool for reliable trend detection in hydroclimatic and environmental time series. MMK is calculated as:

$$S = \sum_{i=1}^{n-1} \sum_{j=i+1}^{n} sgn(\propto_j - \propto_i) \quad (11)$$

where n represents the number of data points, $\propto_i$ and $\propto_j$ are the values in the time series i and j

(j > i), respectively, and sgn(x_j - x_i) is the function as:

$$sgn(\propto_j - \propto_i) = \begin{cases} +1 \; if \;\; \propto_j - \propto_i > 0 \\ 0 \;\; if \;\; \propto_j - \propto_i = 0 \\ -1 \;\; if \;\; \propto_j - \propto_i < 0 \end{cases} \quad (12)$$

The variance is calculated as:

$$Var(S) = \frac{n(n-1)(2n+5) - \sum_{i=1}^{p} t_i(t_i-1)(2t_i+5)}{18} \quad (13)$$

where n represents the number of data points, P is the number of tied groups, and A tied group is a set of sample data having the same value. In cases where the sample size n > 30, the standard normal test statistic Z_S is computed using Eq. (14):

$$Z_s = \begin{cases} \frac{S-1}{\sqrt{Var(S)}}, if \; S > 0 \\ 0 \; if \; S = 0 \\ \frac{S+1}{\sqrt{Var(S)}}, if \; S < 0 \end{cases} \quad (14)$$

If Z_S values are Positive, then it indicate upward trends, whereas negative values denote downward trends. Trend significance is assessed at a specified alpha level. If the absolute Z_S value exceeds $Z_{1-\alpha/2}$ it indicates that the null hypothesis is rejected, meaning a statistically significant trend. The level of significance in this study is 5% (α=0.05). Specifically: At the 5% level, the null hypothesis is rejected if $|Z_S|>1.96$|$Z_S|>1.96$.

3.9.2 Sen's Slope

Sen (1968) introduced a non-parametric approach to determine the trend slope in a dataset consisting of n pairs of observations, also known as Sen's method. It employs a linear model to compute the trend slope, requiring that the residual variance remains constant over time. The calculation is performed as follows:

$$Q_{i=\frac{x_j - x_k}{j-k}} \text{ for } i=1,\ldots,n \quad (15)$$

In this method, X_j and X_k represent the data values at time points j and k (where j > k), respectively. If each period contains only a single observation, the total number of slope estimates (N) is given by $N = \frac{n(n-1)}{2}$, where n is the number of periods. However, if there are multiple observations in any period, N will be less than $N = \frac{n(n-1)}{2}$. The N computed slopes (Q_i) are then sorted in ascending order, and the median of these values, referred to as Sen's slope estimator, is determined as follows:

$$Q_{med} = \begin{cases} Q_{\left[\frac{n+1}{2}\right]}, & \text{if n is odd} \\ \frac{Q_{\left[\frac{n}{2}\right]} + Q_{\left[\frac{n+2}{2}\right]}}{2}, & \text{if n is even} \end{cases} \quad (16)$$

The sign of Q_{med} indicates the direction of the trend (increasing or decreasing), while its magnitude represents the trend's steepness. To assess whether the median slope is statistically significant (i.e., different from zero), the confidence interval of Q_{med} must be calculated at a chosen significance level. Following (Roy & Chakravarty, 2021), the confidence interval for the trend slope can be determined using the following equation:

$$C_{\propto} = Z_{1-\propto_{/2}} \sqrt{Var(S)} \quad (17)$$

Here, Var(S) in Equation (13) and $Z_{1-\alpha/2}$ are derived from the standard normal distribution table. In this study, confidence intervals were computed at significance levels α=0.05. The values $M_1 = (n-C_\alpha)/2$ and $M_2 = (n+C_\alpha)/2$ are then calculated, where C_α represents the confidence interval width. The lower and upper bounds of the confidence interval, Q_{min} and Q_{max}, correspond to the M_1th and (M_2+1)-th largest values, respectively, in the ordered set of slope estimates (Roy & Chakravarty, 2021). The median slope Q_{med} is considered statistically significant (i.e., different from zero) if Q_{min} and Q_{max} share the same sign.

Chapter 4

Results

Different ensemble methods were applied to simulate monthly precipitation, maximum temperature, and minimum temperature across 10 different locations: L1, L2, L3, L4, L5, L6, L7, L8, L9 and L10. The evaluation was done using some key performance metrics, which included RMSE, R^2, KGE, and MAE. The analysis consisted of scatter plots showing the relationship of observed values to the average of 13 GCMs and line plots of observed values compared with those predicted by ML models representing SVR, ANN, and LSTM. Results are summarized in tables for the test period of 2010 to 2023, showing the robustness of these models in capturing monthly variability in PCP, TMAX, and TMIN. A graphical representation of each model's performance compared to observed data is given in the figures below for all 10 locations.

Location 1

A stretch of 10 km of this highway falls in Karnataka NH-150, between Kalaburagi and Yadgiri. It crosses through an area dotted with lakes and rivers, including the Bhima River, and is prone to flooding due to the hilly terrain. The region experiences an average annual rainfall of 838 mm, with temperatures ranging from 39.1°C to 17.1°C. From Table 3, for PCP, the LSTM model demonstrated superior performance under SSP 245, achieving the lowest RMSE (47.43), highest R^2 (0.72), lowest MAE (29.43), and highest KGE (0.82). The SVR model also performed well, with slightly higher errors than LSTM but better accuracy than ANN and the Mean method. Under SSP 585, SVR emerged as the best model with the lowest RMSE (48.52) and highest R^2 (0.71), while LSTM showed a higher RMSE (57.62) but maintained a strong KGE (0.80). The Mean method had the poorest performance in both scenarios, with the highest errors (RMSE: 51.39 for SSP 245, 58.62 for SSP 585) and lowest R^2 values, reinforcing the advantage of machine learning approaches over simple averaging. In the case of TMAX predictions, SVR consistently outperformed other methods in both SSP scenarios, achieving the lowest RMSE (1.16 for both SSP 245 and SSP 585) and highest KGE (0.95). LSTM also performed well, particularly under SSP 245 (RMSE: 1.15), but showed a slight decline in SSP 585 (RMSE: 1.26). The Mean method again had the highest errors (RMSE: 1.31 for SSP 245, 1.46 for SSP 585), indicating its inadequacy for precise temperature forecasting. For TMIN, LSTM was the best-performing model in both scenarios, recording the lowest RMSE (0.99 for

SSP 245, 1.00 for SSP 585) and highest KGE (0.94). SVR and ANN showed competitive results but with marginally higher errors. The Mean method had the highest RMSE (1.05 for SSP 245, 1.22 for SSP 585), further emphasizing the limitations of traditional statistical approaches.

It has been observed that LSTM is the best choice for PCP and TMIN predictions at L-1, demonstrating strong accuracy and stability across both SSP scenarios. SVR is the most reliable model for TMAX, providing consistent and high-precision forecasts. ANN, while not the top performer, showed better results than the Mean of GCMs, suggesting its utility as a secondary model. The Mean method consistently underperformed, reinforcing the need for advanced machine-learning techniques in climate modeling. These results highlight that machine learning models (LSTM and SVR) significantly improve prediction accuracy compared to conventional methods. Future research could explore hybrid models or additional climate variables to enhance projection reliability at the L-1 location further.

Table 3 SSP-245 & 585 Model performance comparison of L-1

L-1 Location		PCP				TMAX				TMIN			
	Method	RMSE	R^2	MAE	KGE	RMSE	R^2	MAE	KGE	RMSE	R^2	MAE	KGE
SSP 245	Mean	51.39	0.67	32.66	0.67	1.31	0.86	1.02	0.93	1.05	0.89	0.82	0.92
	LSTM	47.43	0.72	29.43	0.82	1.15	0.89	0.92	0.93	0.99	0.91	0.73	0.94
	ANN	51.16	0.67	36.97	0.70	1.19	0.88	0.93	0.94	1.04	0.89	0.79	0.92
	SVR	48.52	0.71	30.94	0.68	1.16	0.89	0.92	0.95	1.02	0.90	0.80	0.92
SSP 585	Mean	58.62	0.57	35.36	0.59	1.46	0.82	1.17	0.91	1.22	0.86	0.97	0.89
	ANN	51.14	0.68	36.94	0.70	1.19	0.88	0.90	0.93	1.09	0.89	0.84	0.90
	LSTM	57.62	0.59	32.74	0.80	1.26	0.87	1.00	0.92	1.00	0.90	0.77	0.94
	SVR	48.52	0.71	30.74	0.68	1.16	0.89	0.91	0.95	1.04	0.90	0.83	0.91

Results of PCP under SSP-245 in Figure 15 A) show that MME-Mean has an R^2 value of 0.67. Among three different ML models, the LSTM performed better, followed by the SVR and ANN, respectively. Results of LSTM represent more peaks and patterns than in ANN and SVR, covering extreme rainfall in the L-1 region, while SVR and ANN covered the general trend. LSTM under SSP 245 was overpredicted in 2015 and 2021, indicating that it may produce over-predicted values. Figure 15 B) shows the result of PCP under SSP-585. The mean of GCMs shows an R^2 value of 0.57. Among three different machine learning models, the LSTM showed better performance, followed by SVR and ANN, respectively. Similar to SSP 245,

LSTM also predicted higher values than the observed data in the year 2015 and 2021, showing that it may produce overpredicted values.

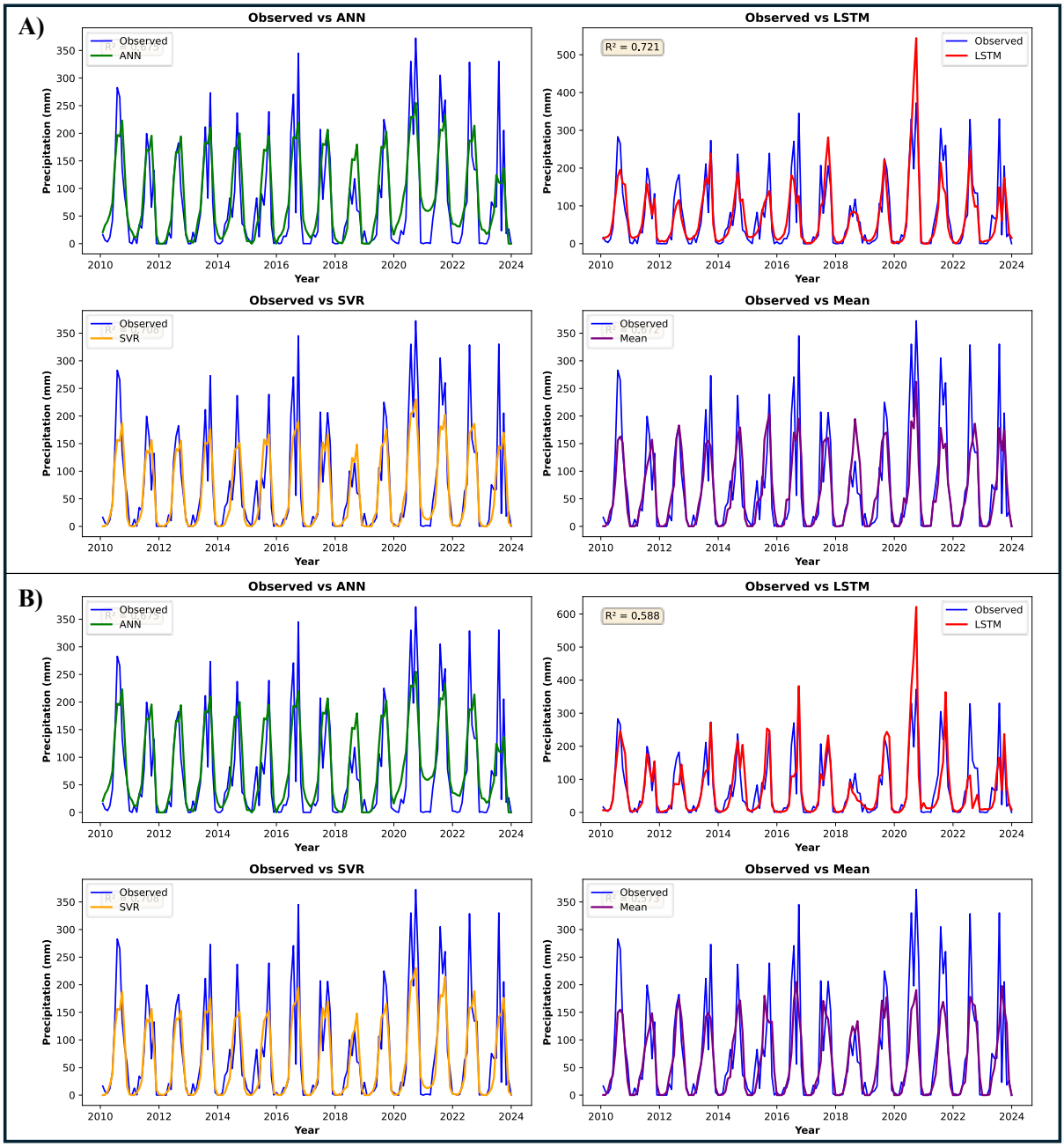

Figure 15 SSP-245 & 585 precipitation Model performance comparison of L1

In Figure 16 A) TMAX, the R^2 value for MME-mean was 0.87. When machine learning was applied, results got better, with all the ML techniques outperforming it. However, there were some differences among the models: compared to the observed data, the ANN model underestimated lower peaks, while both LSTM and SVR overestimated the lower peaks, which may introduce errors in future predictions of this data. In Figure 16 B) TMAX, the R^2 value for MME-mean was 0.83. When ML was applied, results got better, with all the ML techniques

outperforming it. However, there were some differences among the models: compared to the observed data, the ANN model underestimated lower peaks, while both LSTM and SVR overestimated the lower peaks, which may introduce errors in future predictions of this data.

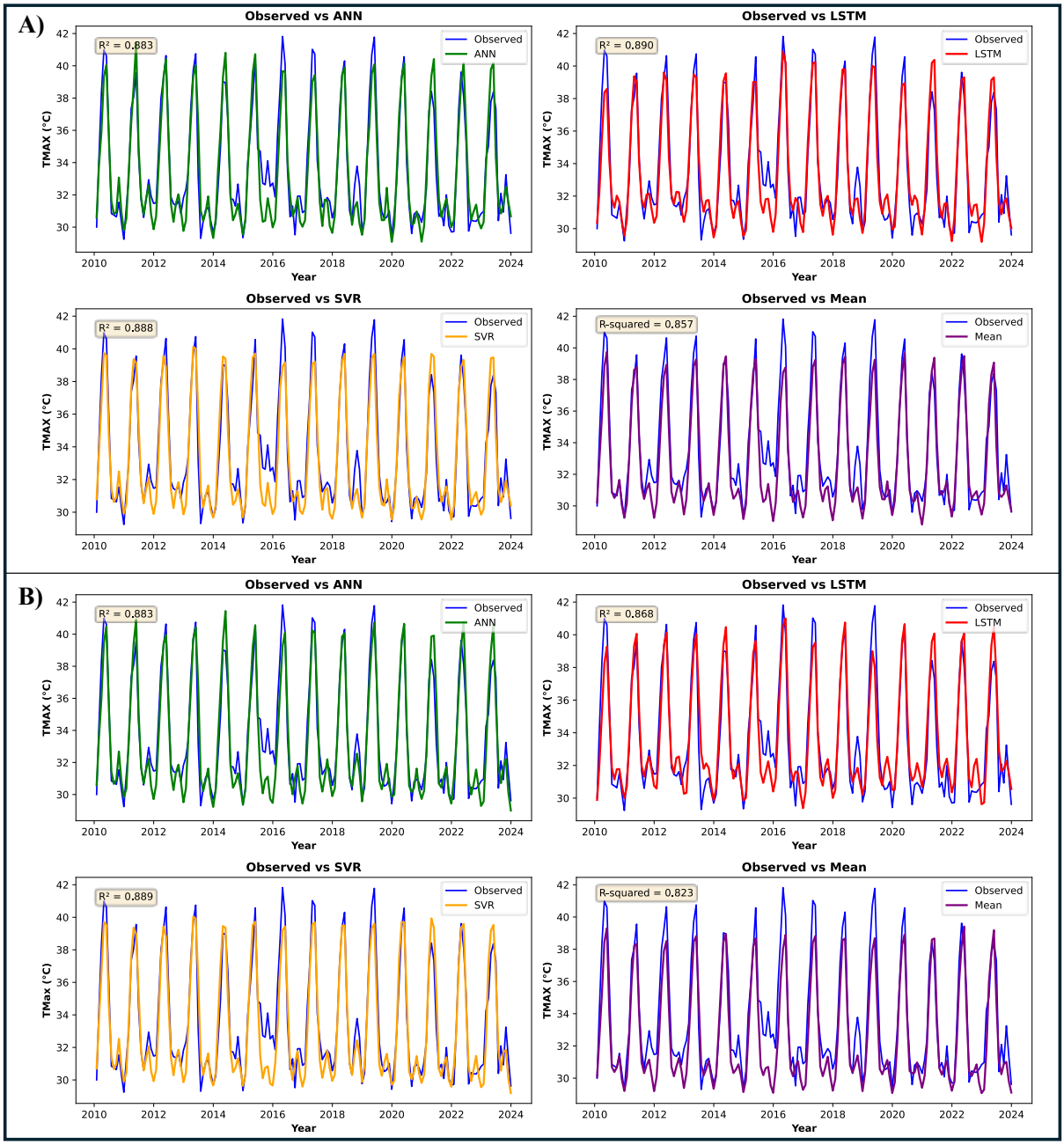

Figure 16 SSP-245 & 585 TMAX Model performance comparison of L1

Under the SSP 245 scenario (TMIN, Figure 17 A), the R^2 value of MME-mean is 0.84. With the application of ML, the results were improved, and all the ML techniques have shown better results with all the techniques. Similarly, under SSP 585 (Figure 17 B), the R2 value is of a similar magnitude to the mean of GCMs. It shows that there is no significant change in the value of TMIN after using ML. It may be due to the temperature not showing a change of high magnitudes.

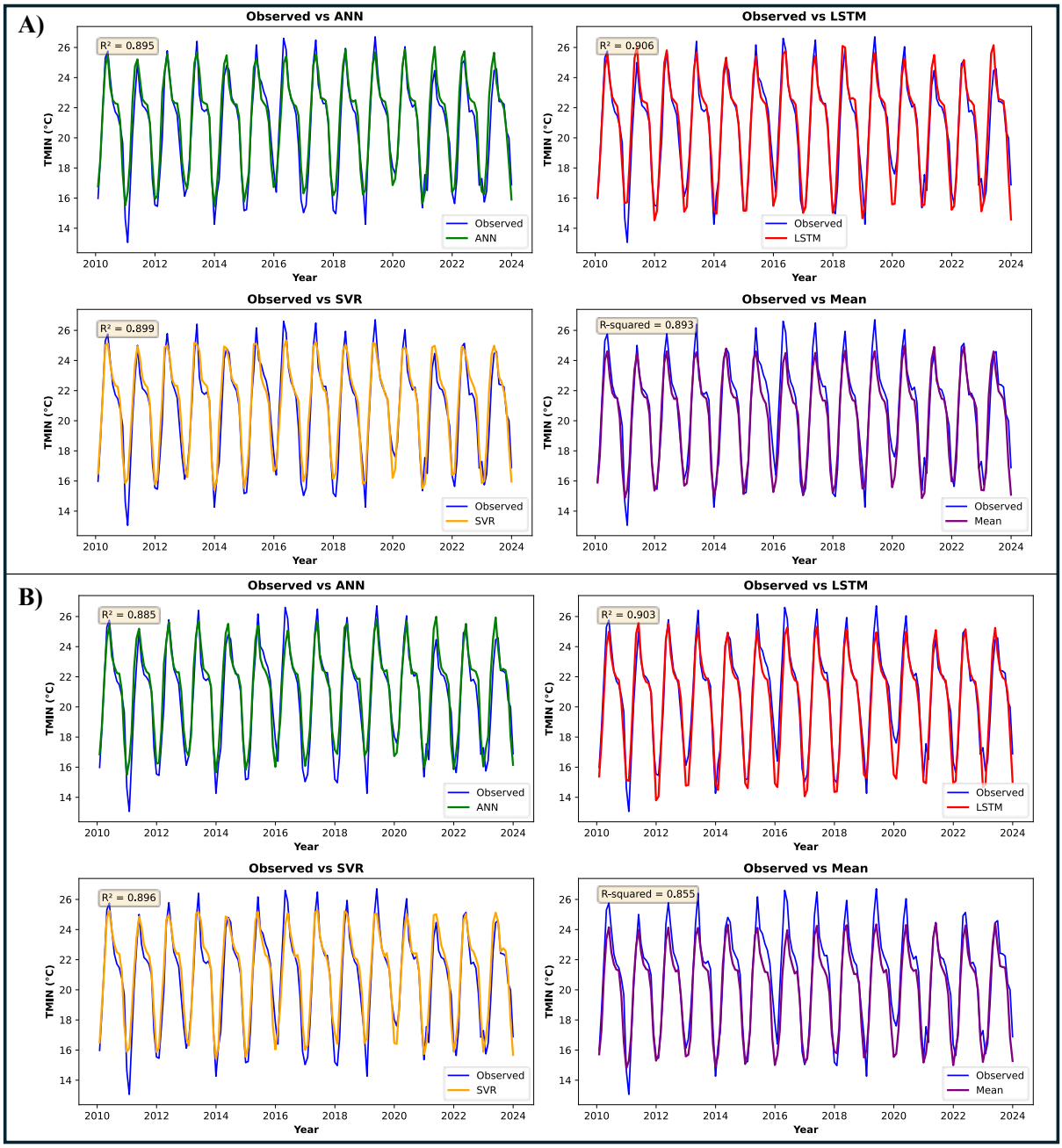

Figure 17 SSP-245 & 585 TMIN- Model performance comparison of L1

Location 2

A stretch of 10 km of this highway falls in Andhra Pradesh, from Guntur to Chilakaluripet. It falls within hilly terrain, owing to which water shows a natural tendency to come down toward the low-lying areas and flood them frequently. Table 4 shows that For PCP, the LSTM model outperformed other methods in both SSP scenarios, achieving the lowest RMSE (46.70 in SSP 245; 51.59 in SSP 585) and highest R^2 (0.73 in SSP 245; 0.67 in SSP 585), indicating better accuracy and predictive capability. The Mean method consistently performed the worst, with the highest RMSE and lowest R^2 values. The ANN and SVR models showed intermediate performance, with SVR slightly better than ANN in terms of MAE and KGE. In TMAX prediction, LSTM again demonstrated superior performance, with the lowest RMSE (1.09 in SSP 245; 1.15 in SSP 585) and highest R^2 (0.85 in SSP 245; 0.84 in SSP 585). The Mean method had the highest errors, particularly under SSP 585, suggesting greater variability in extreme climate conditions. ANN and SVR performed comparably, though SVR had a marginally better KGE, indicating improved hydrological consistency. For TMIN, all machine learning models (LSTM, ANN, SVR) performed well, with high R^2 (≥0.93) and KGE (≥0.94) values. LSTM had the lowest RMSE (0.73 in SSP 245; 0.77 in SSP 585) and MAE, reinforcing its robustness in temperature prediction. The Mean method, while still reasonable (KGE ≥ 0.95), had higher errors, particularly under SSP 585, where RMSE increased to 1.17.

Table 4 SSP-245 & 585 Model performance comparison of L-2

L-2 Location	PCP					TMAX				TMIN			
	Method	RMSE	R^2	MAE	KGE	RMSE	R^2	MAE	KGE	RMSE	R^2	MAE	KGE
SSP 245	Mean	60.36	0.54	40.24	0.64	1.35	0.78	1.10	0.92	0.92	0.90	0.71	0.95
	LSTM	46.70	0.73	32.02	0.82	1.09	0.85	0.87	0.93	0.73	0.94	0.57	0.96
	ANN	54.79	0.62	40.75	0.69	1.17	0.83	0.91	0.90	0.78	0.93	0.63	0.95
	SVR	52.37	0.66	33.35	0.68	1.16	0.84	0.93	0.92	0.79	0.93	0.64	0.96
SSP 585	Mean	62.29	0.51	41.37	0.61	1.53	0.71	1.27	0.89	1.17	0.84	0.93	0.95
	ANN	54.76	0.62	40.68	0.69	1.17	0.83	0.92	0.91	0.80	0.93	0.65	0.94
	LSTM	51.59	0.67	34.24	0.81	1.15	0.84	0.94	0.93	0.77	0.93	0.59	0.95
	SVR	52.11	0.66	32.64	0.67	1.17	0.83	0.92	0.92	0.80	0.93	0.67	0.96

Overall, LSTM consistently outperformed other models across all variables, demonstrating its effectiveness in handling climate prediction tasks. The Mean method, while simple, was the least accurate, highlighting the need for advanced modeling techniques. ANN and SVR provided competitive results but were generally less precise than LSTM. The findings suggest that deep learning approaches like LSTM are particularly effective in capturing complex climate patterns under different emission scenarios. Figure 18 A) shows the precipitation of

SSP-245 MME-Mean having an R^2 value of 0.54. Amongst three different machine learning models, the R^2 value of LSTM was highest, followed by the SVR and SNN, correspondingly. The LSTM model's results represent more peaks and patterns than ANN and SVR, which have done a very good job of representing a general trend. Figure 18 B) shows the result of precipitation for SSP 585, representing that MME-Mean has an R^2 value of 0.51. Amongst three different machine learning models, the LSTM performed better, followed by the ANN and SVR, respectively. The results of LSTM represent more peaks and patterns than ANN and SVR, which have done a very good job of representing a general trend.

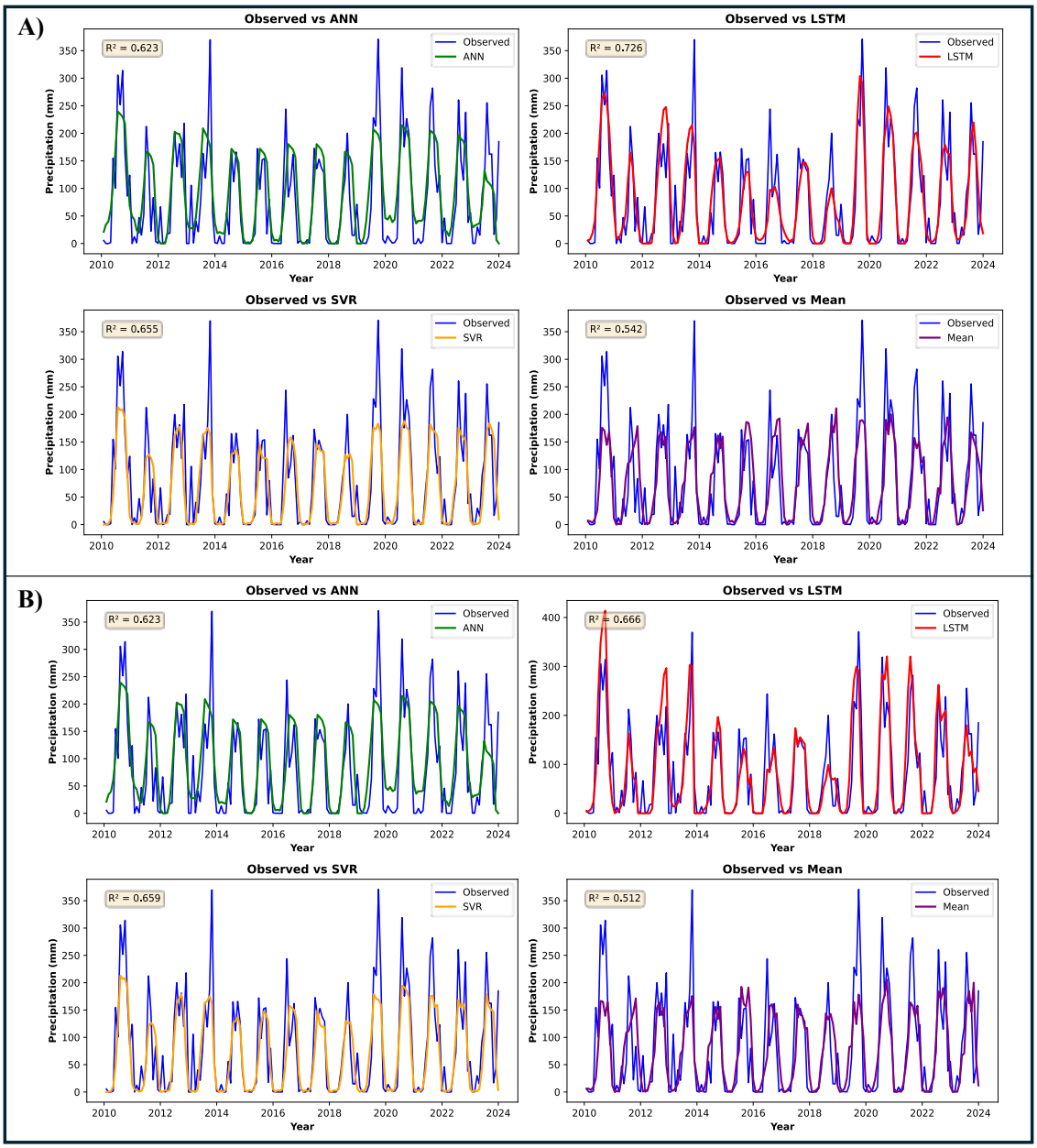

Figure 18 SSP-245 & 585 Precipitation - model performance comparison of L2

In Figure 19 A) TMAX, the R^2 value for MME-mean was 0.78. When machine learning was applied, results got better, with all the ML techniques outperforming it. However, there were some differences among the models: compared to the observed data, the ANN model underestimated lower peaks, while both LSTM and SVR overestimated the lower peaks, which may introduce errors in future predictions of this data. In Figure 19 B) TMAX, the R^2 value for MME-mean was 0.71. When machine learning was applied, results got better, with all the ML techniques outperforming it. However, there were some differences among the models: compared to the observed data, the ANN model underestimated lower peaks, while both LSTM and SVR overestimated the lower peaks, which may introduce errors in future predictions of this data.

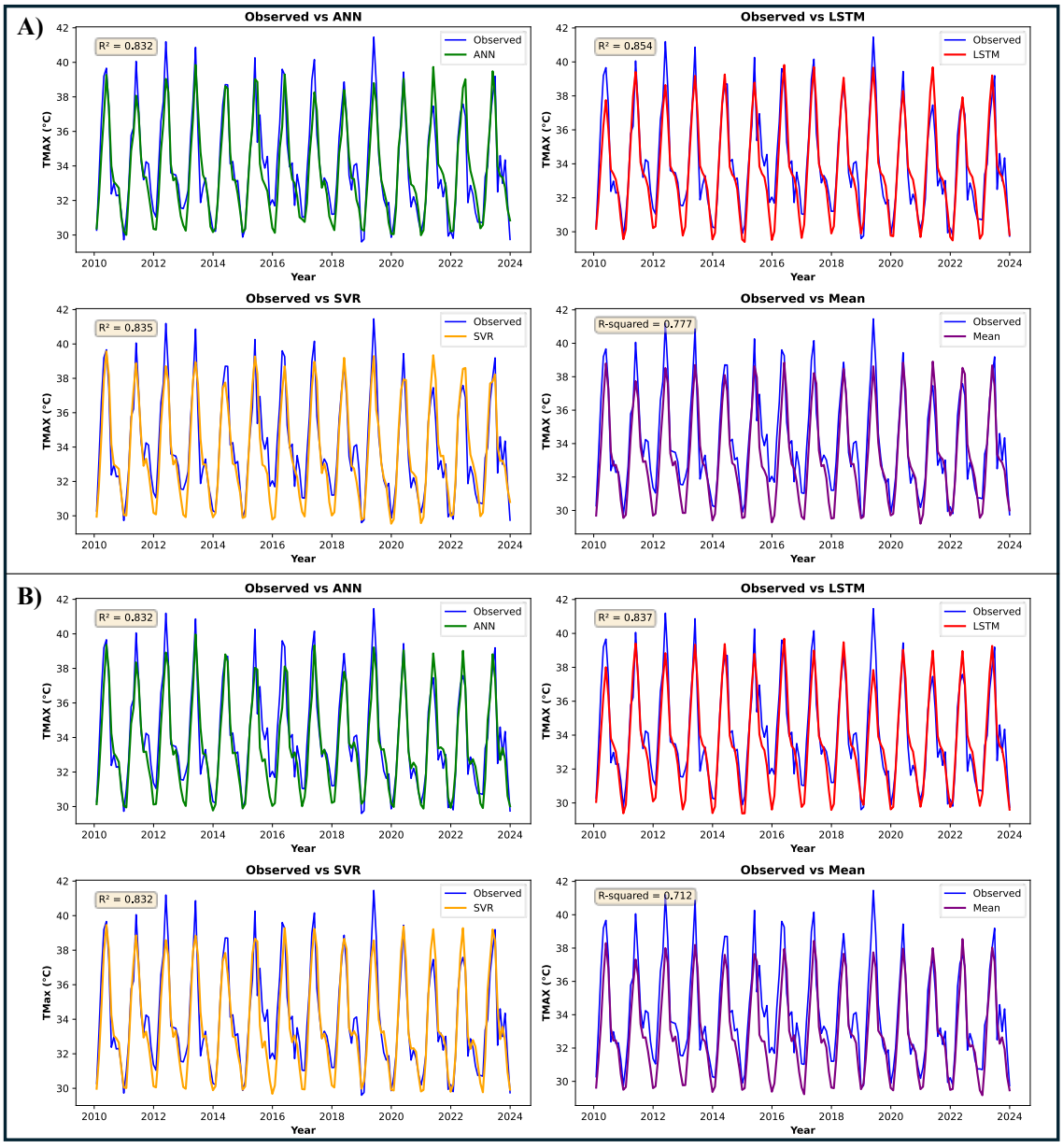

Figure 19 SSP 245 & 585 TMAX – model performance comparison of L2

In figure 20 A) TMIN, the R^2 value of MME-mean is 0.90. With the application of ML, the results were improved, and all the ML techniques have shown better results with all the techniques. In the case of ANN, lower peaks are covered compared to observed data, while in the case of LSTM and SVR, the lower peaks were overestimated, which may generate some error in future prediction of these data. In Figure 20 B) TMIN, the R^2 value of the MME-mean is 0.84. With the application of ML, the results were improved, and all the ML techniques have shown better results with all the techniques. In the case of ANN, lower peaks are covered compared to observed data, while in the case of LSTM and SVR, the lower peaks were overestimated, which may generate some error in future prediction of these data.

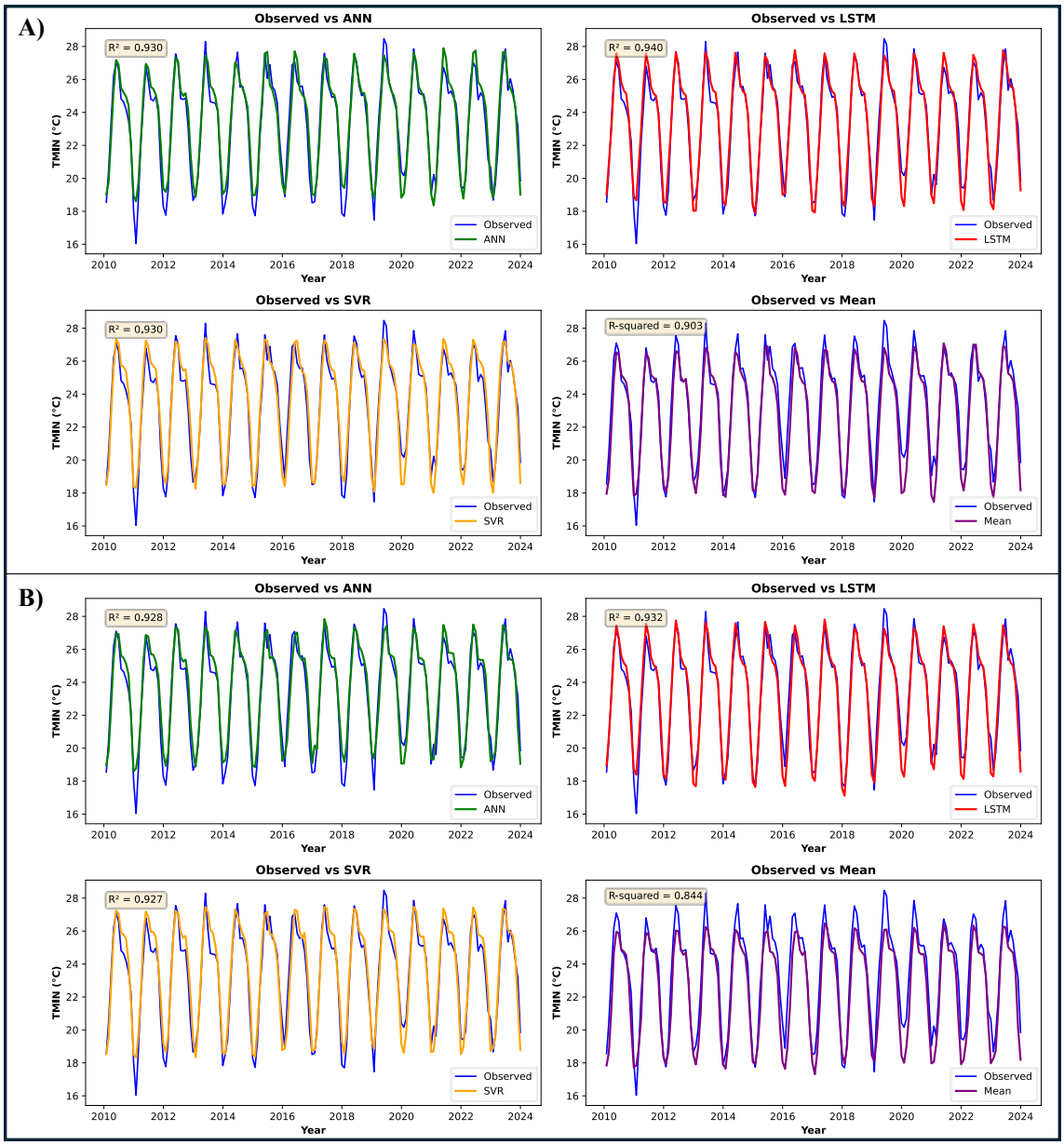

Figure 20 SSP 245 & 585 TMIN – model performance comparison of L-2

Location 3

A stretch of 10 km of this highway falls in Chhattisgarh NH-43, between Manendragarh and Ambikapur. This area is characterized by its proximity to the Hasdeo River, Aaruni Dam, and various waterfalls, making it particularly flood-prone. From Table 5 For PCP, the LSTM model performed best under SSP 245, achieving the lowest RMSE (56.30) and highest R^2 (0.85), indicating strong predictive accuracy. However, under SSP 585, SVR outperformed other methods with the lowest RMSE (61.26) and highest R^2 (0.82). The Mean method had the highest errors in both scenarios, reinforcing the need for advanced modeling techniques. ANN showed intermediate performance, while SVR demonstrated competitive results, particularly in SSP 585. In TMAX prediction, LSTM again excelled under SSP 245, with the lowest RMSE (1.44) and highest R^2 (0.91). Under SSP 585, SVR performed best (RMSE: 1.52, R^2: 0.90), closely followed by LSTM.

Table 5 SSP 245 & 585 Model performance comparison of L-3

L-3 Location	PCP					TMAX				TMIN			
	Method	**RMSE**	**R^2**	**MAE**	**KGE**	**RMSE**	**R^2**	**MAE**	**KGE**	**RMSE**	**R^2**	**MAE**	**KGE**
SSP 245	Mean	73.46	0.75	41.19	0.83	1.61	0.89	1.30	0.92	1.10	0.96	0.88	0.97
	LSTM	56.30	0.85	33.38	0.91	1.44	0.91	1.12	0.95	1.22	0.96	0.98	0.96
	ANN	67.09	0.79	42.81	0.82	1.58	0.89	1.22	0.91	1.09	0.96	0.83	0.97
	SVR	**61.73**	**0.82**	**36.83**	**0.88**	**1.51**	**0.90**	**1.18**	**0.92**	**0.99**	**0.97**	**0.77**	**0.97**
SSP 585	Mean	76.33	0.73	42.83	0.82	1.79	0.86	1.50	0.92	1.45	0.94	1.19	0.94
	ANN	67.12	0.79	42.87	0.82	1.67	0.88	1.32	0.89	1.05	0.97	0.82	0.97
	LSTM	67.78	0.79	37.32	0.86	1.59	0.89	1.27	0.95	1.27	0.95	1.03	0.92
	SVR	61.26	0.82	36.25	0.88	1.52	0.90	1.17	0.94	1.02	0.97	0.81	0.97

The Mean method had the highest errors, particularly under SSP 585 (RMSE: 1.79), suggesting increased variability under higher emissions. ANN was consistent but slightly less accurate than LSTM and SVR. For TMIN, SVR was the top performer in both scenarios, achieving the lowest RMSE (0.99 in SSP 245; 1.02 in SSP 585) and highest R^2 (0.97). The Mean method had higher errors, especially under SSP 585 (RMSE: 1.45), while ANN and LSTM showed strong but slightly inferior results. Notably, LSTM's KGE dropped to 0.92 in SSP 585, indicating reduced hydrological consistency compared to SVR. It has been observed that LSTM is the best model for PCP and TMAX under SSP 245, but SVR outperformed SSP 585, suggesting that different methods may excel under varying climate scenarios. SVR consistently performed

best for TMIN, demonstrating robustness in predicting minimum temperatures. The Mean method consistently had the highest errors, reinforcing the superiority of machine learning models. ANN provided stable but intermediate results, while LSTM and SVR were more scenario-dependent, with LSTM excelling in moderate conditions SSP 245 and SVR performing better under extreme emissions SSP 585.

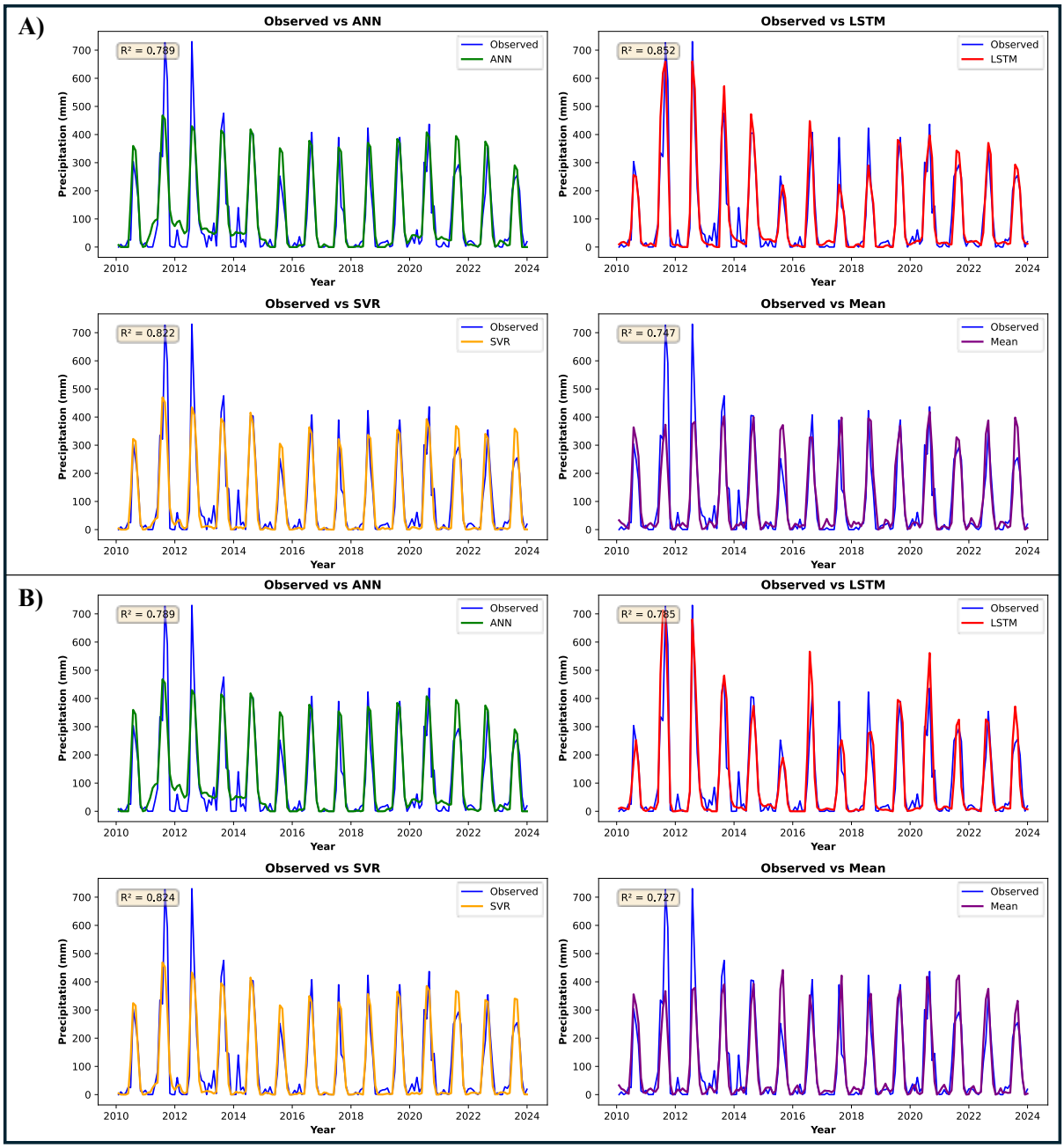

Figure 21 SSP 245 & 585 Precipitation - Model performance comparison of L-3

Figure 21 A) shows the result of precipitation of SSP-245. The panel, that is, represents results for MME-Mean having an R^2 value of 0.75. Amongst three different machine learning models, all ML techniques have shown nearby improvement in the results. In the case of extreme rainfall events that occurred between 2010 and 2014, the peaks are covered better by the LSTM. Figure 21 B) shows the result of precipitation of SSP-245. The panel, that is, represents results for MME-Mean having an R^2 value of 0.73. Amongst three different machine learning models, all ML techniques have shown nearby improvement in the results. In the case of extreme rainfall events that occurred between 2010 and 2014, the peaks are covered better by the LSTM.

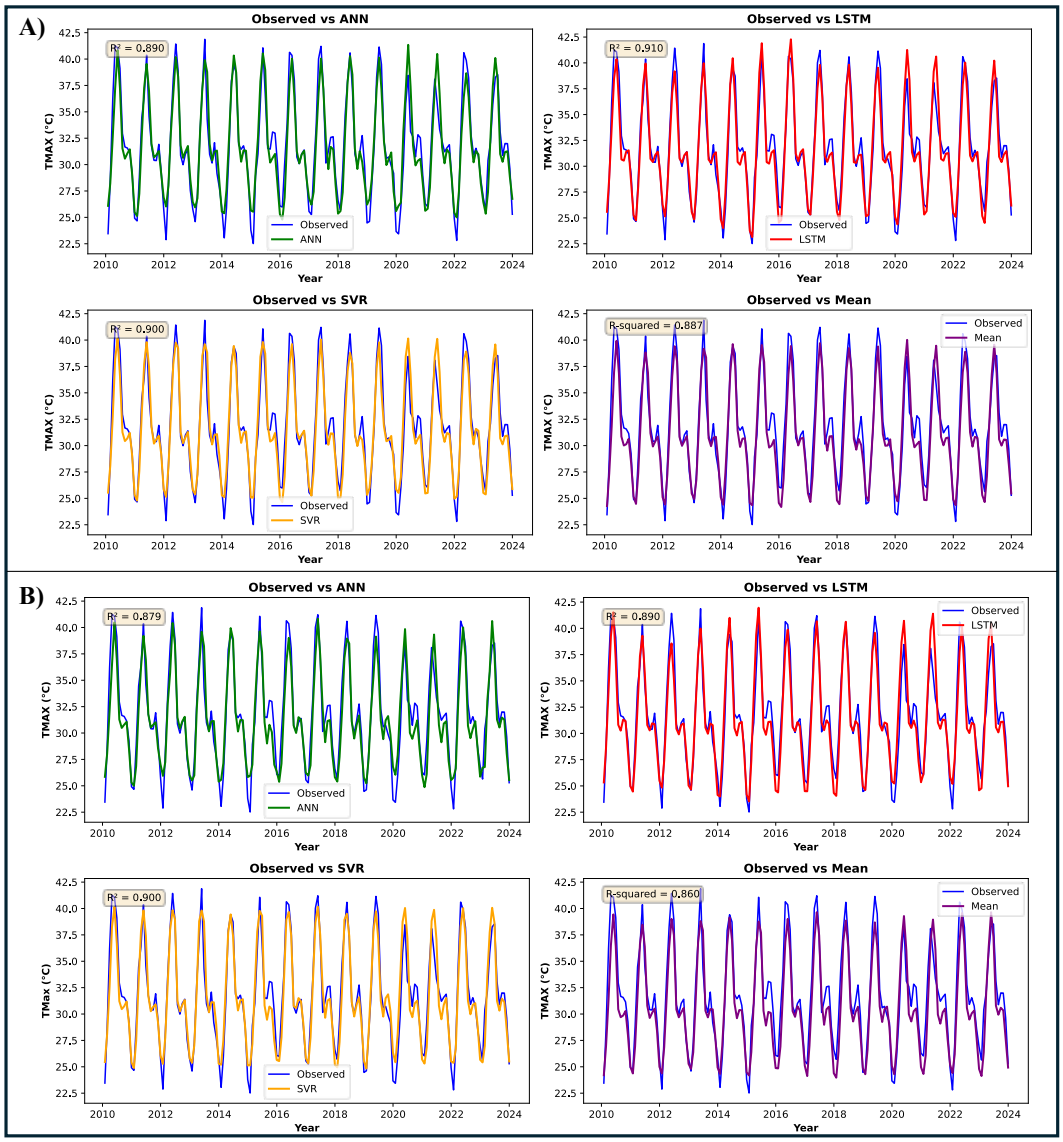

Figure 22 SSP-245 & 585 TMAX - Model performance comparison of L-3

In Figure 22 A) TMAX, the R^2 value for MME-mean was 0.89. When machine learning was applied, results got better, and with all the ML techniques, a slight improvement was observed. All the ML techniques have shown comparable results. In Figure 22 B) TMAX, the R^2 value

for MME-mean was 0.86. When machine learning was applied, the results got better. A slight improvement is observed with all the ML techniques. All the ML techniques have shown comparable results.

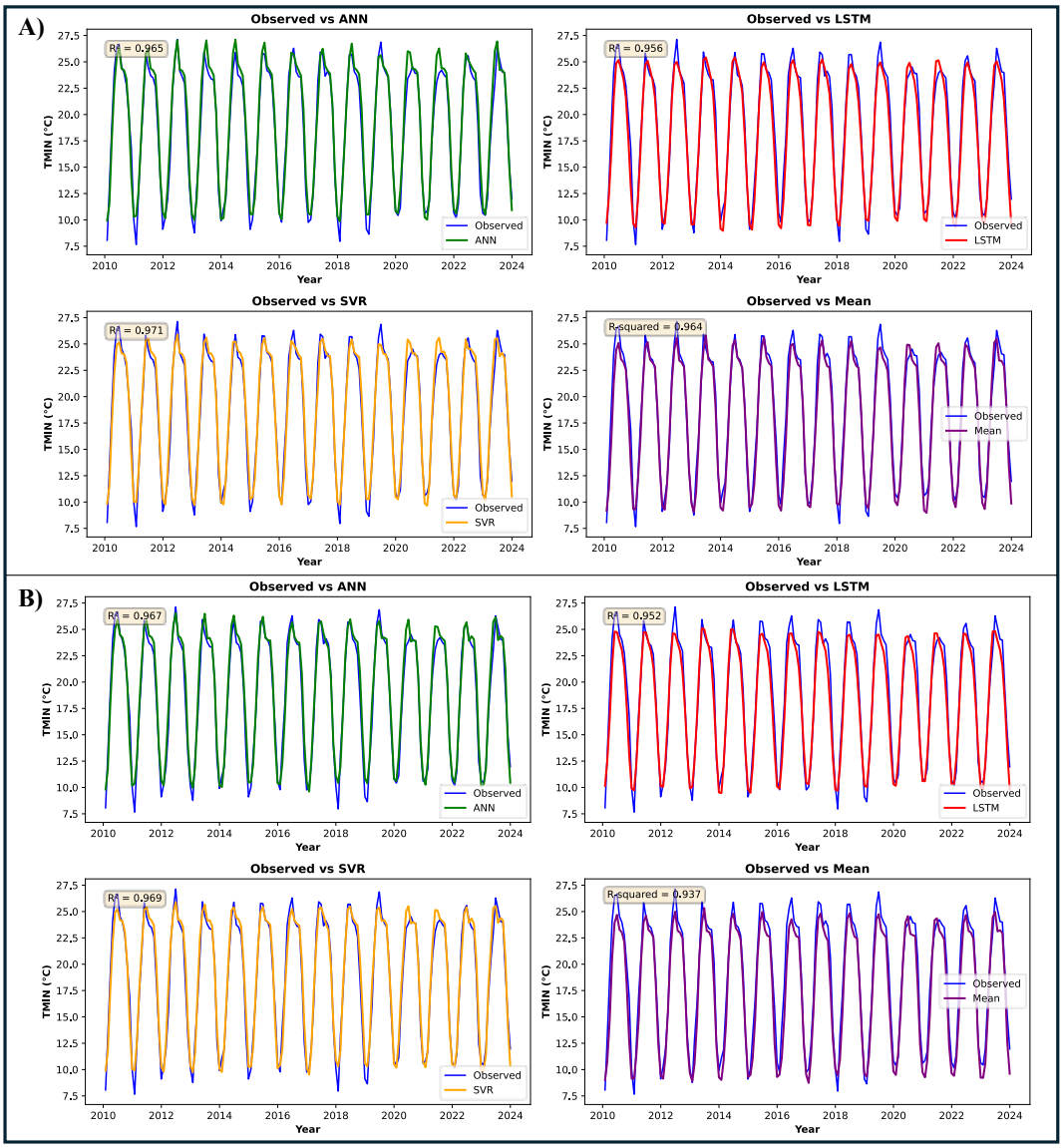

Figure 23 SSP-245 & 585 TMIN - Model performance comparison of L-3

In Figure 23 A) TMIN, the R^2 value for MME-mean was 0.95, which is originally a good correlation between the mean of GCMs and observed data, but when machine learning was applied, the results got better. A slight improvement is observed with all the ML techniques. All the ML techniques have shown comparable results. In Figure 23 B) TMIN, the R^2 value for MME-mean was 0.92, which is originally a good correlation between the mean of GCMs and observed data, but when machine learning was applied, the results got better. A slight

improvement is observed with all the ML techniques. All the ML techniques have shown comparable results.

Location 4

A stretch of 10 km of this highway falls in Madhya Pradesh NH-45, between Shahpura and Jabalpur. Where the Narmada River and several lakes define the local landscape, prone to both flooding and seismic activity (Seismic Zone III), this region experiences an annual rainfall of 1280 mm, with temperatures ranging from 32.1°C to 18.3°C.

Table 6 SSP-245 & 585 Model performance comparison of L-4

L4 Location	PCP					TMAX				TMIN			
	Method	RMSE	R^2	MAE	KGE	RMSE	R^2	MAE	KGE	RMSE	R^2	MAE	KGE
SSP 245	Mean	84.75	0.74	46.34	0.80	1.56	0.90	1.27	0.92	1.15	0.96	0.91	0.96
	LSTM	76.93	0.79	44.45	0.87	1.49	0.91	1.19	0.87	1.10	0.97	0.87	0.93
	ANN	81.33	0.77	52.32	0.79	1.55	0.90	1.20	0.91	1.10	0.97	0.85	0.97
	SVR	78.57	0.78	40.73	0.76	1.46	0.91	1.13	0.93	1.04	0.97	0.82	0.96
SSP 585	Mean	91.50	0.70	47.74	0.78	1.75	0.87	1.49	0.91	1.51	0.93	1.24	0.93
	ANN	81.33	0.77	52.32	0.79	1.55	0.90	1.23	0.93	1.17	0.96	0.89	0.94
	LSTM	61.83	0.86	39.63	0.92	1.47	0.91	1.20	0.95	1.06	0.97	0.83	0.93
	SVR	78.56	0.78	40.91	0.76	1.48	0.91	1.17	0.94	1.11	0.96	0.87	0.96

From Table 6, evaluation metrics for PCP under SSP 245, LSTM performed best with the lowest RMSE (76.93) and highest R^2 (0.79), demonstrating strong predictive capability. SVR followed closely with an RMSE of 78.57, while ANN and Mean had higher errors. Under SSP 585, LSTM significantly outperformed all other models, achieving the lowest RMSE (61.83) and highest R^2 (0.86), suggesting it handles extreme climate scenarios effectively. SVR and ANN showed similar performance, while the Mean method had the highest errors (RMSE: 91.50, R^2: 0.70). For TMAX under SSP 245, SVR was the best model, with the lowest RMSE (1.46) and highest R^2 (0.91). LSTM and ANN were competitive but slightly less accurate. Under SSP 585, LSTM emerged as the top performer (RMSE: 1.47, R^2: 0.91), followed closely by SVR (RMSE: 1.48). The Mean method again had the highest errors, particularly under increased emissions (RMSE: 1.75). For TMIN under SSP 245, ANN and SVR performed best, with low RMSE (1.10 and 1.04, respectively) and high R^2 (0.97). LSTM had a slightly higher RMSE (1.10) but a lower KGE (0.93), indicating some inconsistency in hydrological efficiency. Under SSP 585, SVR maintained strong performance (RMSE: 1.11, R^2: 0.96), while

LSTM had the lowest RMSE (1.06) but a reduced KGE (0.93), suggesting trade-offs between precision and reliability. The Mean method was the least accurate, particularly under extreme conditions (RMSE: 1.51). It has been observed that LSTM performs best for PCP in both scenarios, showing exceptional improvement under SSP 585, likely due to its ability to capture long-term dependencies in precipitation patterns. SVR performed best for TMAX in SSP 245, while LSTM excelled in SSP 585, indicating that model superiority can vary with emission scenarios. For TMIN, ANN and SVR were the most consistent, while LSTM showed slightly reduced KGE values, suggesting that simpler models may sometimes be more reliable for temperature prediction. The Mean method consistently underperformed, reinforcing the need for machine-learning approaches in climate modeling.

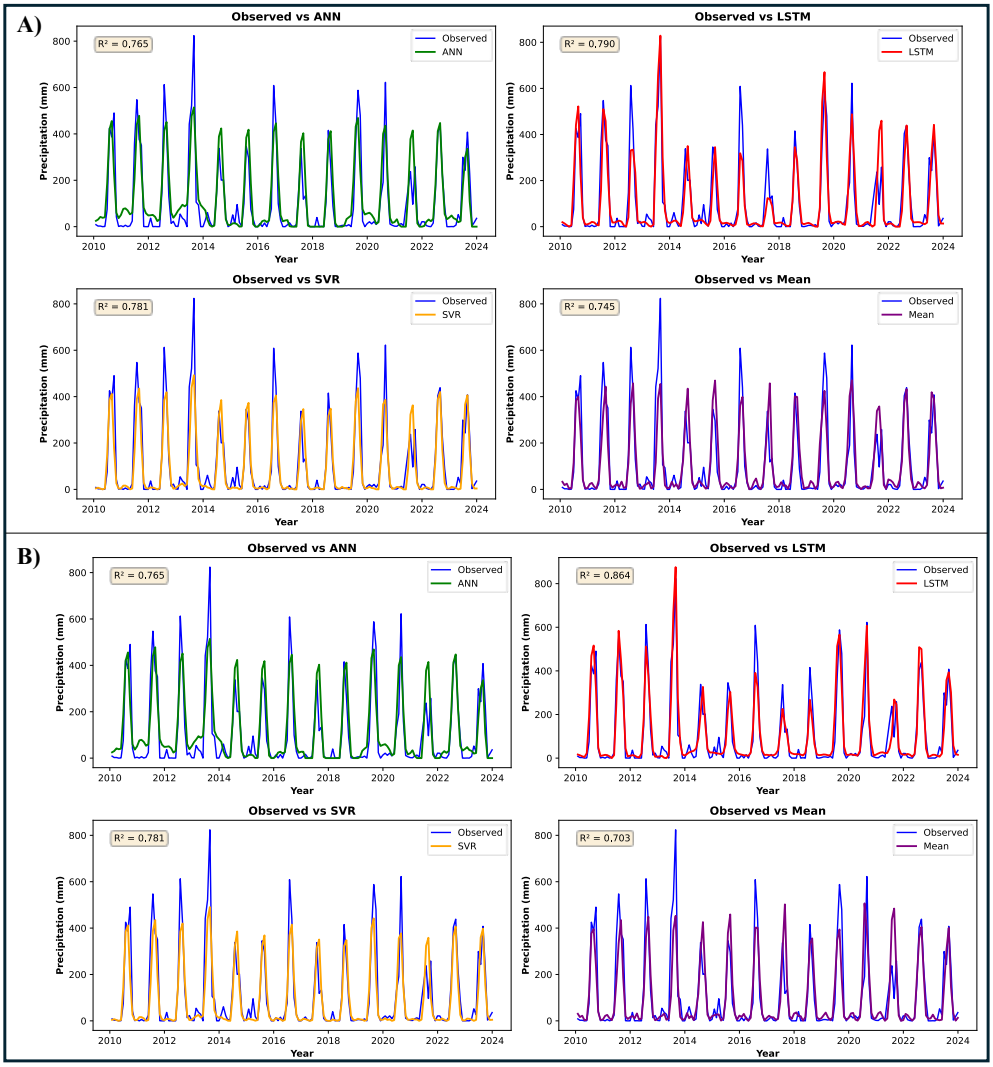

Figure 24 SSP-245 & 585 Precipitation - Model performance comparison of L-4

Figure 24 A) shows the result of the precipitation of SSP 245. The panel, that is, represents results for MME-Mean having an R^2 value of 0.74. Among three different machine learning

models, the LSTM performs better, followed by the ANN and SVR, respectively. The LSTM model's results represent more peaks and patterns than ANN and SVR, which have done a very good job of representing a general trend. Figure 24 B) shows the precipitation of SSP 585, which represents results for MME-Mean, having an R^2 value of 0.70. Among three different machine learning models, the LSTM performed better, followed by the ANN and SVR, respectively. The results of LSTM represent more peaks and patterns than ANN and SVR, which have done a very good job of representing a general trend.

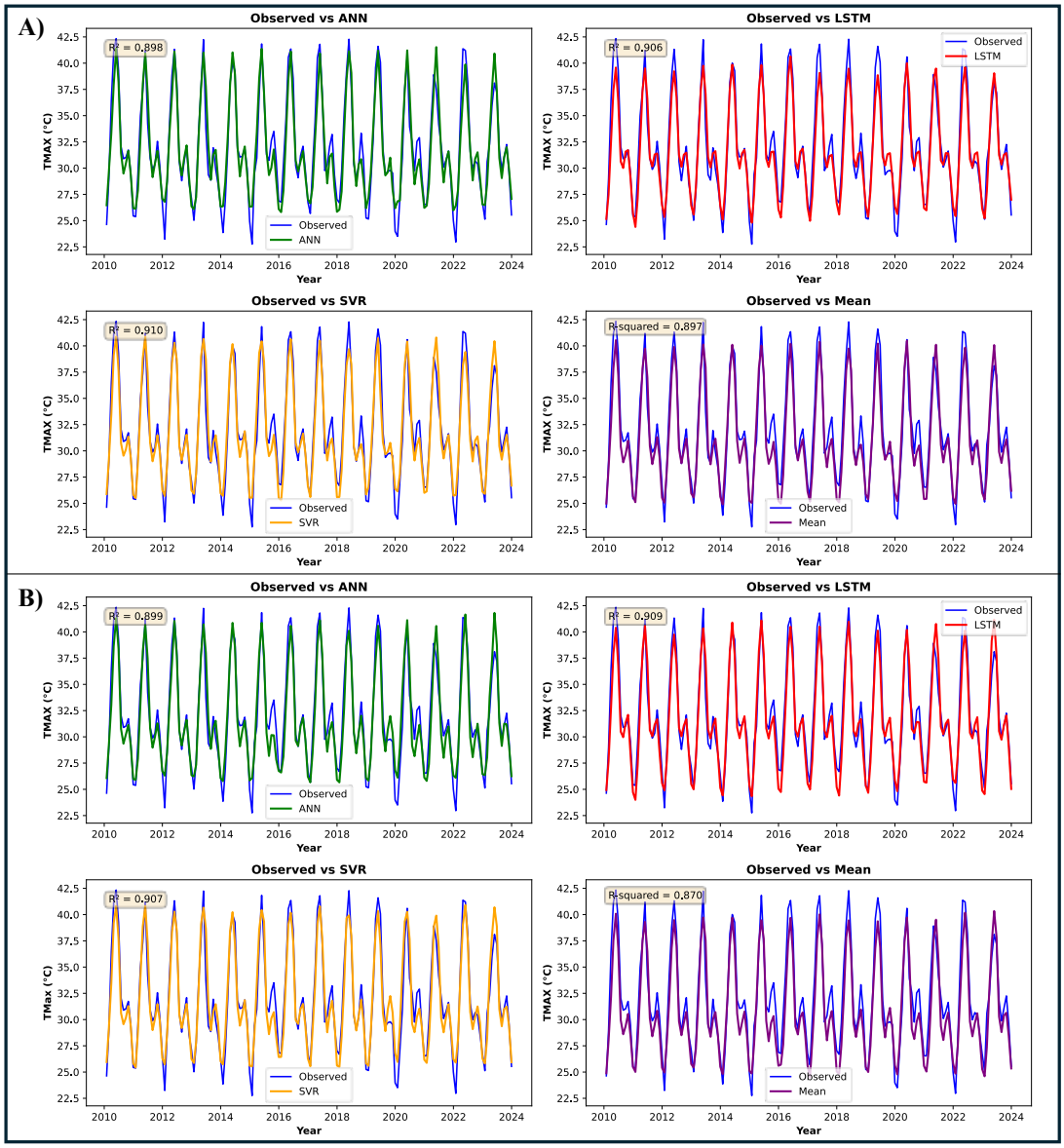

Figure 25 SSP-245 & 585 TMAX - Model performance comparison of L-4

In Figure 25 A) TMAX, the R^2 value for MME-mean was 0.89. When machine learning was applied, results got better, with all the ML techniques outperforming it. However, there were some differences among the models: compared to the observed data, the ANN model underestimated lower peaks, while

both LSTM and SVR overestimated the lower peaks, which may introduce errors in future predictions of this data. In Figure 25 B) TMAX, the R2 value for MME-mean was 0.86. When machine learning was applied, the results got better. A slight improvement is observed with all the ML techniques. All the ML techniques have shown comparable results.

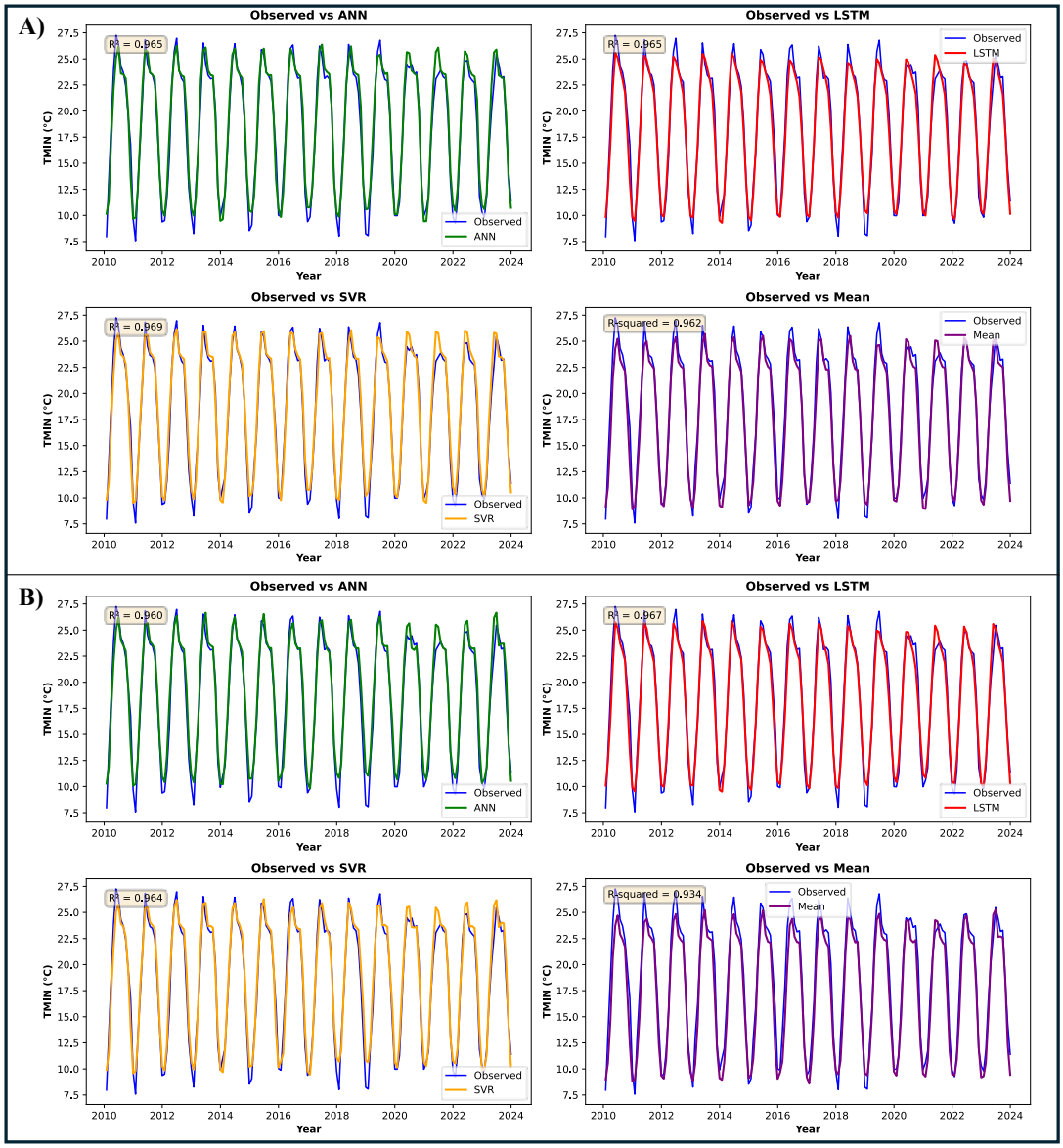

Figure 26 SSP-245 TMIN - Model performance comparison of L-4

In Figure 26 A) TMIN, the R^2 value of the MME-mean is 0.95. With the application of ML, the results were improved, and all the ML techniques have shown better results with all the techniques. In the case of ANN, lower peaks are covered compared to observed data, while in the case of LSTM and SVR, the lower peaks were overestimated, which may generate some error in future prediction of these data. In figure 26 B) TMIN, the R^2 value of MME-mean is 0.92. With the application of ML, the results were improved, and all the ML techniques have

shown better results with all the techniques. In the case of ANN, lower peaks are covered compared to observed data, while in the case of LSTM and SVR, the lower peaks were overestimated, which may generate some error in future prediction of these data.

Location 5

A stretch of 10 km of this highway falls in Maharashtra NH-47, between Betul and Saoner. An area surrounded by dams such as Umri, Kolar, and Nanda. This region, also vulnerable to floods, has a recorded average rainfall of 1060.2 mm, and temperatures fluctuate between 45°C and 12°C. From Table 7, for PCP under SSP 245, LSTM demonstrated the best performance, achieving the lowest RMSE (63.70) and highest R^2 (0.80), indicating strong predictive accuracy. SVR followed closely (RMSE: 67.03, R^2: 0.78), while ANN and Mean had higher errors. Under SSP 585, LSTM significantly outperformed all other models, with the lowest RMSE (54.23) and highest R^2 (0.85), showcasing its robustness in extreme climate conditions. SVR and ANN performed moderately, while the Mean method had the highest errors (RMSE: 78.63, R^2: 0.69). For TMAX under SSP 245, SVR was the top-performing model, with the lowest RMSE (1.39) and highest R^2 (0.91). LSTM and ANN were competitive but slightly less precise. Under SSP 585, LSTM and SVR tied for the best performance (RMSE: 1.44 and 1.40, respectively), both maintaining high R^2 (0.90). The Mean method had the highest RMSE (1.60), particularly under increased emissions. For TMIN under SSP 245, SVR and LSTM performed comparably, with SVR having a slightly lower RMSE (1.21 vs. 1.10) but LSTM maintaining a higher KGE (0.90 vs. 0.95 for SVR). The Mean method was the least accurate (RMSE: 1.12). Under SSP 585, LSTM achieved the lowest RMSE (1.11), but its KGE (0.90) was lower than ANN and SVR (0.95), suggesting a trade-off between precision and consistency. SVR and ANN provided more balanced performance across metrics. It has been observed that LSTM performed best for PCP in both scenarios, with remarkable improvement under SSP 585, highlighting its ability to handle complex precipitation patterns under extreme conditions. SVR excelled in TMAX prediction under SSP 245, while LSTM and SVR were equally strong under SSP 585, indicating that model performance can vary with emission scenarios. For TMIN, SVR and ANN were the most consistent, while LSTM had lower KGE values, suggesting that simpler models may sometimes be more reliable for temperature forecasting. The Mean method consistently underperformed, reinforcing the superiority of machine learning approaches in climate modeling.

Table 7 SSP-245- Model performance comparison of L-5

L5 Location	PCP					TMAX				TMIN			
	Method	RMSE	R^2	MAE	KGE	RMSE	R^2	MAE	KGE	RMSE	R^2	MAE	KGE
SSP 245	Mean	74.62	0.72	41.00	0.68	1.44	0.90	1.19	0.91	1.12	0.95	0.86	0.96
	LSTM	63.70	0.80	37.59	0.84	1.40	0.90	1.12	0.93	1.10	0.95	0.87	0.90
	ANN	71.52	0.75	47.47	0.70	1.40	0.90	1.11	0.92	1.32	0.93	1.02	0.95
	SVR	67.03	0.78	37.26	0.72	1.39	0.91	1.09	0.92	1.21	0.94	0.97	0.95
SSP 585	Mean	78.63	0.69	43.09	0.65	1.60	0.88	1.34	0.90	1.39	0.92	1.10	0.94
	ANN	71.56	0.75	47.57	0.70	1.44	0.90	1.13	0.94	1.29	0.93	1.00	0.95
	LSTM	54.23	0.85	33.43	0.89	1.44	0.90	1.14	0.95	1.11	0.95	0.86	0.90
	SVR	68.20	0.77	36.84	0.70	1.40	0.90	1.11	0.93	1.24	0.94	1.00	0.95

Figure 27 A) shows the result of precipitation of SSP-245. Part a) represents results for MME-Mean having an R^2 value of 0.72. Amongst three different machine learning models, the LSTM performed better, followed by the ANN and SVR, correspondingly. The results of LSTM represent more peaks and patterns than ANN and SVR, which have done a very good job of representing a general trend. Figure 27 B) shows the result of precipitation of SSP-585 representing results for MME-Mean having an R^2 value of 0.694 amongst three different machine learning models. The LSTM performs better, followed by the ANN and SVR, correspondingly. The results of LSTM represent more peaks and patterns than ANN and SVR, which have done a very good job of representing a general trend.

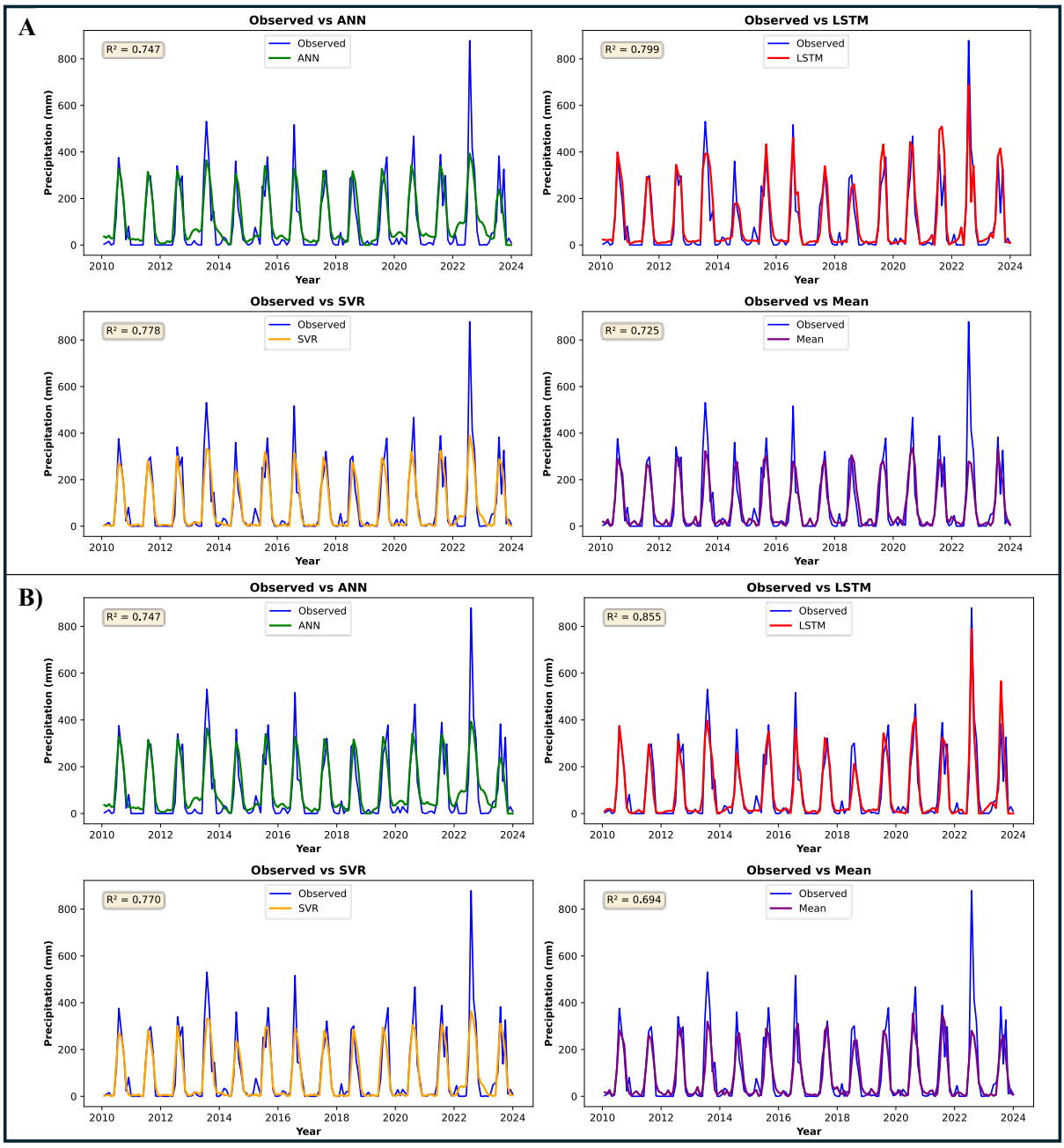

Figure 27 SSP-245 Precipitation - Model performance comparison of L-5

In Figure 28 A) TMAX, the R^2 value for MME-mean was 0.89. When machine learning was applied, results got better, with all the ML techniques outperforming it. However, there were some differences among the models: compared to the observed data, the ANN model underestimated lower peaks, while both LSTM and SVR overestimated the lower peaks, which may introduce errors in future predictions of this data. In Figure 28 B) TMAX, the R^2 value for MME-mean was 0.86. When machine learning was applied, results got better, with all the ML techniques outperforming it. However, there were some differences among the models: compared to the observed data, the ANN model underestimated lower peaks, while both LSTM

and SVR overestimated the lower peaks, which may introduce errors in future predictions of this data.

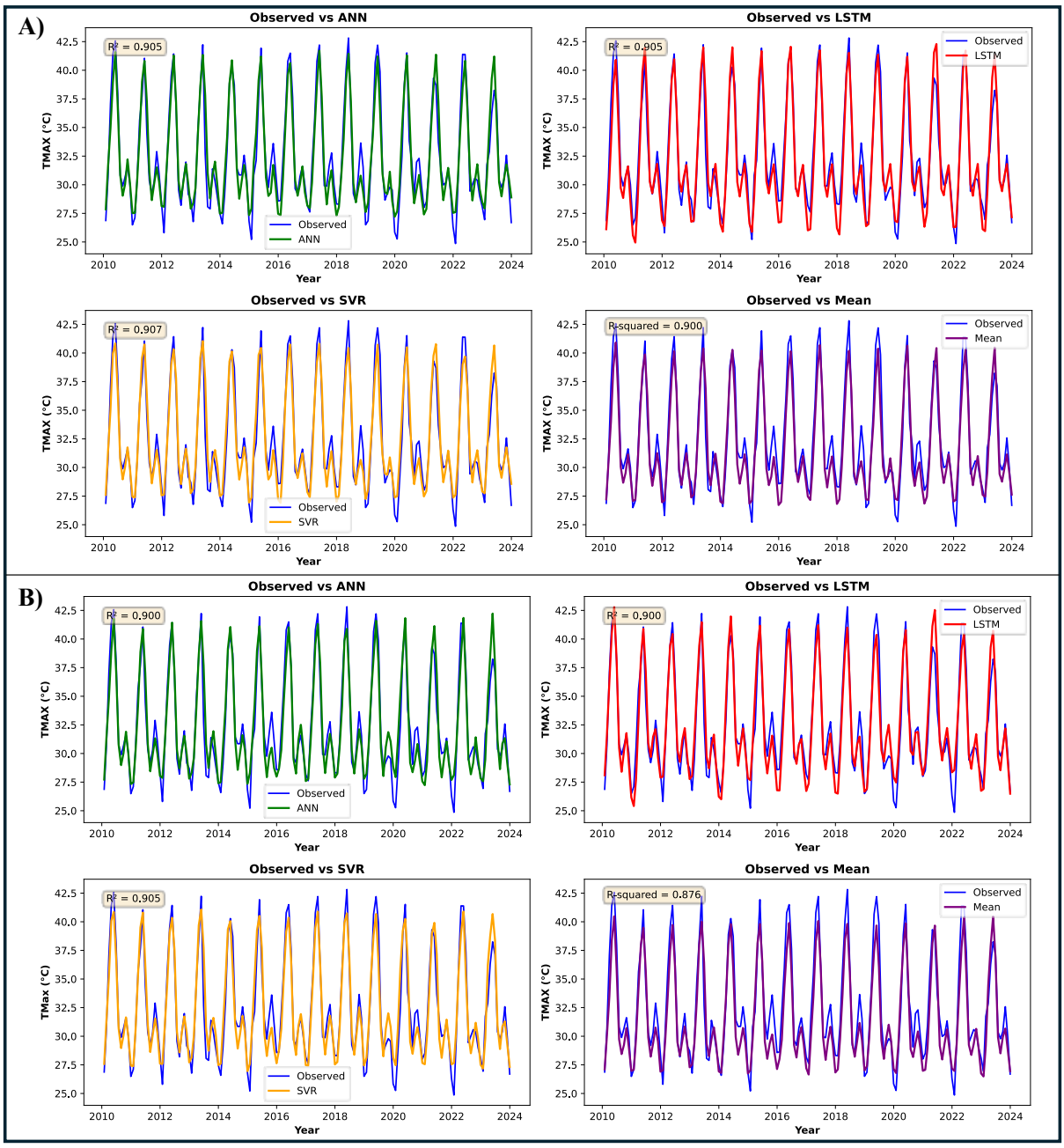

Figure 28 SSP-245 & 585 TMAX- Model performance comparison of L-5

In Figure 29 A) TMIN, the R^2 value of the MME-mean is 0.93. With the application of ML, the results were improved, and all the ML techniques have shown better results with all the techniques. In the case of ANN, lower peaks are covered compared to observed data, while in the case of LSTM and SVR, the lower peaks were overestimated, which may generate some error in future prediction of these data. In figure 29 B) TMIN, the R^2 value of MME-mean is 0.90. With the application of ML, the results were improved, and all the ML techniques have

shown better results with all the techniques. In the case of ANN, lower peaks are covered compared to observed data, while in the case of LSTM and SVR, the lower peaks were overestimated, which may generate some error in future prediction of these data.

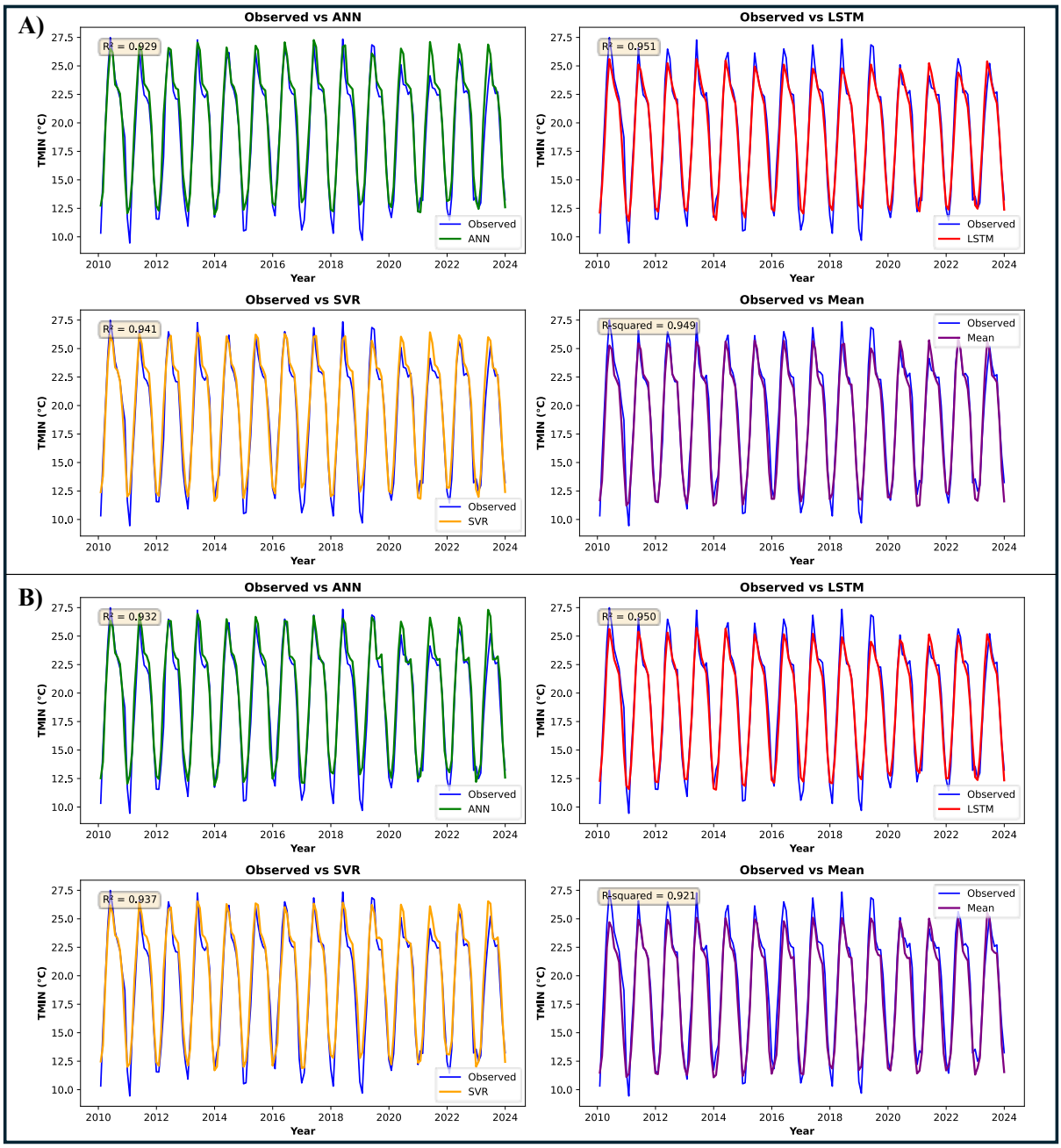

Figure 29 SSP-245 & 585 TMIN- Model performance comparison of L-5

Location 6

A stretch of 10 km of this highway falls in Gujarat NH-48, between Himatnagar and Vadodara. It passes through an industrial zone and intersects with major state highways. This region experiences an annual rainfall of 749 mm, with temperatures varying from 40°C to 14°C. From Table 8, For PCP under SSP 245 Scenario, LSTM emerged as the clear leader with superior performance (RMSE: 61.10, R^2: 0.79), demonstrating a 22% improvement in RMSE over the Mean method. Other machine learning models (ANN, SVR) showed limited improvement over the baseline Mean approach. Under the SSP 585 Scenario, LSTM maintained its advantage (RMSE: 71.27, R^2: 0.71), and the performance gap narrowed compared to SSP 245. Notably, ANN and SVR failed to significantly outperform the Mean method, suggesting challenges in modeling precipitation under extreme climate conditions. For TMAX, both scenarios showed remarkable consistency in model performance rankings. ANN achieved the best balance of accuracy (RMSE: 1.16/1.21) and reliability (KGE: 0.93/0.94) across scenarios, though LSTM and SVR showed competitive RMSE values. The Mean method's performance degraded more noticeably under SSP 585 (14% RMSE increase vs SSP 245), highlighting increased modeling challenges under extreme scenarios. For TMIN, ANN demonstrated exceptional performance with the lowest RMSE (0.82/0.83) and highest R^2 (0.97) in both scenarios, along with outstanding KGE values (0.98). LSTM surprisingly underperformed in TMIN prediction (KGE: 0.87/0.88), suggesting potential limitations in modeling minimum temperature dynamics despite its strong precipitation performance. It has been observed that ANN excelled in temperature prediction while LSTM dominates precipitation forecasting, suggesting different model architectures may be optimal for different climate variables. Performance degradation under SSP 585 was most pronounced for PCP prediction (LSTM's RMSE increased by 16.7%), indicating precipitation modeling becomes more challenging under extreme scenarios. ANN showed remarkable consistency across temperature predictions, maintaining high KGE values (0.93-0.98) in all scenarios. The Mean method's competitive performance in temperature prediction (particularly TMIN) suggests simpler approaches may sometimes suffice for certain climate variables.

.

Table 8 SSP-245 Results Model performance comparison of L-6

L6 Location	PCP					TMAX				TMIN			
	Method	RMSE	R^2	MAE	KGE	RMSE	R^2	MAE	KGE	RMSE	R^2	MAE	KGE
SSP 245	Mean	78.50	0.65	39.32	0.72	1.17	0.90	0.98	0.89	1.20	0.94	0.99	0.95
	LSTM	61.10	0.79	34.33	0.82	1.14	0.91	0.92	0.89	1.28	0.93	1.07	0.87
	ANN	77.63	0.65	45.32	0.71	1.16	0.90	0.94	0.93	0.82	0.97	0.60	0.98
	SVR	78.09	0.65	37.41	0.65	1.14	0.91	0.92	0.87	0.86	0.97	0.64	0.93
SSP 585	Mean	82.88	0.60	41.05	0.67	1.39	0.86	1.14	0.88	1.61	0.90	1.38	0.93
	ANN	77.62	0.65	45.27	0.71	1.21	0.90	0.97	0.94	0.83	0.97	0.65	0.98
	LSTM	71.27	0.71	33.68	0.72	1.23	0.89	1.00	0.88	1.30	0.93	1.11	0.88
	SVR	77.89	0.65	37.44	0.66	1.16	0.90	0.93	0.88	0.87	0.97	0.66	0.93

Figure 30 A) shows the result of precipitation of SSP-245. The panel, that is, represents results for MME-Mean having an R^2 value of 0.65. Amongst three different machine learning models, the LSTM performed better, followed by the ANN and SVR, correspondingly. The results of LSTM represent more peaks and patterns than ANN and SVR, which have done a very good job of representing a general trend. Figure 30 B) shows the result of precipitation of SSP-585. a) represents results for MME-Mean having an R^2 value of 0.60. Amongst three different machine learning models, the LSTM performs better, followed by the ANN and SVR, respectively. The results of LSTM represent more peaks and patterns than ANN and SVR, which have done a very good job of representing a general trend.

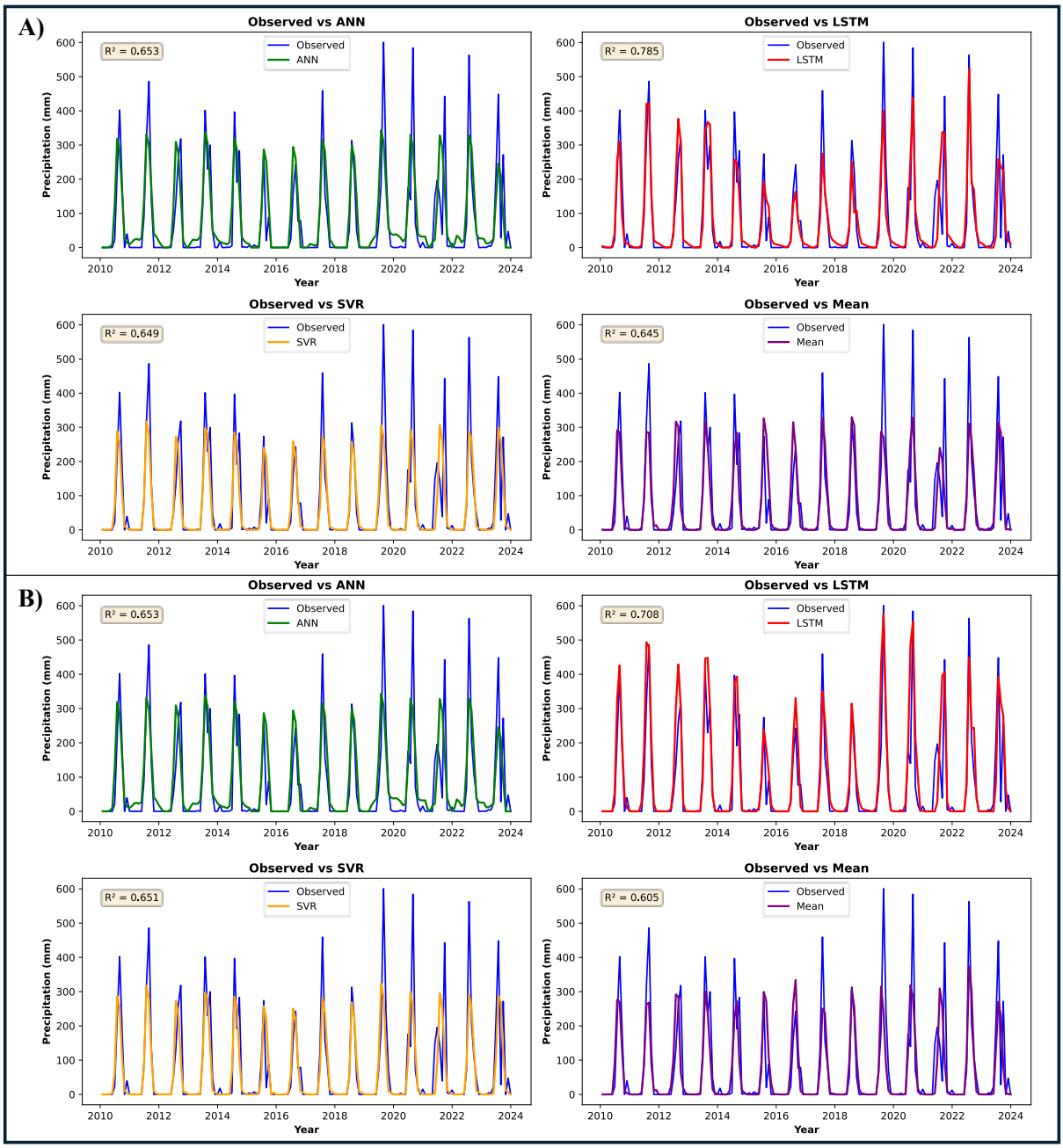

Figure 30 SSP-245 Precipitation- Model performance comparison of L-6

Figure 31 A) shows that in TMAX, the R^2 value for MME-mean was 0.89. When machine learning was applied, results got better, with all the ML techniques outperforming it. However, there were some differences among the models: compared to the observed data, the ANN model underestimated lower peaks, while both LSTM and SVR overestimated the lower peaks, which may introduce errors in future predictions of this data. In Figure 31 B) TMAX, the R^2 value for MME-mean was 0.84. When machine learning was applied, results got better, with all the ML techniques outperforming it. However, there were some differences among the models: compared to the observed data, the ANN model underestimated lower peaks, while both LSTM

and SVR overestimated the lower peaks, which may introduce errors in future predictions of this data.

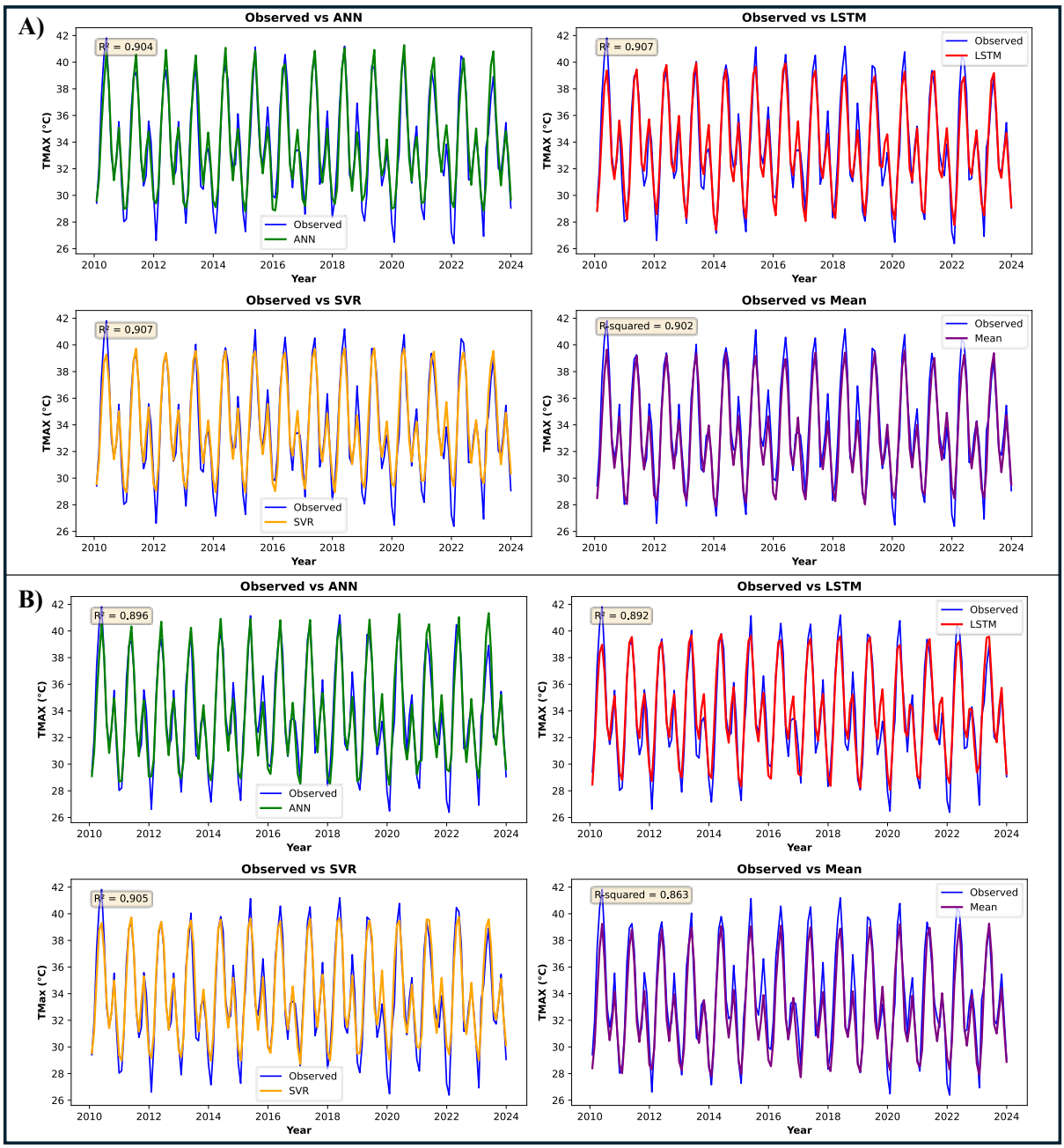

Figure 31 SSP-245 & 585 TMAX- Model performance comparison of L-6

In Figure 32 A) TMIN, the R^2 value of the MME-mean is 0.92. With the application of ML, the results were improved, and all the ML techniques have shown better results with all the techniques. In the case of ANN, lower peaks are covered compared to observed data, while in the case of LSTM and SVR, the lower peaks were overestimated, which may generate some error in future prediction of these data. In figure 32 B) TMIN, the R^2 value of MME-mean is 0.92. With the application of ML, the results were improved, and all the ML techniques have

shown better results with all the techniques. In the case of ANN, lower peaks are covered compared to observed data, while in the case of LSTM and SVR, the lower peaks were overestimated, which may generate some error in future prediction of these data.

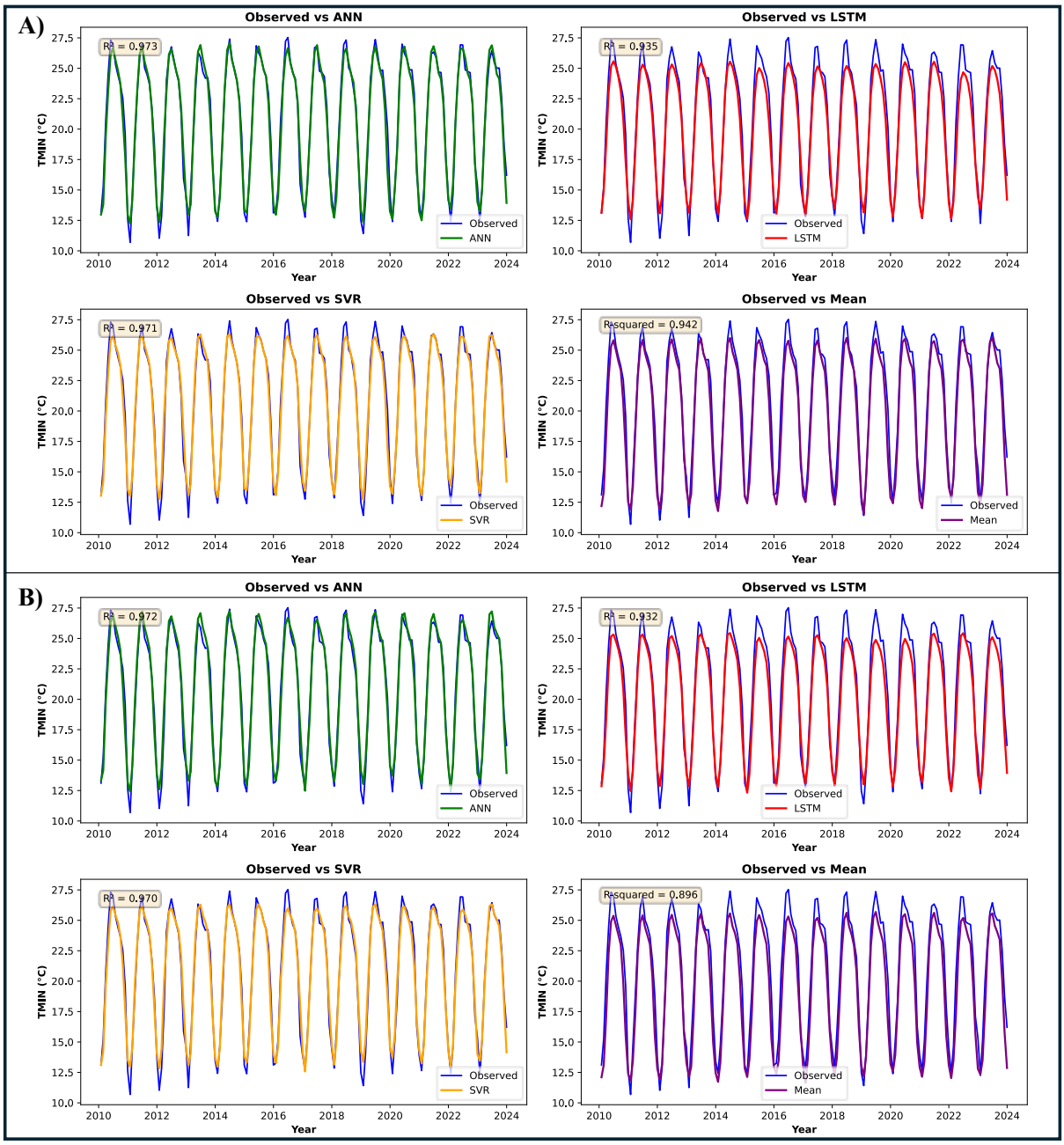

Figure 32 SSP-245 & 585 TMIN -Model performance comparison of L-6

Location 7

A stretch of 10 km of this highway falls in Maharashtra NH-48_C, between Lonavala and Khandala. a popular tourist destination in Maharashtra. Known for its waterfalls and scenic viewpoints, the area has been severely affected by flooding in recent years, receiving an average annual rainfall of 4223 mm, with temperatures ranging from 34°C to 11°C. From Table 9, for PCP under the SSP 245 Scenario, LSTM emerged as the clear leader with superior performance (RMSE: 61.10, R^2: 0.79), demonstrating a 22% improvement in RMSE over the Mean method. Other machine learning models (ANN, SVR) showed limited improvement over the baseline Mean approach. Under the SSP 585 Scenario, LSTM maintained its advantage (RMSE: 71.27, R^2: 0.71), and the performance gap narrowed compared to SSP 245. Notably, ANN and SVR failed to significantly outperform the Mean method, suggesting challenges in modeling precipitation under extreme climate conditions. For TMAX, both scenarios showed remarkable consistency in model performance rankings. ANN achieved the best balance of accuracy (RMSE: 1.16/1.21) and reliability (KGE: 0.93/0.94) across scenarios, though LSTM and SVR showed competitive RMSE values. The Mean method's performance degraded more noticeably under SSP 585 (14% RMSE increase vs SSP 245), highlighting increased modeling challenges under extreme scenarios. For TMIN, ANN demonstrated exceptional performance with the lowest RMSE (0.82/0.83) and highest R^2 (0.97) in both scenarios, along with outstanding KGE values (0.98). LSTM surprisingly underperformed in TMIN prediction (KGE: 0.87/0.88), suggesting potential limitations in modeling minimum temperature dynamics despite its strong precipitation performance. It has been observed that ANN excelled in temperature prediction while LSTM dominates precipitation forecasting, suggesting different model architectures may be optimal for different climate variables. Performance degradation under SSP 585 was most pronounced for PCP prediction (LSTM's RMSE increased by 16.7%), indicating precipitation modeling becomes more challenging under extreme scenarios. ANN showed remarkable consistency across temperature predictions, maintaining high KGE values (0.93-0.98) in all scenarios. The Mean method's competitive performance in temperature prediction (particularly TMIN) suggests simpler approaches may sometimes suffice for certain climate variables.

Table 9 SSP-245 & 585 Model performance comparison of L-7

L7 Location	PCP					TMAX				TMIN			
	Method	RMSE	R^2	MAE	KGE	RMSE	R^2	MAE	KGE	RMSE	R^2	MAE	KGE
SSP 245	Mean	167.13	0.76	89.26	0.71	1.12	0.83	0.89	0.85	0.97	0.90	0.75	0.94
	LSTM	126.17	0.86	70.49	0.87	0.99	0.87	0.81	0.91	0.82	0.93	0.62	0.95
	ANN	142.75	0.82	92.36	0.80	0.92	0.88	0.73	0.93	0.81	0.93	0.63	0.96
	SVR	135.11	0.84	72.89	0.78	0.92	0.88	0.73	0.86	0.82	0.93	0.65	0.93
SSP 585	Mean	178.19	0.73	93.60	0.67	1.42	0.72	1.16	0.79	1.23	0.83	0.99	0.92
	ANN	142.77	0.82	92.38	0.80	1.06	0.84	0.86	0.90	0.87	0.92	0.69	0.95
	LSTM	119.39	0.88	66.17	0.91	1.10	0.83	0.88	0.92	0.79	0.93	0.59	0.96
	SVR	136.83	0.84	73.77	0.78	0.99	0.86	0.80	0.86	0.84	0.92	0.68	0.92

Figure 33 A) shows the result of precipitation of SSP-245. The panel, that is, represents results for MME-Mean having an R^2 value of 0.77. Amongst three different machine learning models, the LSTM performed better, followed by the ANN and SVR, correspondingly. The results of LSTM represent more peaks and patterns than ANN and SVR, which have done a very good job of representing a general trend. Figure 33 B) shows the result of precipitation of SSP-585. a) represents results for MME-Mean having an R^2 value of 0.73. Amongst three different machine learning models, the LSTM was the best, followed by the ANN and SVR, correspondingly. The LSTM model's results represent more peaks and patterns than ANN and SVR, which have done a very good job of representing a general trend.

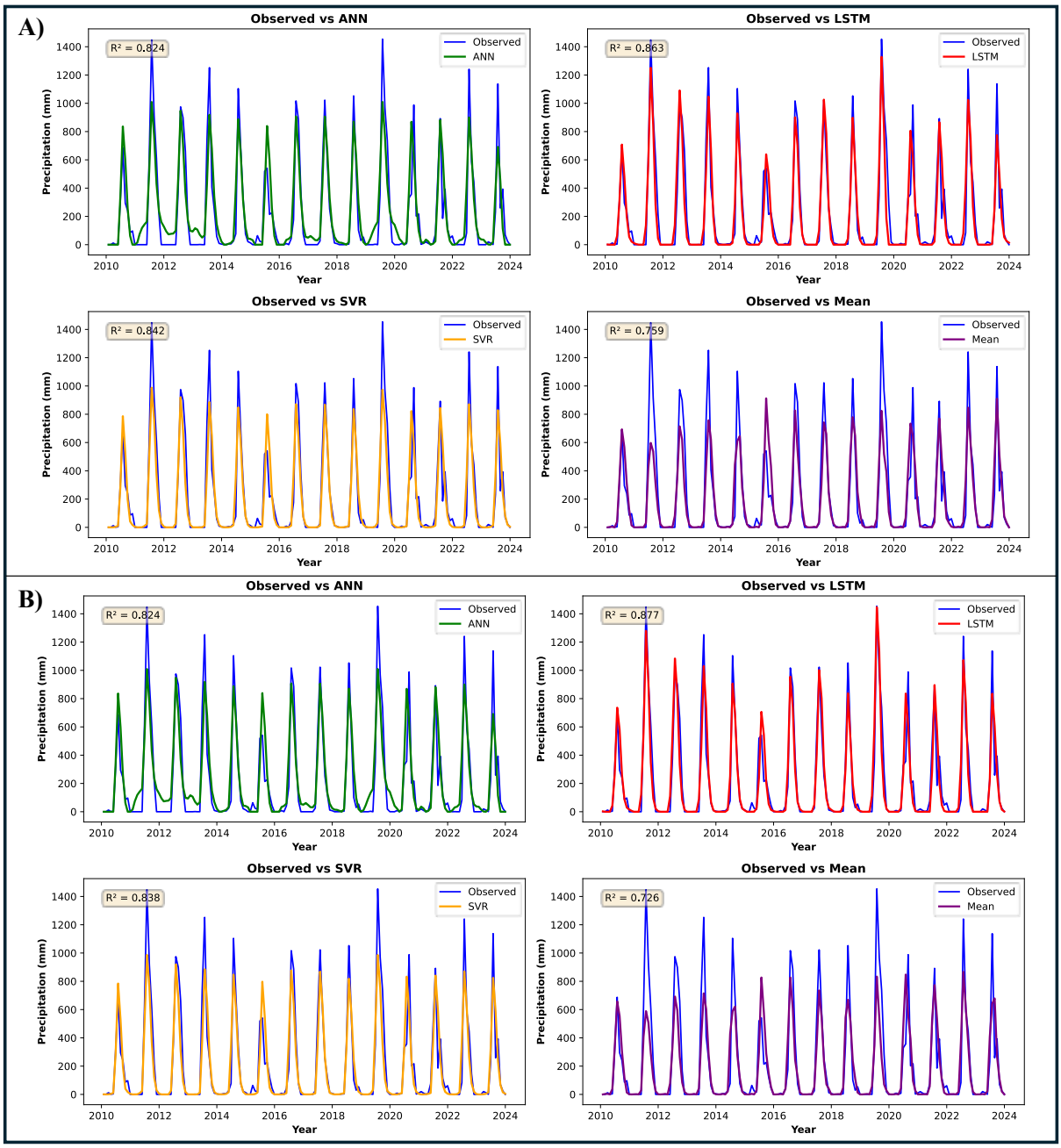

Figure 33 SSP-245 & 585 precipitation- Model performance comparison of L-7

In Figure 34 A) TMAX, the R^2 value for MME-mean was 0.83. When machine learning was applied, results got better, with all the ML techniques outperforming it. However, there were some differences among the models: compared to the observed data, the ANN model underestimated lower peaks, while both LSTM and SVR overestimated the lower peaks, which may introduce errors in future predictions of this data. In Figure 34 B) TMAX, the R^2 value for MME-mean was 0.71. When machine learning was applied, results got better, with all the ML techniques outperforming it. However, there were some differences among the models: compared to the observed data, the ANN model underestimated lower peaks, while both LSTM

and SVR overestimated the lower peaks, which may introduce errors in future predictions of this data.

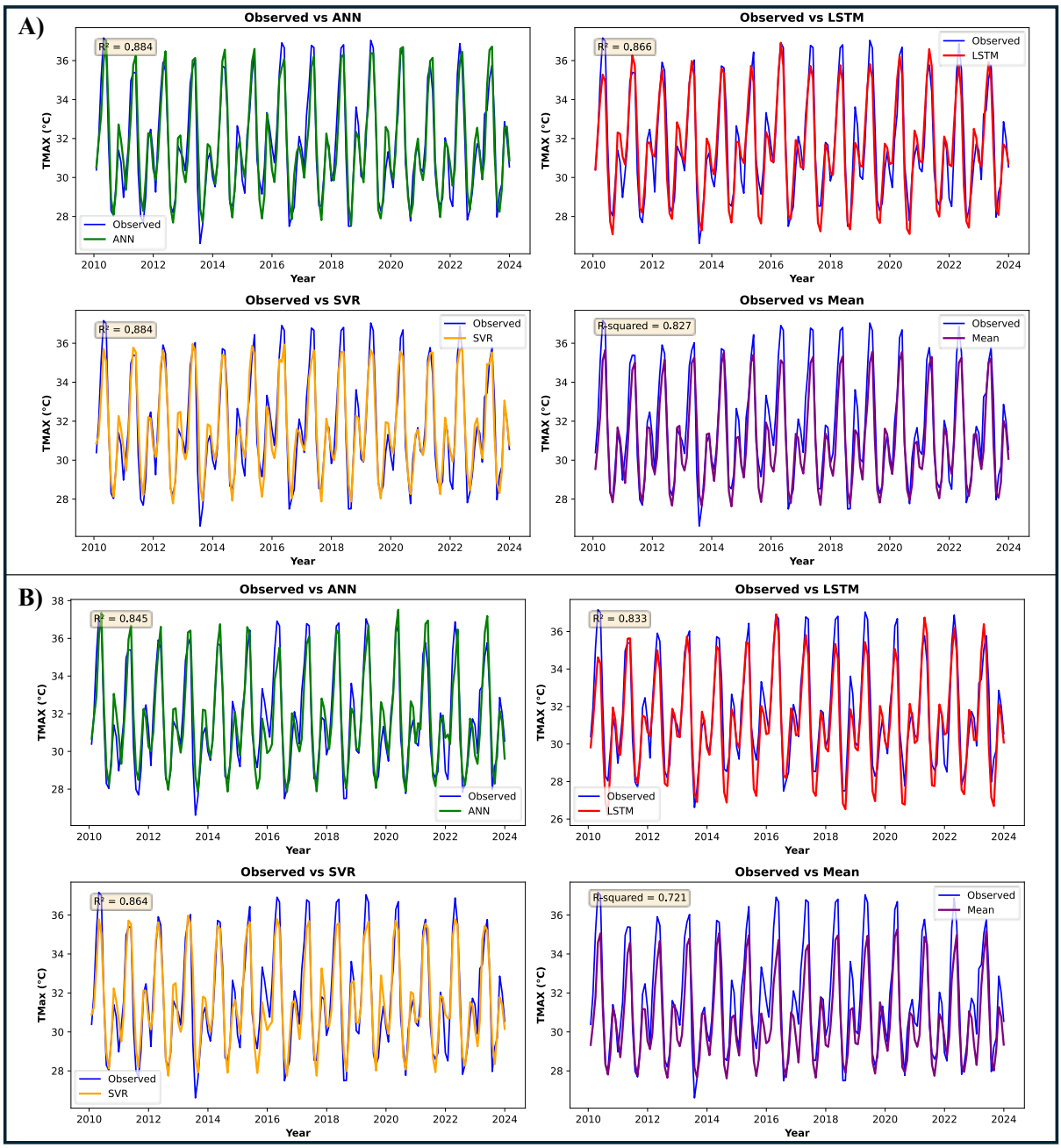

Figure 34 SSP-245 TMAX- Model performance comparison of L-7

In Figure 35 A) TMIN, the R^2 value of the MME-mean is 0.86. With the application of ML, the results were improved, and all the ML techniques have shown better results with all the techniques. In the case of ANN, lower peaks are covered compared to observed data, while in the case of LSTM and SVR, the lower peaks were overestimated, which may generate some error in future prediction of these data. In Figure 35 B), in the case of TMIN, the R^2 value of MME-mean is 0.78. With the application of ML, the results were improved, and all the ML

techniques have shown better results with all the techniques. In the case of ANN, lower peaks are covered compared to observed data, while in the case of LSTM and SVR, the lower peaks were overestimated, which may generate some error in future prediction of these data.

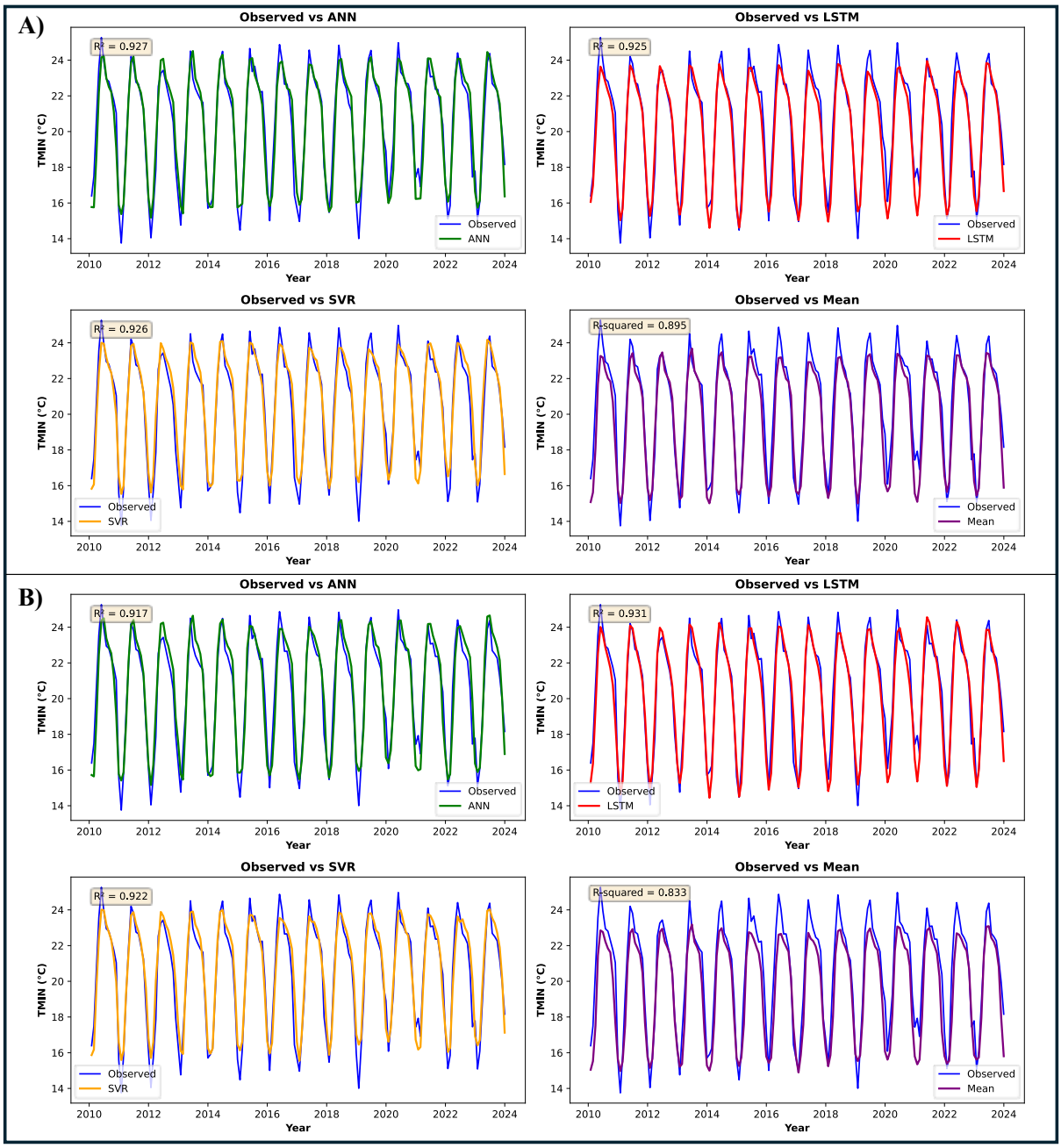

Figure 35 SSP-245 & 585 TMIN- Model performance comparison of L-7

Location 8

A stretch of 10 km of this highway falls in Madhya Pradesh, NH-52, between Dewas and Sendhwa, an area marked by both industrial and agricultural activities. The Narmada River, which flows through this region, contributes to its vulnerability to floods. The area sees an average rainfall of 833.6 mm and temperatures ranging between 44°C and 10°C. From Table 10, for PCP prediction, LSTM emerged as the superior model, achieving the lowest RMSE (52.30 in SSP 245; 50.22 in SSP 585) and highest R^2 (0.79-0.80), representing a 12-23% improvement over the Mean baseline. While SVR showed competitive PCP results with better MAE values (26.38 in SSP 245), its overall performance was slightly inferior to LSTM. Temperature predictions revealed different optimal models: ANN consistently delivered the best TMIN forecasts with the lowest RMSE (1.02 in SSP 245; 1.05 in SSP 585) and maintained high KGE values (0.97), while all machine learning methods performed comparably for TMAX prediction, with ANN showing a slight edge in KGE (0.91-0.92). The analysis highlights several key patterns: LSTM's clear advantage in precipitation prediction is maintained across scenarios, ANN's superior performance in minimum temperature forecasting, and the general consistency of machine learning methods for maximum temperature prediction. Notably, the Mean method was consistently outperformed, particularly for PCP under SSP 585, where LSTM achieved a 23% lower RMSE. These results suggest that optimal climate forecasting at Location L-8 would benefit from employing LSTM for precipitation and ANN for temperature predictions, with particular attention to scenario conditions, as model performance shows some variation between SSP 245 and SSP 585. The findings support the use of specialized models for different climate variables and highlight the value of machine-learning approaches over traditional baseline methods.

Table 10 SSP-245 Model performance comparison of L-8

L8 Location	PCP					TMAX				TMIN			
	Method	RMSE	R^2	MAE	KGE	RMSE	R^2	MAE	KGE	RMSE	R^2	MAE	KGE
SSP 245	Mean	60.00	0.72	30.85	0.73	1.32	0.91	1.09	0.89	1.12	0.95	0.84	0.97
	ANN	59.80	0.72	33.55	0.74	1.33	0.91	1.05	0.92	1.02	0.96	0.79	0.97
	LSTM	52.30	0.79	28.14	0.88	1.35	0.91	1.10	0.88	1.15	0.95	0.90	0.95
	SVR	54.71	0.76	26.38	0.76	1.35	0.91	1.06	0.90	1.05	0.96	0.85	0.96
SSP 585	Mean	64.88	0.67	31.98	0.68	1.49	0.89	1.24	0.88	1.46	0.92	1.13	0.94
	ANN	59.74	0.72	33.26	0.74	1.37	0.90	1.06	0.91	1.05	0.96	0.83	0.97
	LSTM	50.22	0.80	29.22	0.75	1.33	0.91	1.05	0.92	1.15	0.95	0.90	0.94
	SVR	55.35	0.76	26.96	0.76	1.36	0.91	1.07	0.90	1.09	0.95	0.87	0.96

Figure 36 A) shows the precipitation of SSP-585, which represents results for MME-Mean having an R^2 value of 0.71. Amongst three different machine learning models, the LSTM performed better, followed by the ANN and SVR, correspondingly. The results of LSTM represent more peaks and patterns than ANN and SVR, which have done a very good job of representing a general trend. Figure 36 B) shows the result of precipitation of SSP-585 representing results for MME-Mean having an R^2 value of 0.66. Amongst three different machine learning models, the LSTM was the best, followed by the ANN and SVR, correspondingly.

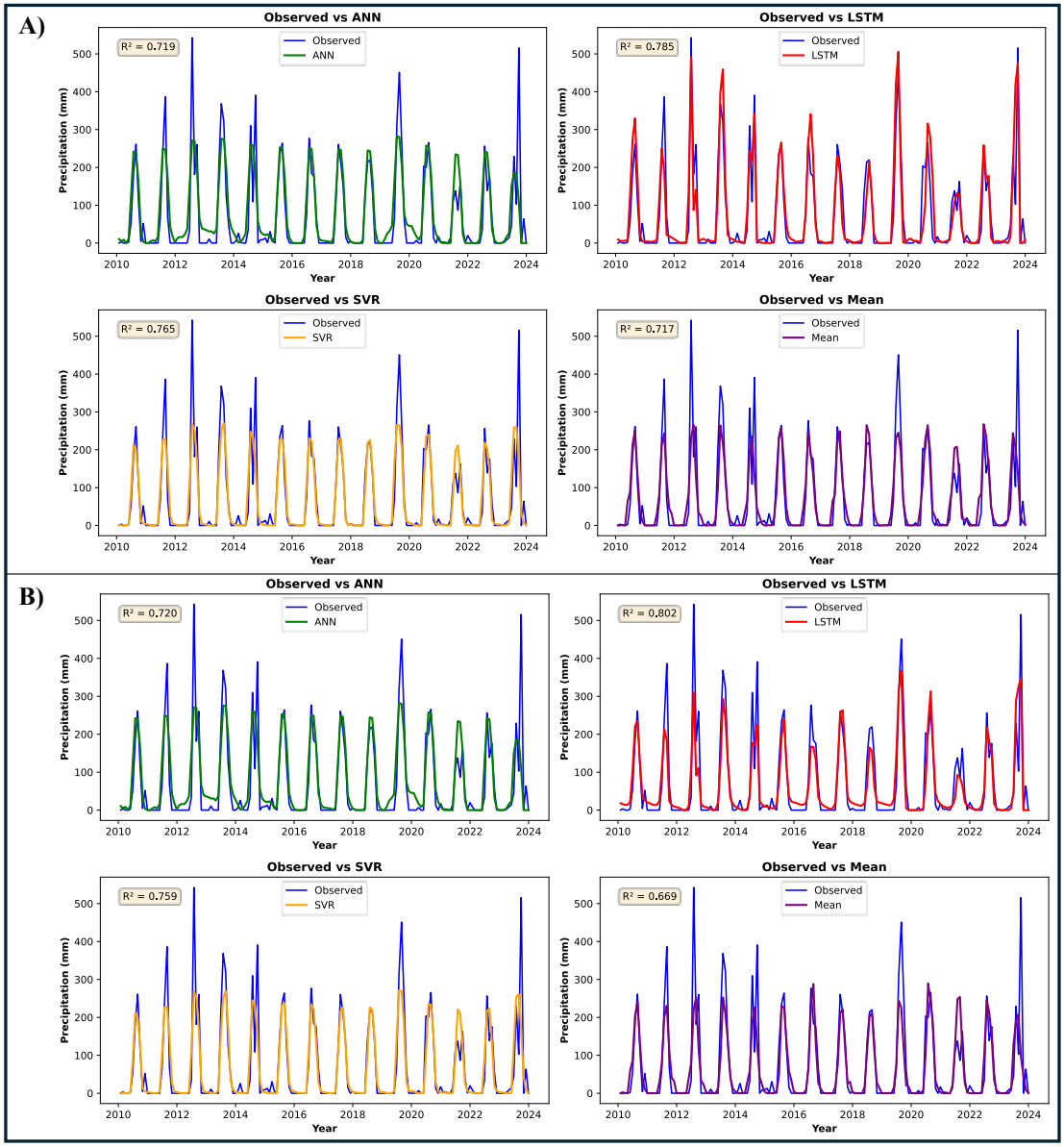

Figure 36 SSP-245 & 585 Precipitation- Model performance comparison of L-8

In Figure 37 A) TMAX, the R^2 value for MME-mean was 0.89. When machine learning was applied, results got better, with all the ML techniques outperforming it. However, there were some differences among the models: compared to the observed data, the ANN model underestimated lower peaks, while both LSTM and SVR overestimated the lower peaks, which may introduce errors in future predictions of this data. In figure 37 B) TMAX, the R^2 value for MME-mean was 0.87. When machine learning was applied, results got better, with all the ML techniques outperforming it. However, there were some differences among the models: compared to the observed data, the ANN model underestimated lower peaks, while both LSTM and SVR overestimated the lower peaks, which may introduce errors in future predictions of this data.

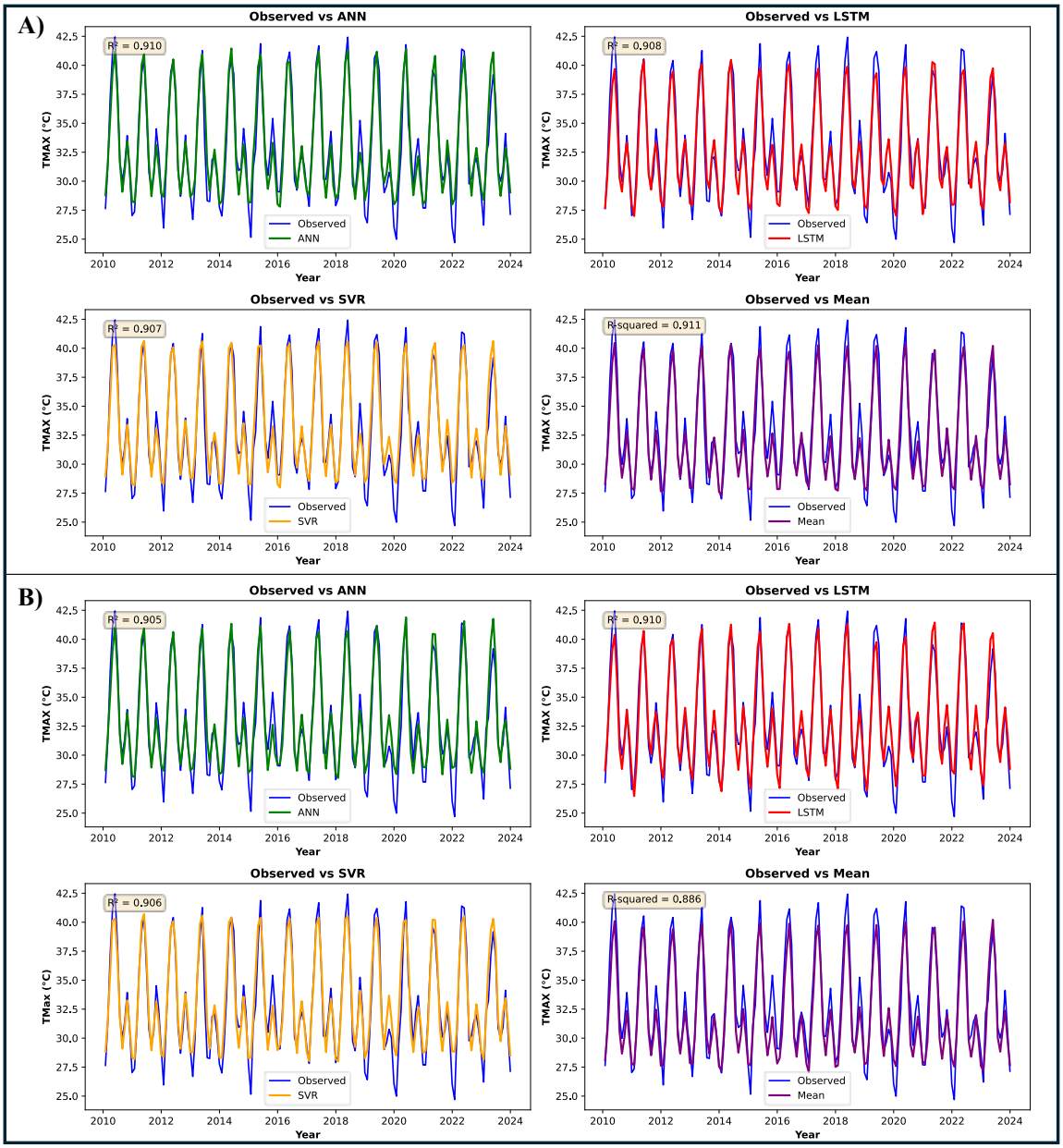

Figure 37 SSP-245 & 585 TMAX- Model performance comparison of L-8

In Figure 38 A) TMIN, the R^2 value of the MME-mean is 0.89. With the application of ML, the results were improved, and all the ML techniques have shown better results with all the techniques. In the case of ANN, lower peaks are covered compared to observed data, while in the case of LSTM and SVR, the lower peaks were overestimated, which may generate some error in future prediction of these data. In Figure 38 B) TMIN, the R^2 value of the MME-mean is 0.89. With the application of ML, the results were improved, and all the ML techniques have shown better results with all the techniques. In the case of ANN, lower peaks are covered compared to observed data, while in the case of LSTM and SVR, the lower peaks were overestimated, which may generate some error in future prediction of these data.

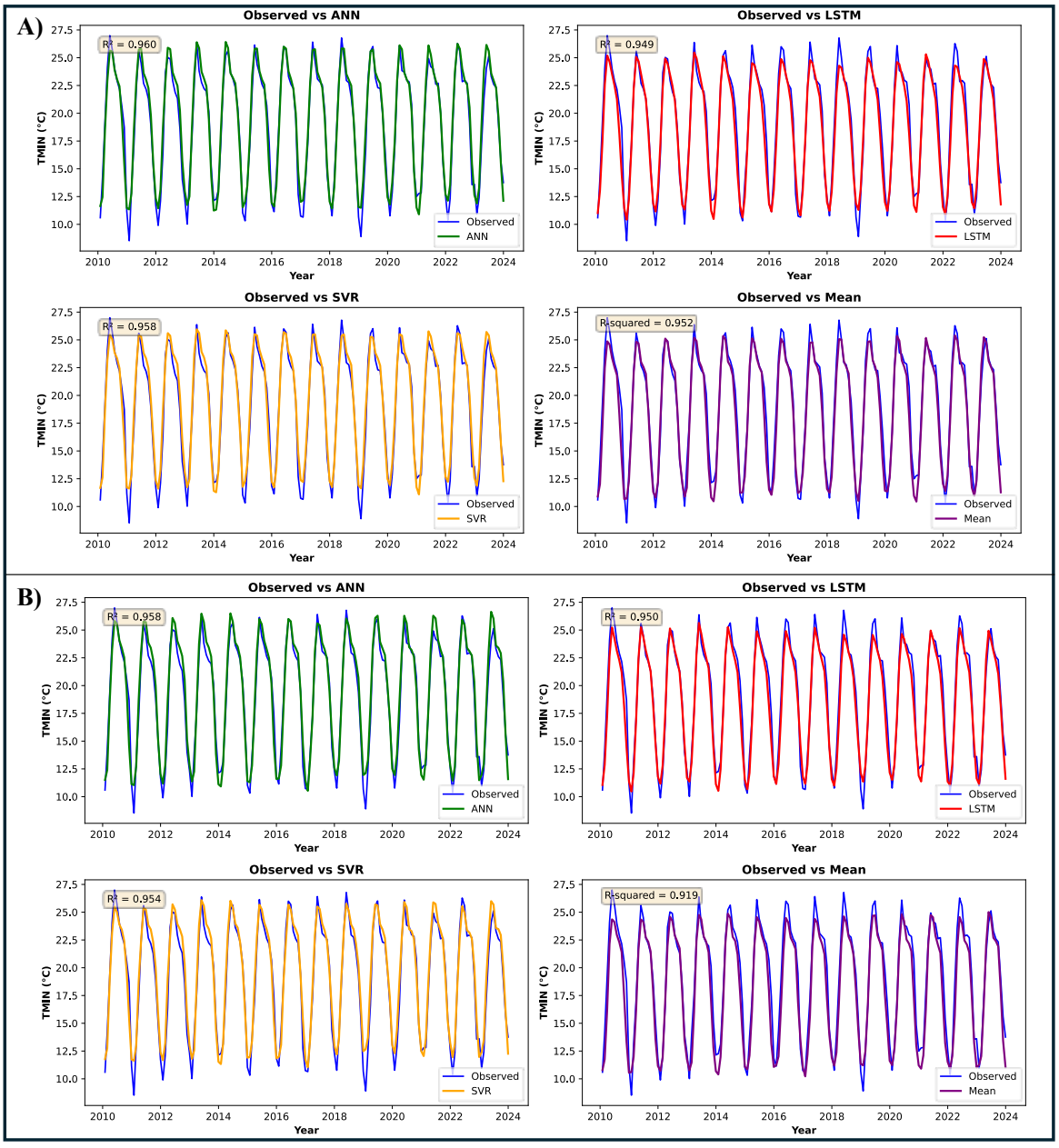

Figure 38 SSP-245 & 585 TMIN- Model performance comparison of L-8

Location 9

A stretch of 10 km of this highway falls in Gujarat NH-64, between Ahmedabad and Nadiad. It runs through a dense urban area. The region's rainfall averages 749 mm annually, and temperatures range from 40°C to 14°C. From Table 11, for PCP forecasting, LSTM demonstrates clear superiority, achieving an 18% lower RMSE (63.48-63.97) compared to the Mean baseline while maintaining robust performance under both SSP scenarios. Temperature predictions show different optimal models: ANN emerges as the best performer for both maximum (TMAX) and minimum (TMIN) temperatures, particularly excelling in TMIN prediction with exceptional consistency (RMSE: 0.83, KGE: 0.99). While SVR shows competitive results for TMAX, ANN's superior reliability in temperature forecasting is evident through its consistently high KGE values (0.93-0.95). The analysis highlights the limitations of the Mean method, which consistently underperforms across all variables, particularly in extreme scenarios (SSP 585). These findings suggest that optimal climate forecasting at Location L-9 requires a tailored approach, employing LSTM for precipitation and ANN for temperature predictions. The results underscore the importance of variable-specific model selection and demonstrate the value of machine learning approaches in improving climate prediction accuracy, especially under changing climate conditions. Future research could explore hybrid modeling approaches to enhance predictive performance across all climate variables further.

Table 11 SSP-245 & 585 Model performance comparison of L-9

L9 Location	PCP					TMAX				TMIN			
	Method	RMSE	R^2	MAE	KGE	RMSE	R^2	MAE	KGE	RMSE	R^2	MAE	KGE
SSP 245	Mean	77.30	0.63	38.37	0.68	1.19	0.90	1.00	0.89	1.19	0.95	0.98	0.95
	LSTM	63.48	0.75	36.28	0.79	1.17	0.91	0.94	0.86	1.15	0.95	0.96	0.93
	ANN	74.47	0.66	44.64	0.68	1.13	0.91	0.93	0.95	0.83	0.97	0.61	0.95
	SVR	74.36	0.66	35.52	0.62	1.13	0.91	0.91	0.88	0.84	0.97	0.64	0.94
SSP 585	Mean	81.49	0.59	39.91	0.63	1.41	0.87	1.17	0.89	1.61	0.90	1.39	0.93
	ANN	74.46	0.66	44.64	0.68	1.18	0.91	0.95	0.93	0.83	0.97	0.65	0.99
	LSTM	63.97	0.75	31.31	0.86	1.18	0.91	0.96	0.89	1.17	0.95	0.93	0.96
	SVR	74.99	0.65	35.83	0.63	1.14	0.91	0.92	0.88	0.86	0.97	0.66	0.93

Figure 39 A) shows the result of precipitation of SSP-245. a) represents results for MME-Mean having an R^2 value of 0.63. Amongst three different machine learning models, the LSTM

performed better, followed by the ANN and SVR, correspondingly. The results of LSTM represent more peaks and patterns than ANN and SVR, which have done a very good job of representing a general trend. Figure 39 B) shows the result of precipitation of SSP-585. a) represents results for MME-Mean having an R^2 value of 0.59. Amongst three different machine learning models, the LSTM was the best, followed by the ANN and SVR, correspondingly. The LSTM model's results represent more peaks and patterns than ANN and SVR, which have done a very good job of representing a general trend.

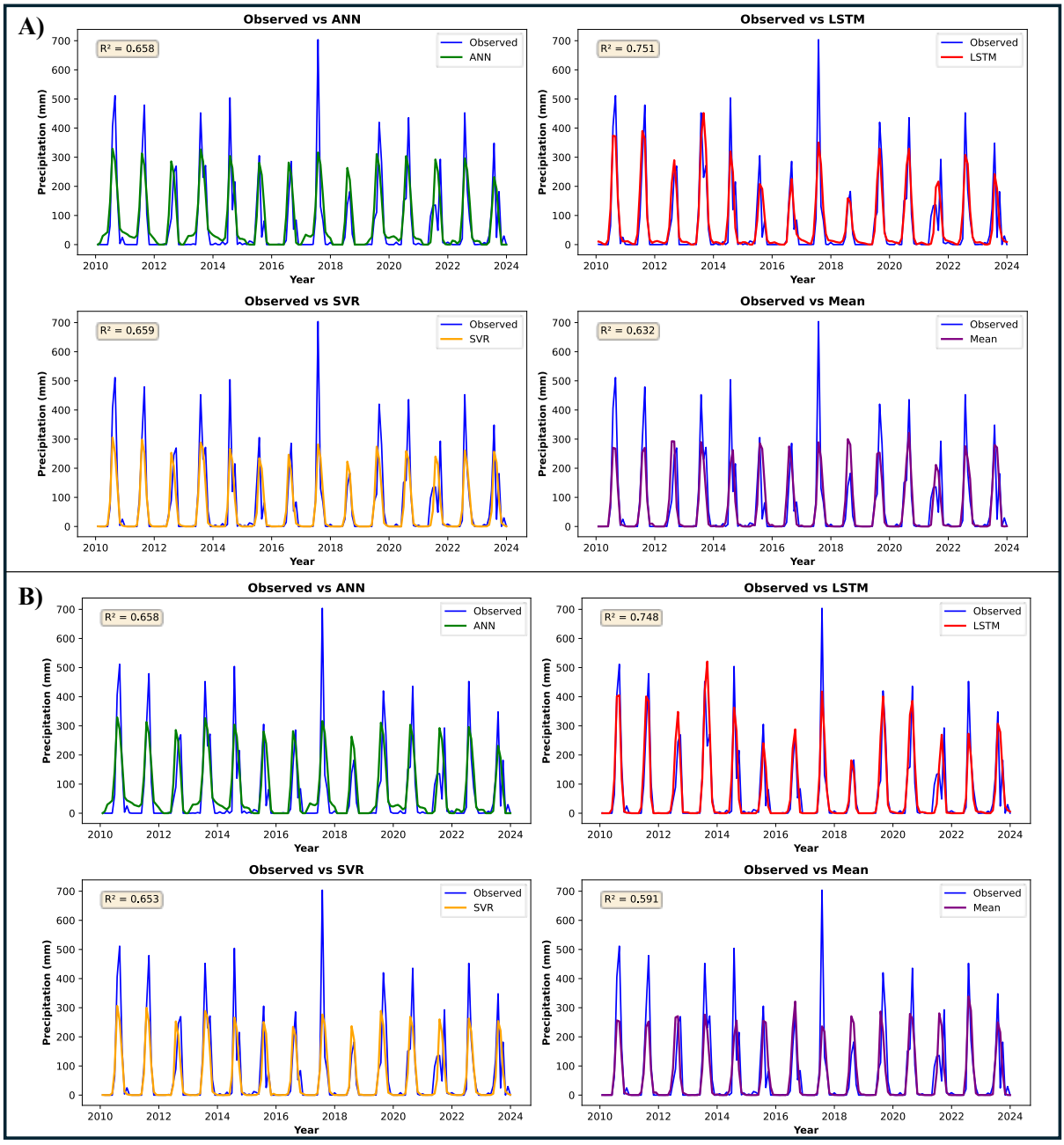

Figure 39 SSP-245 Precipitation- Model performance comparison of L-9

In Figure 40 A), TMAX, the R^2 value for MME-mean was 0.89. When machine learning was applied, results got better, with all the ML techniques outperforming it. However, there were some differences among the models: compared to the observed data, the ANN model underestimated lower peaks, while both LSTM and SVR overestimated the lower peaks, which may introduce errors in future predictions of this data. Figure 40 B), the R^2 value for MME-mean was 0.85. When machine learning was applied, results got better, with all the ML techniques outperforming it. However, there were some differences among the models: compared to the observed data, the ANN model underestimated lower peaks, while both LSTM and SVR overestimated the lower peaks, which may introduce errors in future predictions of this data.

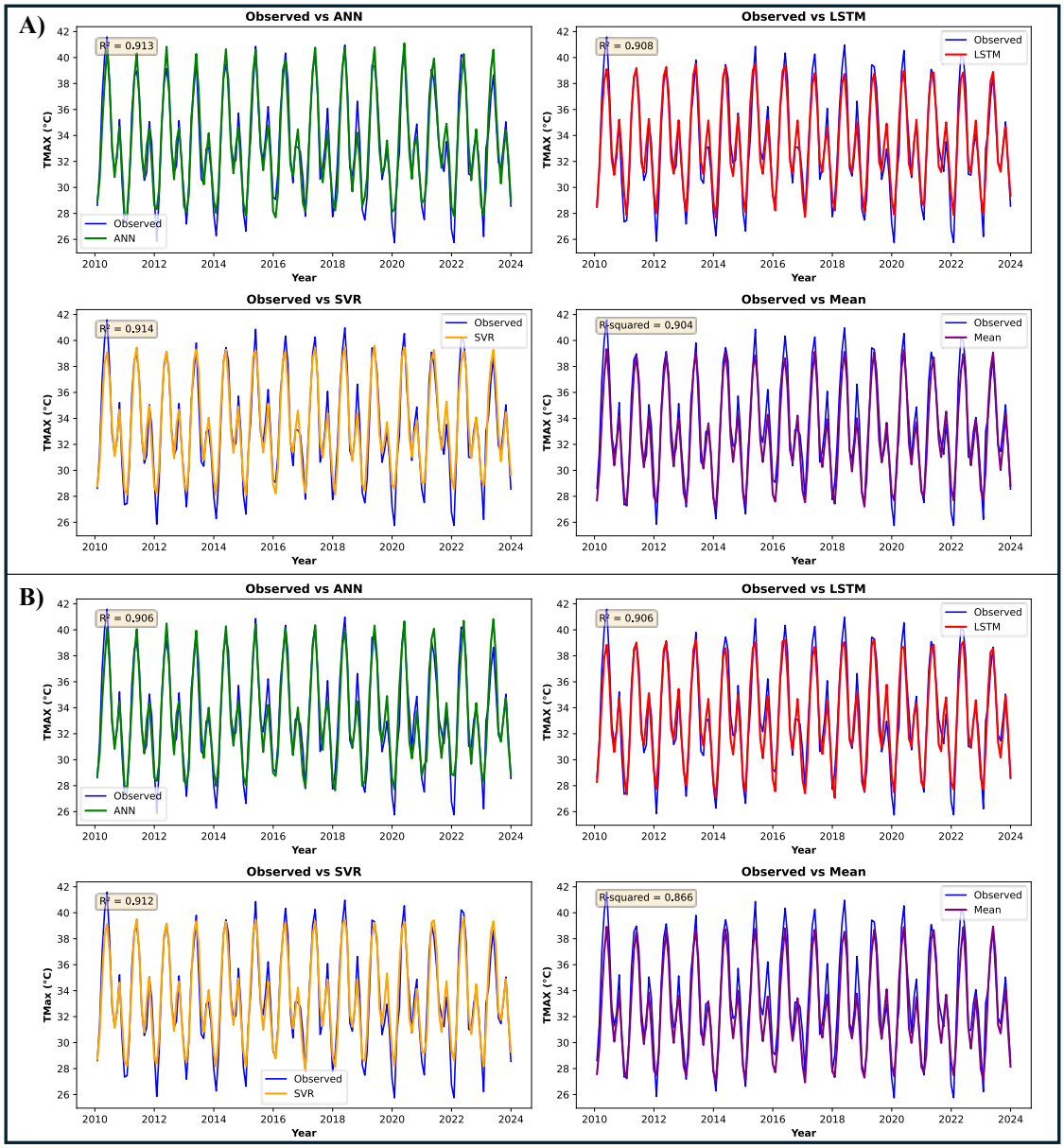

Figure 40 SSP-245 TMAX - Model performance comparison of L-9

In Figure 41 A) TMIN, the R^2 value of the MME-mean is 0.92. With the application of ML, the results were improved, and all the ML techniques have shown better results with all the techniques. In the case of ANN, lower peaks are covered compared to observed data, while in the case of LSTM and SVR, the lower peaks were overestimated, which may generate some error in future prediction of these data. In Figure 41 B) TMIN, the R^2 value of the MME-mean is 0.87. With the application of ML, the results were improved, and all the ML techniques have shown better results with all the techniques. In the case of ANN, lower peaks are covered compared to observed data, while in the case of LSTM and SVR, the lower peaks were overestimated, which may generate some error in future prediction of these data.

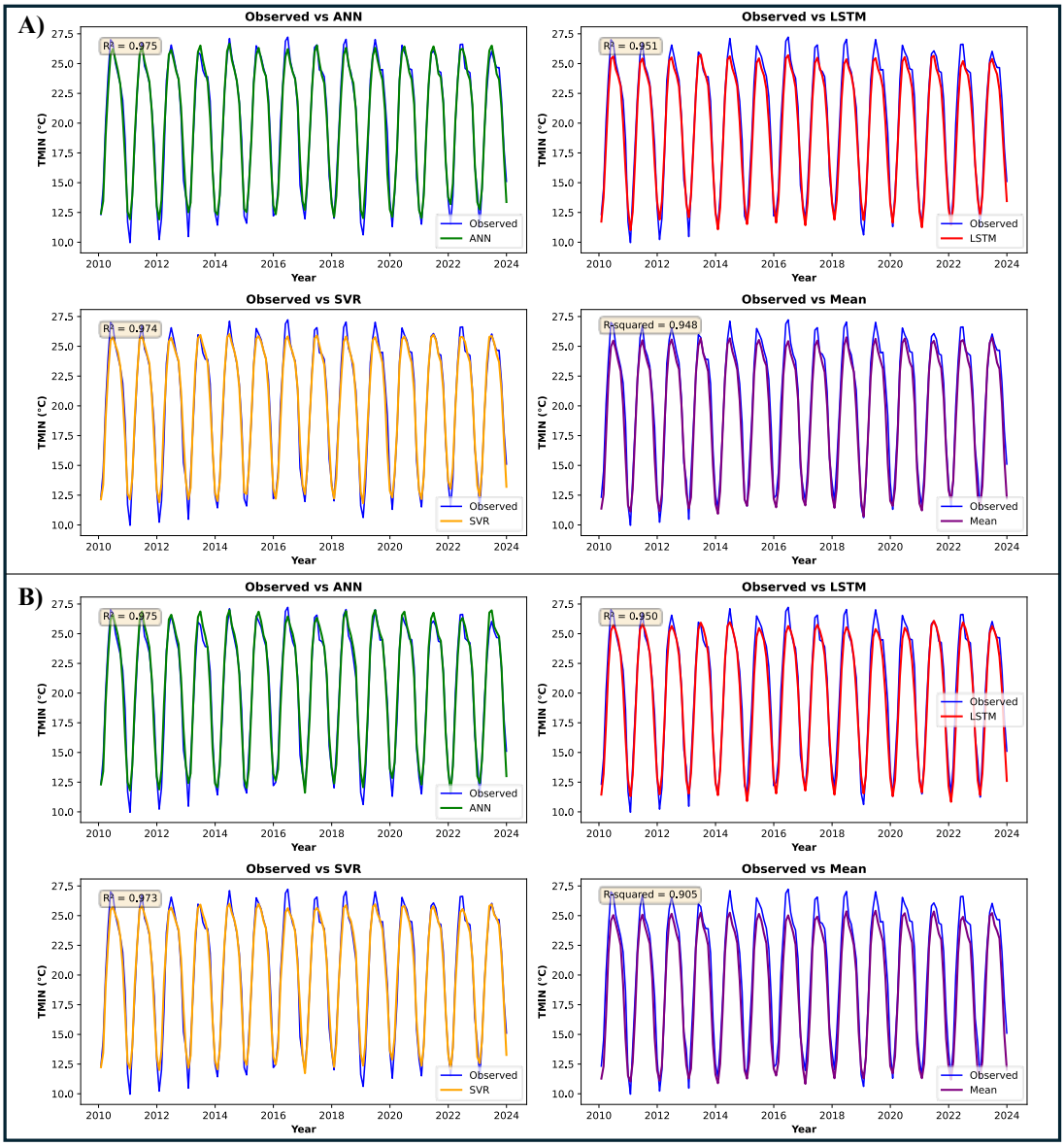

Figure 41 SSP-245 & 585 TMIN- Model performance comparison of L-9

Location 10

A stretch of 10 km of this highway falls in Tamil Nadu NH-87, between Ramanathapuram to Mandapam. It runs close to the coastline, making it particularly vulnerable to both floods and cyclones. The region receives an annual rainfall of 821 mm, with temperatures ranging between 40°C and 21°C. From Table 11 for PCP, the LSTM model outperformed other methods in both SSP scenarios, achieving the lowest RMSE (71.16 in SSP 245; 71.72 in SSP 585) and highest KGE (0.74 in SSP 245; 0.76 in SSP 585), indicating better accuracy and reliability. The Mean method consistently performed the worst, with higher errors and lower R^2 values. In TMAX predictions, SVR and ANN showed strong performance, particularly under SSP 585, where SVR achieved the highest R^2 (0.87) and lowest MAE (0.60). However, LSTM also performed well in SSP 245, with a high KGE of 0.94. The Mean method again had the highest errors, especially in SSP 585 (RMSE = 1.40). For TMIN, LSTM demonstrated the best results in both scenarios, with the lowest RMSE (0.45 in SSP 245; 0.47 in SSP 585) and highest KGE (0.97 in SSP 245; 0.95 in SSP 585). ANN and SVR also performed well but were slightly less accurate than LSTM. The Mean method had the weakest performance, particularly in SSP 585 (R^2 = 0.66). Overall, machine learning models (LSTM, ANN, SVR) significantly improved prediction accuracy over the Mean baseline, with LSTM excelling in PCP and TMIN, while SVR and ANN were competitive in TMAX.

Table 12 SSP-245 Model performance comparison of L-10

	PCP					TMAX				TMIN			
L10 Location	**Method**	**RMSE**	R^2	**MAE**	**KGE**	**RMSE**	R^2	**MAE**	**KGE**	**RMSE**	R^2	**MAE**	**KGE**
SSP 245	Mean	78.90	0.46	53.50	0.55	1.19	0.70	0.97	0.85	0.76	0.79	0.64	0.92
	LSTM	71.16	0.56	49.33	0.74	1.04	0.77	0.84	0.94	0.45	0.92	0.34	0.97
	ANN	73.49	0.53	56.51	0.61	0.91	0.82	0.73	0.90	0.55	0.89	0.45	0.91
	SVR	73.36	0.53	47.86	0.61	0.82	0.85	0.64	0.89	0.55	0.89	0.42	0.92
SSP 585	Mean	80.17	0.44	52.86	0.48	1.40	0.58	1.20	0.80	0.97	0.66	0.88	0.88
	ANN	73.49	0.53	56.51	0.61	0.78	0.87	0.61	0.93	0.49	0.91	0.38	0.89
	LSTM	71.72	0.55	51.92	0.76	1.04	0.77	0.84	0.94	0.47	0.92	0.34	0.95
	SVR	72.47	0.54	47.55	0.62	0.79	0.87	0.60	0.90	0.51	0.90	0.38	0.93

Figure 42 A) shows the precipitation of the SSP 245 Panel, which represents the results for MME-Mean with an R^2 value of 0.46. Among three different machine learning models, the LSTM performed better, followed by the ANN and SVR, respectively. The results of LSTM represent more peaks and patterns than ANN and SVR, which have done a very good job of

representing a general trend. Figure 42 B) shows the result of precipitation of SSP585, representing results for MME-Mean, having an R^2 value of 0.44. Among three different machine learning models, the LSTM performed better, followed by the ANN and SVR, respectively. The results of LSTM represent more peaks and patterns than ANN and SVR, which have done a very good job of representing a general trend.

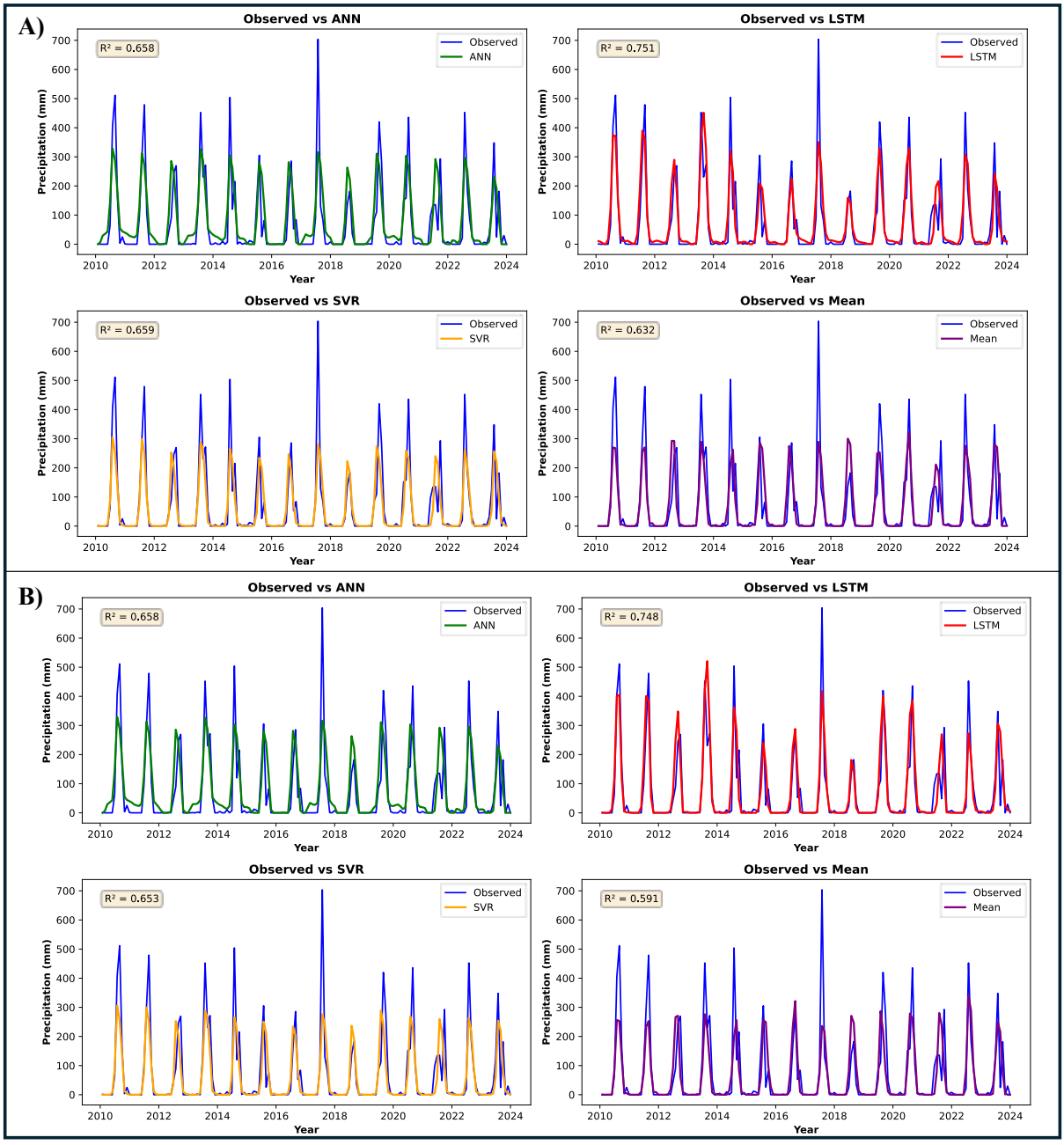

Figure 42 SSP-245 & 585 Precipitation- Model performance comparison of L-10

In Figure 43 A) TMAX, the R^2 value for MME-mean was 0.73. When machine learning was applied, results got better, with all the ML techniques outperforming it. However, there were some differences among the models: compared to the observed data, the ANN model

underestimated lower peaks, while both LSTM and SVR overestimated the lower peaks, which may introduce errors in future predictions of this data. Figure 43 B) TMAX, the R^2 value for MME-mean was 0.60. When machine learning was applied, results got better, with all the ML techniques outperforming it. However, there were some differences among the models: compared to the observed data, the ANN model underestimated lower peaks, while both LSTM and SVR overestimated the lower peaks, which may introduce errors in future predictions of this data.

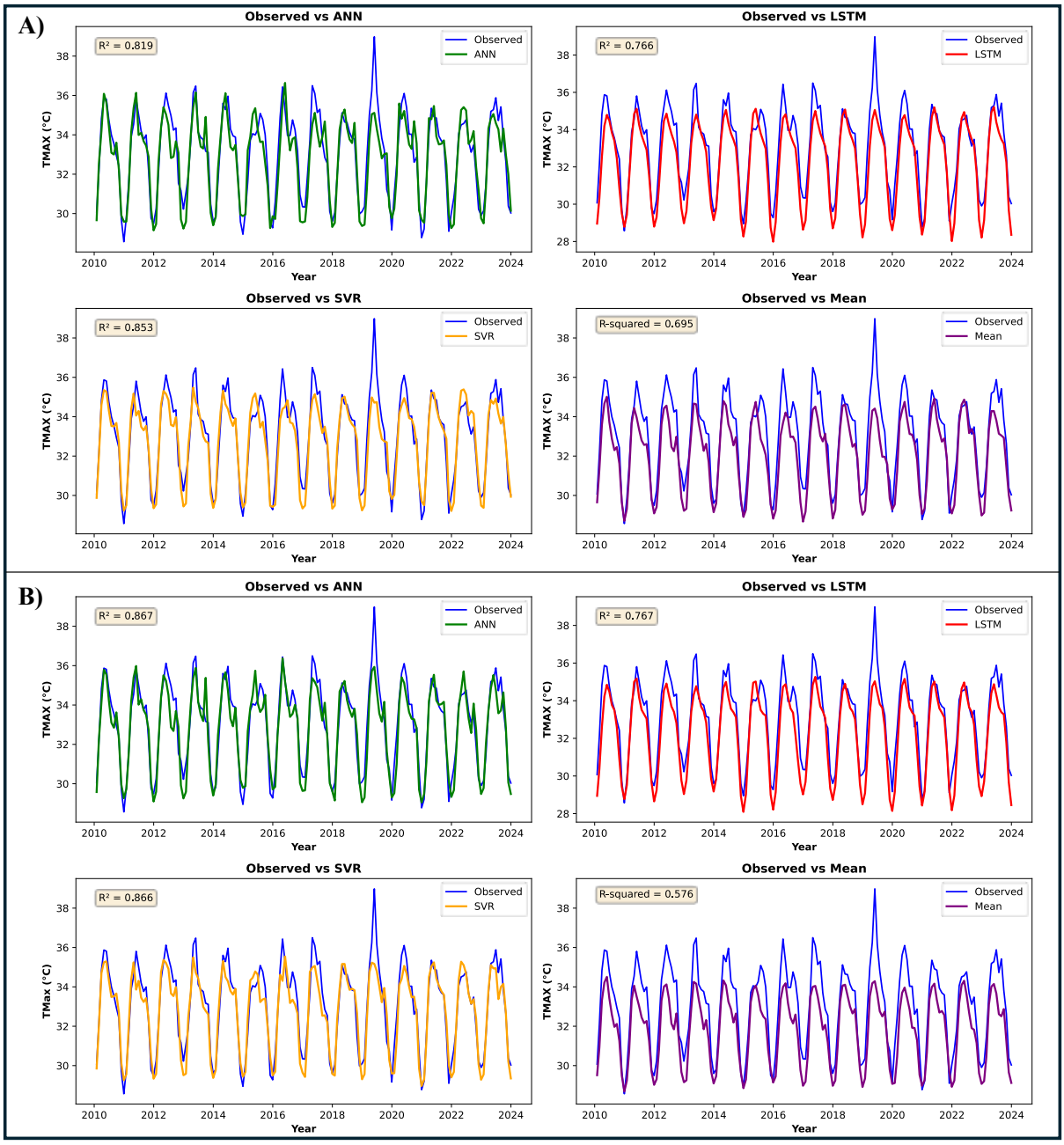

Figure 43 SSP-245 & 585 TMAX- Model performance comparison of L-10

In Figure 44 A) TMIN, the R^2 value of the MME-mean is 0.71. With the application of ML, the results were improved, and all the ML techniques have shown better results with all the techniques. In the case of ANN, lower peaks are covered compared to observed data, while in the case of LSTM and SVR, the lower peaks were overestimated, which may generate some error in future prediction of these data. In Figure 44 B) TMIN, the R^2 value of the MME-mean is 0.54. With the application of ML, the results were improved, and all the ML techniques have shown better results with all the techniques. In the case of ANN, lower peaks are covered compared to observed data, while in the case of LSTM and SVR, the lower peaks were overestimated, which may generate some error in future prediction of these data.

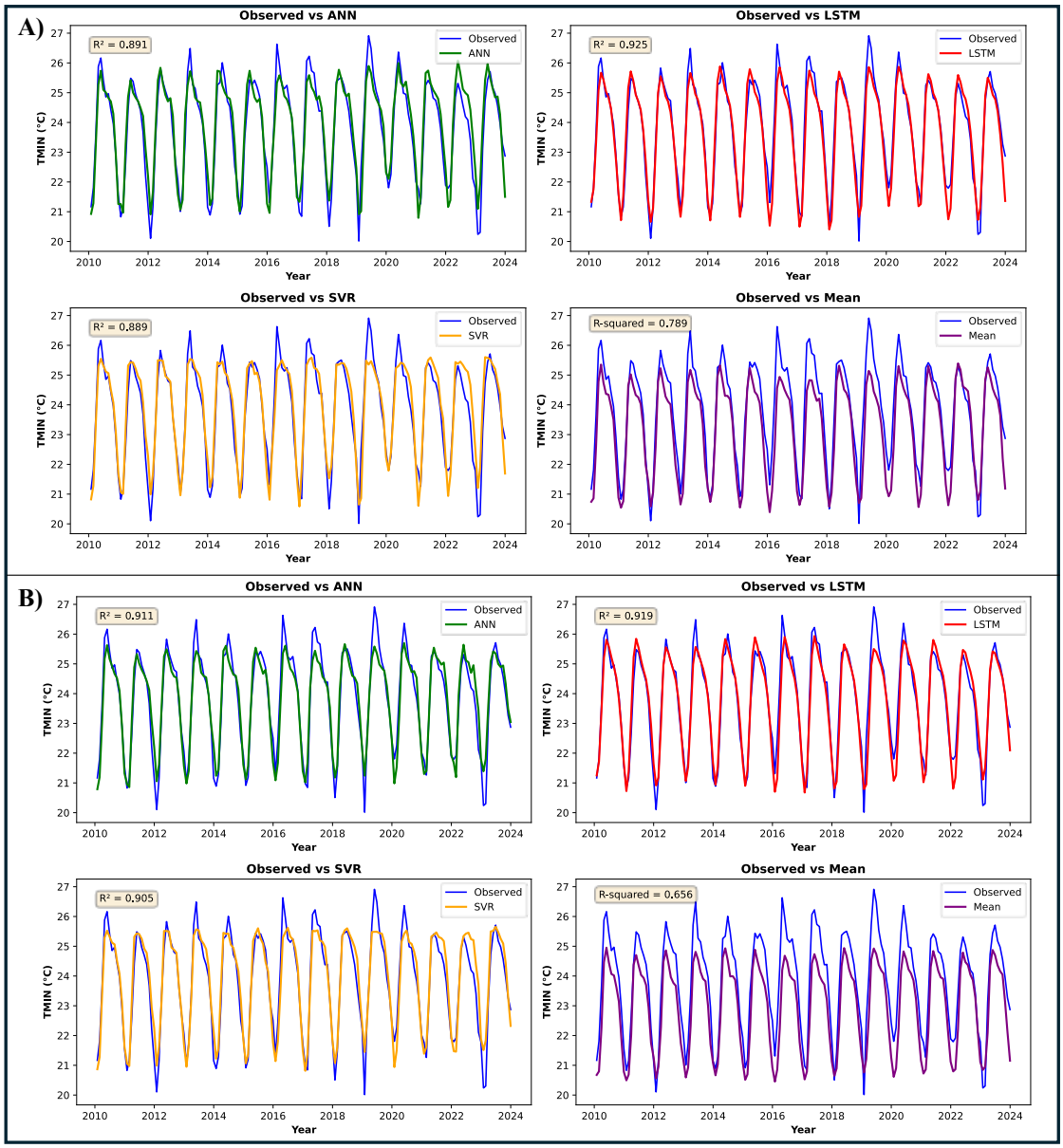

Figure 44 SSP-245 & 585 TMIN- Model performance comparison of L-10

4.1 Trend Analysis

The trend analysis of CMIP6 multi-model ensembles using machine learning (ML) techniques revealed significant variations in model performance across different scenarios (SSP245 and SSP585) and geographical locations. Table 13 and Table 14 show that the means of GCMs consistently exhibited strong, statistically significant increasing trends ($p < 0.05$) in all regions, with particularly steep Sen's slope values under SSP585 (e.g., L7: +10.55 units/year). It suggests that conventional MME provides a robust, consensus-based projection of warming trends, reinforcing its reliability in climate change assessments. In contrast, ML-based ensembles (ANN, LSTM, SVR) displayed greater variability in trend detection. LSTM demonstrated the most divergent behavior, with sharp increasing trends in some regions (e.g., L2 SSP585: Zc = 3.95, slope = +3.75) but significant decreasing trends in others (e.g., L7 SSP585: Zc = -10.03, slope = -5.08). This inconsistency suggests that while LSTM captures complex temporal dependencies, its projections may be highly sensitive to regional climate dynamics. ANN, meanwhile, produced more moderate but spatially consistent trends, particularly under SSP585 (e.g., L5 SSP585: slope = +0.056, $p < 0.001$), indicating better stability compared to LSTM. SVR performed least reliably, with mostly non-significant trends (e.g., L8 SSP245: p = 0.36) except in a few cases (e.g., L8 SSP585: Zc = 5.27, p = 1.40E-07), while various machine learning models demonstrate unique strengths in climate trend analysis, each exhibits notable limitations in long-term climate trend detection. The Multi-Model Ensemble (MME) stands out as the most reliable for large-scale, consensus-based projections, offering robust and widely accepted trends. However, LSTM models, though successful in capturing extreme trends, suffer from high variability, making them unsuitable for standalone use in policy-relevant assessments. Artificial Neural Networks (ANN) present a balanced compromise, delivering moderate yet more stable trends compared to LSTM, though they may lack the precision required for detailed long-term projections. Conversely, Support Vector Regression (SVR) underperforms in climate trend detection, indicating limited potential for refining ensemble models.

Table 13 Trend Analysis of SSP 245 for different models at all 10 locations

Location	Model	Near future			Far future		
		Corrected Zc	new P-value	Sen's slope	Corrected Zc	new P-value	Sen's slope
L1	ANN	0.8376	0.4023	0.0745	0.8188	0.4129	0.0127
	LSTM	0.5500	0.5823	2.8192	-0.6023	0.5470	-1.6622
	Mean	0.7767	0.4373	1.1205	2.0697	0.0385	0.7487
	SVR	-0.8376	0.4023	-0.5597	1.5726	0.1158	0.2046
L2	ANN	1.1902	0.2340	0.0866	0.6357	0.5250	0.0169
	LSTM	-0.8376	0.4023	-1.9796	-1.7733	0.0762	-1.4446
	Mean	1.5870	0.1125	2.4252	2.4091	0.0160	1.4968
	SVR	-1.4157	0.1569	-0.5537	1.1618	0.2453	0.1733
L3	ANN	0.5731	0.5666	0.0178	0.6190	0.5359	0.0168
	LSTM	0.9698	0.3321	3.9872	2.5596	0.0105	3.9737
	Mean	0.0000	1.0000	-0.1052	9.5803	0.0000	1.8538
	SVR	-1.7736	0.0761	-0.5520	-0.5688	0.5695	-0.1081
L4	ANN	0.7053	0.4806	0.0368	0.0578	0.9539	0.0019
	LSTM	0.2204	0.8255	0.9114	1.0707	0.2843	2.7564
	Mean	-0.5731	0.5666	-1.6008	1.4118	0.1580	1.1809
	SVR	0.0882	0.9297	0.0331	-0.9536	0.3403	-0.1176
L5	ANN	2.2042	0.0275	0.0772	0.4852	0.6276	0.0159
	LSTM	-1.6739	0.0942	-4.6941	1.4103	0.1585	1.6563
	Mean	0.3046	0.7606	0.4478	2.1061	0.0352	1.5046
	SVR	1.0139	0.3106	0.5178	0.5521	0.5809	0.0277
L6	ANN	1.5429	0.1229	0.1151	0.3513	0.7253	0.0128
	LSTM	-0.3527	0.7243	-3.6543	-2.9420	0.0033	-2.5586
	Mean	0.6380	0.5235	1.5349	2.5095	0.0121	1.9683
	SVR	0.7122	0.4764	0.2678	-0.3011	0.7633	-0.0523
L7	ANN	0.2204	0.8255	0.0117	0.6190	0.5359	0.0144
	LSTM	-0.1322	0.8948	-0.1608	-1.0038	0.3155	-1.7446
	Mean	0.9257	0.3546	4.2946	1.3623	0.1731	1.6266
	SVR	-0.4408	0.6593	-0.3231	1.0874	0.2768	0.2608
L8	ANN	0.8817	0.3780	0.1250	0.9201	0.3575	0.0426
	LSTM	-0.0441	0.9648	-0.1020	0.1673	0.8671	0.1812
	Mean	0.3527	0.7243	0.2915	1.4722	0.1410	0.9652
	SVR	-0.9257	0.3546	-0.6663	-0.2596	0.7952	-0.0530
L9	ANN	1.4979	0.1342	0.1117	0.2844	0.7761	0.0092
	LSTM	-0.7053	0.4806	-3.0653	0.0340	0.9729	0.2637
	Mean	0.5273	0.5980	1.5482	2.3422	0.0192	1.7379
	SVR	0.2204	0.8255	0.0861	1.0425	0.2972	0.1807
L10	ANN	1.4988	0.1339	0.0166	3.9010	0.0001	0.0128
	LSTM	-0.1600	0.8729	-1.6714	-3.0857	0.0020	-2.2940
	Mean	0.3527	0.7243	0.6428	0.9834	0.3254	0.6444
	SVR	-1.1133	0.2656	-0.6818	2.4367	0.0148	0.4459

4.2 Entropy

In this study, entropy analysis is done based on the standardized variability Index, which Normalizes the variability index between 0 and 1, for which two indices, SVI_{AE} and SVI_{ME}, are used. The analysis of SVI_{AE} is done based on the Monthly and Seasonal scales, while SVI_{ME} is done on the Monthly, Seasonal, and Annual scales for both scenarios, i.e., SSP 245 and SSP 585, to understand the variability in the models used for ensembling of GCMs.

4.2.1 Monthly and Seasonal Variability under SSP 245 and SSP 585 based on SVI_{AE}

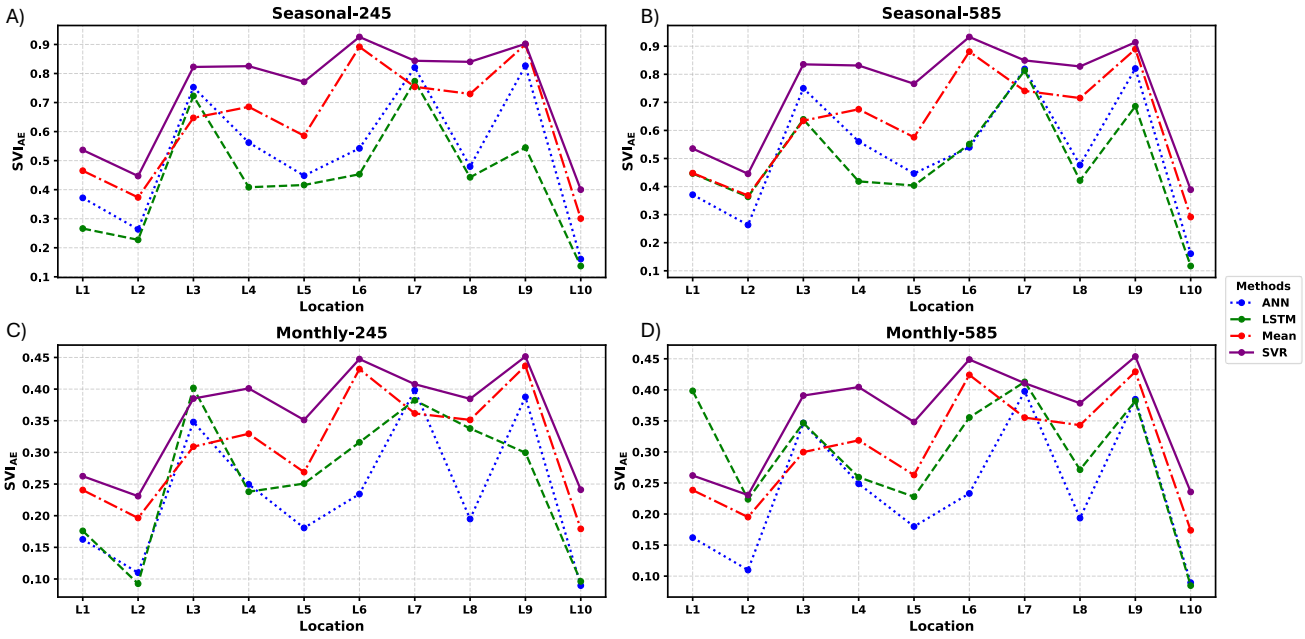

Figure 45 SVI_{AE} plots of Seasonal and Monthly analysis for SSP 245 and 585

The seasonal and monthly evaluation of SVI_{AE} across both scenarios reveals noticeable variability patterns among the models. From Figure 45 A) and B), SVR demonstrates the highest variability, followed closely by the mean of the GCM ensemble. In contrast, Figures 45 C) and D) show that both the ANN and LSTM exhibit significantly lower variability, which suggests that SVR and Mean of GCMs have predicted overpredicted values, which led to higher variability. The performance of machine learning (ML)-based ensemble techniques (ANN, LSTM, SVR) was evaluated against the traditional multi-model mean (MME) for seasonal and monthly CMIP6 projections under SSP245 and SSP585 scenarios. Overall, the results demonstrate distinct patterns in model performance across different temporal scales and emission scenarios. For SSP245, the SVR model consistently outperformed other methods, achieving the highest values across most locations (e.g., L6: 0.926, L4: 0.825). The MME ranked second in performance, particularly excelling in L6 (0.892) and L9 (0.900), while ANN

and LSTM showed intermediate results, with LSTM generally underperforming (e.g., L10: 0.137). Under SSP585, a similar trend emerged, with SVR maintaining dominance (e.g., L6: 0.933, L3: 0.835) and MME remaining competitive (L6: 0.881, L9: 0.889). Notably, LSTM exhibited slight improvements under SSP585 in some locations (e.g., L1: 0.447 vs. 0.266 in SSP245), though it still lagged behind SVR and MME. The MME demonstrated superior performance in monthly SSP245 projections for most locations (e.g., L6: 0.432, L9: 0.437), followed closely by SVR (L6: 0.447, L9: 0.451). ANN and LSTM displayed higher variability, with LSTM occasionally outperforming ANN (e.g., L3: 0.402 vs. 0.348) but remaining inconsistent (e.g., L8: 0.338 vs. 0.194 for ANN). Under SSP585, SVR again led in most cases (e.g., L6: 0.449, L3: 0.391), while MME retained strong performance (L6: 0.424, L9: 0.429). LSTM showed improved results in some regions (e.g., L1: 0.398 vs. 0.176 in SSP245), but its overall performance remained less stable compared to SVR and MME.

4.2.2 Inter-annual rainfall variability based on SVI_{ME} across different time-scales

To investigate the inter-annual rainfall variability over monthly, seasonal, and annual variation, which gives an understanding of the variability obtained out of the maximum variability possible that can be associated with the time-series data. The calculation of SVI_{ME} is based on the amount of rainfall for each location. Table 14 reveals an annual analysis of SVI_{ME} across 10 locations, demonstrating that LSTM and Mean exhibit a low value. At the same time, ANN and SVR showed very low values in the order of 10^{-6} to 10^{-8} under both scenarios, SSP 245 and SSP 585. Table 16 also revealed that the SVI_{ME} value at the annual scale is smaller under both scenarios. Mishra et al., 2009 revealed that the inter-annual variability will be larger at a smaller time scale and becomes smaller at a larger time scale.

Table 14 Annual analysis of SVI_{ME} for SSP 245 and 585

Scenario	245				585			
Location	**ANN**	**LSTM**	**SVR**	**Mean**	**ANN**	**LSTM**	**SVR**	**Mean**
L1	6.54757E-07	0.004084297	5.16E-05	0.00054	1.04E-06	0.00823	5.09E-05	0.0018331
L2	5.12415E-07	0.000719058	8.59E-05	0.00057	6.34E-07	0.001739	5.11E-05	0.0013519
L3	5.15443E-07	0.0018456	2.40E-05	0.00061	9.08E-07	0.003596	2.81E-05	0.0011505
L4	2.09585E-07	0.002008581	2.13E-05	0.00077	4.27E-07	0.001498	2.85E-05	0.0014204
L5	3.64125E-07	0.001368517	4.98E-05	0.0006	5.36E-07	0.001114	6.55E-05	0.0016597
L6	9.29437E-07	0.00712296	3.65E-05	0.00129	1.32E-06	0.003513	3.32E-05	0.0025927
L7	1.3261E-07	0.001100878	1.48E-05	0.00082	1.58E-07	0.001758	1.49E-05	0.0018422
L8	1.45636E-06	0.001029011	5.49E-05	0.00097	1.61E-06	0.002171	5.83E-05	0.0021957
L9	1.61062E-06	0.005475886	6.50E-05	0.00132	2.50E-06	0.005599	5.66E-05	0.0026087
L10	1.1515E-08	0.002365263	6.19E-05	0.00083	1.10E-08	0.003392	9.51E-05	0.0017842

Figures 46 and 47 show that the SVI_{ME} value at the annual scale is higher for LSTM, followed by the Mean of GCMs, which indicates that the model performance is highly variable, backing up the results we obtained in the trend analysis of SSP 245 in Table 13 that LSTM shows highly variable results in Near future at some locations it shows increasing while at others it shows decreasing indicating variability in the model performance.

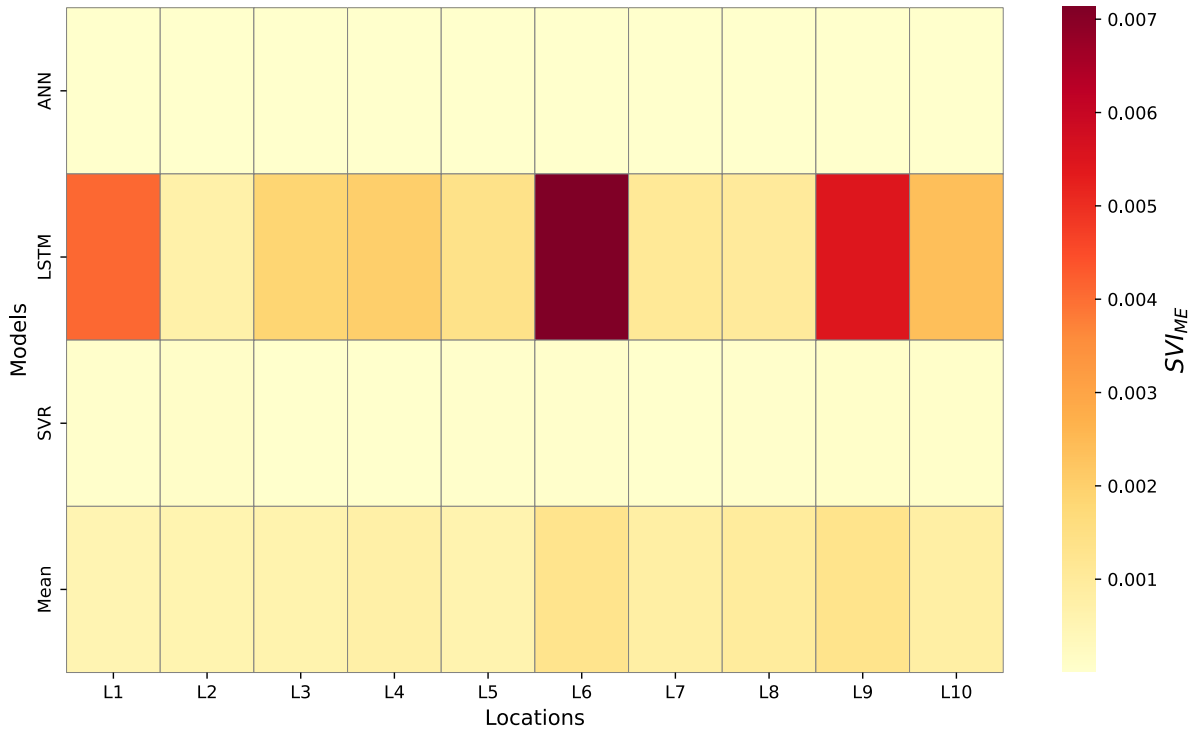

Figure 46 Heatmap of SSP 245 SVI_{ME} Annual values

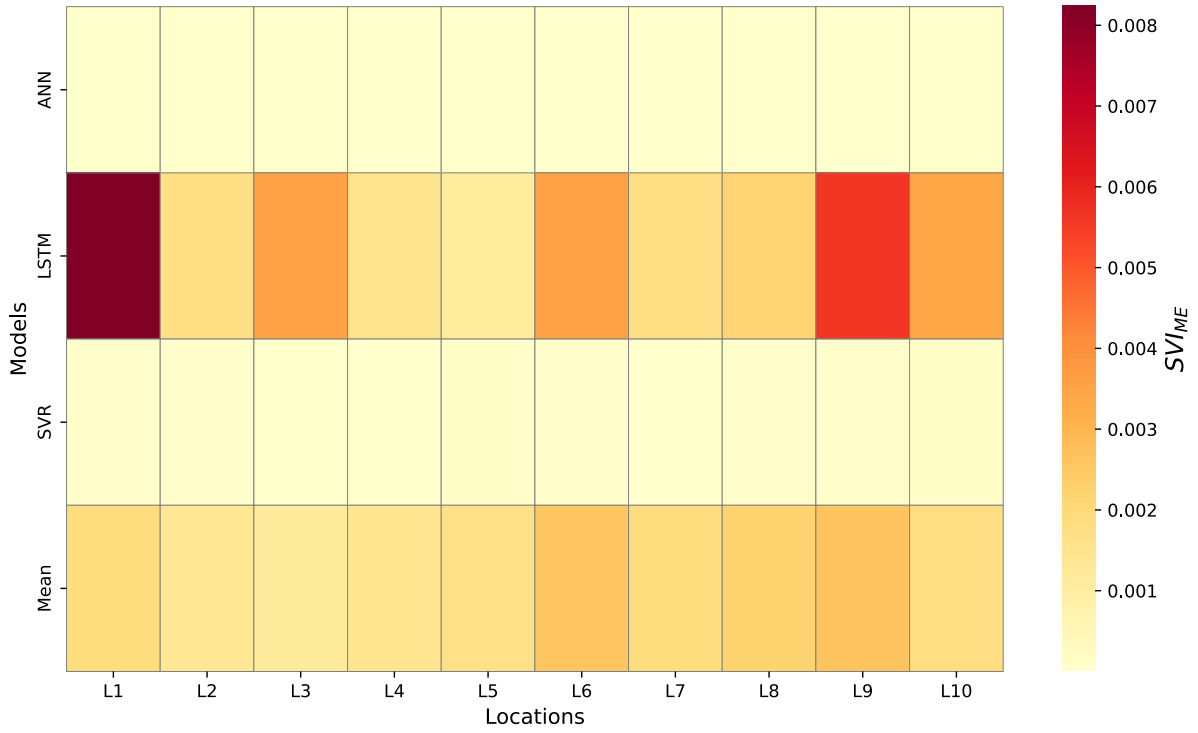

Figure 47 Heatmap of SSP 585 SVI_{ME} Annual values

SVI_{ME} value at the Seasonal and Annual scale was very insignificant under both Scenarios, SSP 245 and SSP 585, for all four ensembling methods. For more information, refer to Annexure-1 Tables 18,19,20 and 21.

Chapter 5

Conclusion

In this study, 13 GCMs are ensembled using simple mean and 3 ML, and their performance is measured on the basis of evaluation metrics like R^2, RMSE, MAE, and KGE based on the trained model's future data. This future ensembled data is used to calculate the trend analysis using MMK and Sen's slope. An entropy analysis of future ensembles is also performed to understand the variability of precipitation ensembles using Mean and 3 ML techniques. Based on the results, the following conclusion has been drawn:

1. According to the Multi-model ensemble by Mean and 3 ML techniques like LSTM, ANN, and SVR on the basis of performance evaluation metrics, LSTM performed better, followed by other ANN and SVR, which shows the ML technique has improved the value of different parameter of evaluation metrics.
2. In the case of temperature, on the basis of the evaluation metric, all ensembling techniques performed better as the temperature parameter does not show a sharp change with respect to time.
3. Mann-Kendall and Sen's slope tests show that the ensemble means exhibited a statistically significant increasing trend across all 10 different locations. However, LSTM showed an increasing trend in most of the locations.
4. In the case of trend analysis of temperature, LSTM showed a decreasing trend while all other ML techniques showed an increasing trend, which shows that it fails to capture short-term change, i.e., Temperature.
5. Standard variability analysis using SVI_{AE} reveals that SVR and MME-mean exhibit high variability. At the same time, SVI_{ME} analysis at the annual scale showed low values for LSTM and MME-Mean and insignificant for SVR and ANN.

5.1 Limitations

1. The study has several limitations that warrant consideration. First, the reliance on CMIP6 GCMs introduces inherent biases and uncertainties, particularly in regional precipitation and temperature projections, which may affect the accuracy of downscaled data. While advanced bias correction techniques like quantile delta mapping (QDM) and machine learning approaches are employed, challenges such as overcorrection and distortion of climate signals persist.

2. The MME methods, including traditional techniques like simple and weighted mean, may underestimate true uncertainties or fail to capture extreme events due to structural differences among models fully.
3. The study acknowledges computational constraints and the limited ability of current ML-based ensembles to address all nonlinear climate dynamics comprehensively.
4. The evaluation metrics, though comprehensive, may not fully align with practical outcomes in imbalanced data scenarios, potentially limiting the interpretability of results for specific applications. These limitations highlight the need for further refinement in model integration, bias correction, and metric selection to enhance the reliability of climate projections.

5.2 Future scope

The study opens several promising avenues for future research to enhance the accuracy and reliability of climate projections. First, advancements in bias correction techniques, such as integrating hybrid methods that combine quantile mapping with machine learning (e.g., deep learning or wavelet-based approaches), could further reduce systematic biases in CMIP6 models, particularly for regional precipitation and temperature variability. Second, improving Multi-Model Ensemble (MME) methods by incorporating dynamic weighting schemes, Bayesian optimization, or ensemble selection algorithms could better address inter-model spread and uncertainty, especially for extreme weather events. Another critical direction is the development of hybrid frameworks that seamlessly merge traditional GCMs with machine learning models, such as transformer-based architectures or physics-informed neural networks, to enhance downscaling and parameterization while preserving physical consistency. Additionally, future work could explore the integration of high-resolution observational datasets and emerging climate reanalysis products to constrain model uncertainties better. Further research is also needed to refine evaluation metrics, particularly for imbalanced or non-Gaussian data, by developing domain-specific performance indicators that align with real-world risk assessment needs.

References

- Ali, S., Tirumala, S. S., & Sarrafzadeh, A. (2015). Ensemble learning methods for decision making: Status and future prospects. *2015 International Conference on Machine Learning and Cybernetics (ICMLC)*, *1*, 211–216. https://doi.org/10.1109/ICMLC.2015.7340924
- Almazroui, M., Ashfaq, M., Islam, M. N., Rashid, I. U., Kamil, S., Abid, M. A., O'Brien, E., Ismail, M., Reboita, M. S., Sörensson, A. A., Arias, P. A., Alves, L. M., Tippett, M. K., Saeed, S., Haarsma, R., Doblas-Reyes, F. J., Saeed, F., Kucharski, F., Nadeem, I., … Sylla, M. B. (2021). Assessment of CMIP6 Performance and Projected Temperature and Precipitation Changes Over South America. *Earth Systems and Environment*, *5*(2), 155–183. https://doi.org/10.1007/s41748-021-00233-6
- Anil, S., & Anand Raj, P. (2022). Deciphering the projected changes in CMIP-6 based precipitation simulations over the Krishna River Basin. *Journal of Water and Climate Change*, *13*(3), 1389–1407. https://doi.org/10.2166/wcc.2022.399
- Bayar, A. S., Yılmaz, M. T., Yücel, İ., & Dirmeyer, P. (2023). CMIP6 Earth System Models Project Greater Acceleration of Climate Zone Change Due To Stronger Warming Rates. *Earth's Future*, *11*(4), e2022EF002972. https://doi.org/https://doi.org/10.1029/2022EF002972
- Bian, G., Zhang, J., Song, M., Qian, X., Guan, T., & Wang, G. (2023). Projections of flood regime changes over the upper-middle Huaihe River Basin in China based on CMIP6 models. *Frontiers in Environmental Science*, *Volume 11*. https://doi.org/10.3389/fenvs.2023.1247753
- Bojer, A. K., Woldetsadik, M., & Biru, B. H. (2024). Machine learning and CORDEX-Africa regional model for assessing the impact of climate change on the Gilgel Gibe Watershed, Ethiopia. *Journal of Environmental Management*, *363*, 121394. https://doi.org/https://doi.org/10.1016/j.jenvman.2024.121394
- Botchkarev, A. (2019). A New Typology Design of Performance Metrics to Measure Errors in Machine Learning Regression Algorithms. *Interdisciplinary Journal of Information, Knowledge, and Management*, *14*, 045–076. https://doi.org/10.28945/4184
- Brassington, G. (2017). Mean absolute error and root mean square error: which is the better metric for assessing model performance? *EGU General Assembly Conference Abstracts*, 3574.
- Cannon, A. J. (2015). Selecting GCM Scenarios that Span the Range of Changes in a Multimodel Ensemble: Application to CMIP5 Climate Extremes Indices. *Journal of Climate*, *28*(3), 1260–1267. https://doi.org/10.1175/JCLI-D-14-00636.1

- Chai, T., & Draxler, R. R. (2014a). Root mean square error (RMSE) or mean absolute error (MAE)? – Arguments against avoiding RMSE in the literature. *Geoscientific Model Development*, *7*(3), 1247–1250. https://doi.org/10.5194/gmd-7-1247-2014
- Chai, T., & Draxler, R. R. (2014b). Root mean square error (RMSE) or mean absolute error (MAE)? – Arguments against avoiding RMSE in the literature. *Geoscientific Model Development*, *7*(3), 1247–1250. https://doi.org/10.5194/gmd-7-1247-2014
- Chandel, V. S., Bhatia, U., Ganguly, A. R., & Ghosh, S. (2024). State-of-the-art bias correction of climate models misrepresent climate science and misinform adaptation. *Environmental Research Letters*, *19*(9), 94052. https://doi.org/10.1088/1748-9326/ad6d82
- Correndo, A. A., Rosso, L. H. M., Hernandez, C. H., Bastos, L. M., Nieto, L., Holzworth, D., & Ciampitti, I. A. (2022). metrica: an R package to evaluate prediction performance of regression and classification point-forecast models. *Journal of Open Source Software*, *7*(79), 4655. https://doi.org/10.21105/joss.04655
- Das, A., Jain, K., Majumder, D., & Karmakar, R. (2024). An Ensemble Learning Paradigm for Efficient Stock Market Predictions. *2024 15th International Conference on Computing Communication and Networking Technologies (ICCCNT)*, 1–7. https://doi.org/10.1109/ICCCNT61001.2024.10726086
- Dessain, J. (2023). Credit Scoring Models: Which Performance Metrics for Optimal Financial Decision-Making? *SSRN Electronic Journal*. https://doi.org/10.2139/ssrn.4624501
- Dong, X., Yu, Z., Cao, W., Shi, Y., & Ma, Q. (2020). A survey on ensemble learning. *Frontiers of Computer Science*, *14*(2), 241–258. https://doi.org/10.1007/s11704-019-8208-z
- Dumbre, S. U., Dixit, P. R., & Londhe, S. (2024). *Performance Evaluation of CMIP6 - GCMs Using Three Spatial Interpolation Methods Over Catchment Area of Koyna Reservoir ,. 1*, 103–121.
- Dutta, D., & Bhattacharjya, R. K. (2022). A statistical bias correction technique for global climate model predicted near-surface temperature in India using the generalized regression neural network. *Journal of Water and Climate Change*, *13*(2), 854–871. https://doi.org/10.2166/wcc.2022.214
- Exbrayat, J.-F., Bloom, A. A., Falloon, P., Ito, A., Smallman, T. L., & Williams, M. (2018). Reliability ensemble averaging of 21st~century projections of terrestrial net primary productivity reduces global and regional uncertainties. *Earth System Dynamics*, *9*(1), 153–165. https://doi.org/10.5194/esd-9-153-2018

- Eyring, V., Bony, S., Meehl, G. A., Senior, C. A., Stevens, B., Stouffer, R. J., & Taylor, K. E. (2016). Overview of the Coupled Model Intercomparison Project Phase 6 (CMIP6) experimental design and organization. *Geoscientific Model Development*, *9*(5), 1937–1958. https://doi.org/10.5194/gmd-9-1937-2016
- Foyhirun, Chutipat, Kongkitkul, Duangrudee K., & Ekkawatpanit, Chaiwat. (2019). Performance of Global Climate Model (GCMs) for Wind Data Analysis. *E3S Web Conf.*, *117*, 6. https://doi.org/10.1051/e3sconf/201911700006
- Frei, A., Mukundan, R., Chen, J., Gelda, R. K., Owens, E. M., Gass, J., & Ravindranath, A. (2022). A Cascading Bias Correction Method for Global Climate Model Simulated Multiyear Precipitation Variability. *Journal of Hydrometeorology*, *23*(5), 697–713. https://doi.org/10.1175/JHM-D-21-0148.1
- Ganguly, T., & Arya, D. S. (2023). A novel framework for a multimodel ensemble of GCMs and its application in the analysis of projected extremes. *International Journal of Climatology*, *43*(15), 7308–7325. https://doi.org/https://doi.org/10.1002/joc.8266
- Gao, J. (2024). R-squared (R2) – How much variation is explained? *Research Methods in Medicine \& Health Sciences*, *5*(4), 104–109. https://doi.org/10.1177/26320843231186398
- Gao, W., Li, J., Cheng, D., Liu, L., Liu, J., Le, T. D., Du, X., Chen, X., Zhao, Y., & Chen, Y. (2024). *A Deconfounding Approach to Climate Model Bias Correction*. https://arxiv.org/abs/2408.12063
- González-Abad, J., & Baño-Medina, J. (2023). *Deep Ensembles to Improve Uncertainty Quantification of Statistical Downscaling Models under Climate Change Conditions*. https://arxiv.org/abs/2305.00975
- Grillakis, M. G., Koutroulis, A. G., & Tsanis, I. K. (2013). Multisegment statistical bias correction of daily GCM precipitation output. *Journal of Geophysical Research: Atmospheres*, *118*(8), 3150–3162. https://doi.org/https://doi.org/10.1002/jgrd.50323
- Guan, T., Liu, Y., Sun, Z., Zhang, J., Chen, H., Wang, G., Jin, J., Bao, Z., & Qi, W. (2022). A Framework to Identify the Uncertainty and Credibility of GCMs for Projected Future Precipitation: A Case Study in the Yellow River Basin, China. *Frontiers in Environmental Science*, *Volume 10*. https://doi.org/10.3389/fenvs.2022.863575
- Hamed, K. H., & Rao, A. R. (1998). Hydrology A modified Mann-Kendall trend test for autocorrelated data. In *Journal of Hydrology* (Vol. 204).

- Hirabayashi, Y., Tanoue, M., Sasaki, O., Zhou, X., & Yamazaki, D. (2021). Global exposure to flooding from the new CMIP6 climate model projections. *Scientific Reports*, *11*(1), 3740. https://doi.org/10.1038/s41598-021-83279-w
- Hodson, T. O. (2022). Root-mean-square error (RMSE) or mean absolute error (MAE): when to use them or not. *Geoscientific Model Development*, *15*(14), 5481–5487. https://doi.org/10.5194/gmd-15-5481-2022
- Jose, D. M., Vincent, A. M., & Dwarakish, G. S. (2022). Improving multiple model ensemble predictions of daily precipitation and temperature through machine learning techniques. *Scientific Reports*, *12*(1). https://doi.org/10.1038/s41598-022-08786-w
- Kim, Y., Evans, J. P., & Sharma, A. (2023). Multivariate bias correction of regional climate model boundary conditions. *Climate Dynamics*, *61*(7), 3253–3269. https://doi.org/10.1007/s00382-023-06718-6
- Kim, Y. H., Min, S. K., Zhang, X., Sillmann, J., & Sandstad, M. (2020). Evaluation of the CMIP6 multi-model ensemble for climate extreme indices. *Weather and Climate Extremes*, *29*. https://doi.org/10.1016/j.wace.2020.100269
- Knoben, W. J. M., Freer, J. E., & Woods, R. A. (2019). Technical note: Inherent benchmark or not? Comparing Nash–Sutcliffe and Kling–Gupta efficiency scores. *Hydrology and Earth System Sciences*, *23*(10), 4323–4331. https://doi.org/10.5194/hess-23-4323-2019
- Knutti, R., Furrer, R., Tebaldi, C., Cermak, J., & Meehl, G. A. (2010). Challenges in Combining Projections from Multiple Climate Models. *Journal of Climate*, *23*(10), 2739–2758. https://doi.org/10.1175/2009JCLI3361.1
- Krishnamoorthy, G., & Sistla, S. M. K. (2023). Leveraging Deep Learning for Climate Change Prediction Models : A Dive into Cutting-Edge Techniques. *Journal of Knowledge Learning and Science Technology ISSN: 2959-6386 (Online)*, *2*(2), 108–113. https://doi.org/10.60087/jklst.vol2.n2.p113
- Kusumastuti, C., Jiang, Z., Mehrotra, R., & Sharma, A. (2022). Correcting Systematic Bias in Climate Model Simulations in the Time-Frequency Domain. *Geophysical Research Letters*, *49*(19), e2022GL100550. https://doi.org/https://doi.org/10.1029/2022GL100550
- Labe, Z. M., & Barnes, E. A. (2022). Comparison of Climate Model Large Ensembles With Observations in the Arctic Using Simple Neural Networks. *Earth and Space Science*, *9*(7), e2022EA002348. https://doi.org/https://doi.org/10.1029/2022EA002348
- Lehner, F., Deser, C., Maher, N., Marotzke, J., Fischer, E. M., Brunner, L., Knutti, R., & Hawkins, E. (2020). Partitioning climate projection uncertainty with multiple large ensembles

and CMIP5/6. *Earth System Dynamics*, *11*(2), 491–508. https://doi.org/10.5194/esd-11-491-2020

- Li, X., & Li, Z. (2023). Evaluation of bias correction techniques for generating high-resolution daily temperature projections from CMIP6 models. *Climate Dynamics*, *61*(7), 3893–3910. https://doi.org/10.1007/s00382-023-06778-8
- MA, S., & Stratonovitch, P. (2010). Use of multi-model ensembles from global climate models for assessment of climate change impacts . *Climate Research*, *41*(1), 1–14. https://www.int-res.com/abstracts/cr/v41/n1/p1-14
- Maruyama, T., Kawachi, T., & Singh, V. P. (2005). Entropy-based assessment and clustering of potential water resources availability. *Journal of Hydrology*, *309*(1), 104–113. https://doi.org/https://doi.org/10.1016/j.jhydrol.2004.11.020
- Mathevet, T., Le Moine, N., Andréassian, V., Gupta, H., & Oudin, L. (2023). Multi-objective assessment of hydrological model performances using Nash–Sutcliffe and Kling–Gupta efficiencies on a worldwide large sample of watersheds. *Comptes Rendus - Geoscience*, *355*(S1), 117–141. https://doi.org/10.5802/crgeos.189
- McKenna, C. M., & Maycock, A. C. (2021). Sources of Uncertainty in Multimodel Large Ensemble Projections of the Winter North Atlantic Oscillation. *Geophysical Research Letters*, *48*(14), e2021GL093258. https://doi.org/https://doi.org/10.1029/2021GL093258
- Miles, J. (2005). R-squared, Adjusted R-squared. In *Encyclopedia of Statistics in Behavioral Science*. John Wiley & Sons, Ltd. https://doi.org/https://doi.org/10.1002/0470013192.bsa526
- Mishra, A. K., Özger, M., & Singh, V. P. (2009). An entropy-based investigation into the variability of precipitation. *Journal of Hydrology*, *370*(1), 139–154. https://doi.org/https://doi.org/10.1016/j.jhydrol.2009.03.006
- Moradkhani, M. A., GAO, R., Hosseini, S. H., & SONG, M. (2024). Estimation of frost layer characteristics during natural convection on vertical and inverted cold surfaces based on smart approaches. *Applied Thermal Engineering*, *239*. https://doi.org/10.1016/j.applthermaleng.2023.122090
- Nashwan, M. S., & Shahid, S. (2020). A novel framework for selecting general circulation models based on the spatial patterns of climate. *International Journal of Climatology*, *40*(10), 4422–4443. https://doi.org/10.1002/joc.6465
- Onyutha, C. (2020). From R-squared to coefficient of model accuracy for assessing "goodness-of-fits." *Geoscientific Model Development Discussions*, *2020*, 1–25. https://doi.org/10.5194/gmd-2020-51

- Osso, A., Craig, P., & Allan, R. P. (2023). An assessment of CMIP6 climate signals and biases in temperature, precipitation and soil moisture over Europe. *International Journal of Climatology*, *43*(12), 5698–5719. https://doi.org/10.1002/joc.8169
- Pai, D. S., Sridhar, L., Rajeevan, M., Sreejith, O. P., Satbhai, N. S., & Mukhopadyay, B. (2014). *Development of a new high spatial resolution (0.25° × 0.25°) Long Period (1901-2010) daily gridded rainfall data set over India and its comparison with existing data sets over the region* (Vol. 65, Issue 1).
- Peng, S., Wang, C., Li, Z., Mihara, K., Kuramochi, K., Toma, Y., & Hatano, R. (2023). Climate change multi-model projections in CMIP6 scenarios in Central Hokkaido, Japan. *Scientific Reports*, *13*(1), 230. https://doi.org/10.1038/s41598-022-27357-7
- Pierce, D. W., Cayan, D. R., Maurer, E. P., Abatzoglou, J. T., & Hegewisch, K. C. (2015). Improved Bias Correction Techniques for Hydrological Simulations of Climate Change. *Journal of Hydrometeorology*, *16*(6), 2421–2442. https://doi.org/10.1175/JHM-D-14-0236.1
- Plevris, V., Solorzano, G., Bakas, N. P., & Ben Seghier, M. E. A. (2022). Investigation of Performance Metrics in Regression Analysis and Machine Learning-Based Prediction Models. *World Congress in Computational Mechanics and ECCOMAS Congress*, 0–25. https://doi.org/10.23967/eccomas.2022.155
- Rampal, N., Hobeichi, S., Gibson, P. B., Baño-Medina, J., Abramowitz, G., Beucler, T., González-Abad, J., Chapman, W., Harder, P., & Gutiérrez, J. M. (2024). Enhancing Regional Climate Downscaling through Advances in Machine Learning. *Artificial Intelligence for the Earth Systems*, *3*(2), 230066. https://doi.org/10.1175/AIES-D-23-0066.1
- Rane, N., Choudhary, S. P., & Rane, J. (2024). Ensemble deep learning and machine learning: applications, opportunities, challenges, and future directions. *Studies in Medical and Health Sciences*, *1*(2), 18–41. https://doi.org/10.48185/smhs.v1i2.1225
- Ren, Y., Zhang, L., & Suganthan, P. N. (2016). Ensemble Classification and Regression-Recent Developments, Applications and Future Directions [Review Article]. *IEEE Computational Intelligence Magazine*, *11*(1), 41–53. https://doi.org/10.1109/MCI.2015.2471235
- Robertson, D. E., Chiew, F. H. S., & Potter, N. (2023). Adapting rainfall bias-corrections to improve hydrological simulations generated from climate model forcings. *Journal of Hydrology*, *619*, 129322. https://doi.org/https://doi.org/10.1016/j.jhydrol.2023.129322
- Roy, S., & Chakravarty, N. (2021). *Rainfall Analysis by Using Mann-Kendall Trend, Sen's Slope and Variability at Six Stations of Andaman & Nicobar Islands*.

- Sa'adi, Z., Shahid, S., Ismail, T., Chung, E.-S., & Wang, X.-J. (2019). Trends analysis of rainfall and rainfall extremes in Sarawak, Malaysia using modified Mann–Kendall test. *Meteorology and Atmospheric Physics*, *131*(3), 263–277. https://doi.org/10.1007/s00703-017-0564-3
- Sanderson, B. M., & Knutti, R. (2012). On the interpretation of constrained climate model ensembles. *Geophysical Research Letters*, *39*(16). https://doi.org/https://doi.org/10.1029/2012GL052665
- Semenov, M. A., Senapati, N., Coleman, K., & Collins, A. L. (2024). A dataset of CMIP6-based climate scenarios for climate change impact assessment in Great Britain. *Data in Brief*, *55*, 110709. https://doi.org/https://doi.org/10.1016/j.dib.2024.110709
- Shetty, S., Umesh, P., & Shetty, A. (2023). The effectiveness of machine learning-based multi-model ensemble predictions of CMIP6 in Western Ghats of India. *International Journal of Climatology*, *43*(11), 5029–5054. https://doi.org/https://doi.org/10.1002/joc.8131
- Shiru, M. S., & Chung, E.-S. (2021). Performance evaluation of CMIP6 global climate models for selecting models for climate projection over Nigeria. *Theoretical and Applied Climatology*, *146*(1), 599–615. https://doi.org/10.1007/s00704-021-03746-2
- Srivastava, A. K., Rajeevan, M., & Kshirsagar, S. R. (2009). Development of a high resolution daily gridded temperature data set (1969-2005) for the Indian region. *Atmospheric Science Letters*, *10*(4), 249–254. https://doi.org/10.1002/asl.232
- Stitson, M. O., Weston, J. A. E., Gammerman, A., Vovk, V., & Vapnik, V. (1996). *Theory of Support Vector Machines: Vol. +*.
- Sun, L., Lan, Y., & Jiang, R. (2023). Using CNN framework to improve multi-GCM ensemble predictions of monthly precipitation at local areas: An application over China and comparison with other methods. *Journal of Hydrology*, *623*, 129866. https://doi.org/https://doi.org/10.1016/j.jhydrol.2023.129866
- Talukder, A., Shaid, S., Hwang, S., Alam, E., Islam, K., & Kamruzzaman, M. (2025). Optimizing the multi-model ensemble of CMIP6 GCMs for climate simulation over Bangladesh. *Scientific Reports*, *15*(1), 11343. https://doi.org/10.1038/s41598-025-96446-0
- Tang, A., Shen, L., Luo, Y., Yin, N., Zhang, L., & Tao, D. (2024). *Merging Multi-Task Models via Weight-Ensembling Mixture of Experts*. https://arxiv.org/abs/2402.00433
- Thrasher, B., Wang, W., Michaelis, A., Melton, F., Lee, T., & Nemani, R. (2022). NASA Global Daily Downscaled Projections, CMIP6. *Scientific Data*, *9*(1), 262. https://doi.org/10.1038/s41597-022-01393-4

- Tunkel, S., & Herbold, S. (2022). Exploring the relationship between performance metrics and cost saving potential of defect prediction models. *Empirical Software Engineering*, *27*(7), 182. https://doi.org/10.1007/s10664-022-10224-4
- Tyagi, S., Sahany, S., Saraswat, D., Mishra, S. K., Dubey, A., & Niyogi, D. (2024). Implications of CMIP6 Models-Based Climate Biases and Runoff Sensitivity on Runoff Projection Uncertainties Over Central India. *International Journal of Climatology*, *44*(16), 5727–5744. https://doi.org/https://doi.org/10.1002/joc.8661
- Vrac, M., Allard, D., Mariéthoz, G., Thao, S., & Schmutz, L. (2024). Distribution-based pooling for combination and multi-model bias correction of climate simulations. *Earth System Dynamics*, *15*(3), 735–762. https://doi.org/10.5194/esd-15-735-2024
- Vrugt, J. A., & de Oliveira, D. Y. (2022). Confidence intervals of the Kling-Gupta efficiency. *Journal of Hydrology*, *612*, 127968. https://doi.org/https://doi.org/10.1016/j.jhydrol.2022.127968
- Willmott, C. J. (2005a). Advantages of the mean absolute error (MAE) over the root mean square error (RMSE) in assessing average model performance . *Climate Research*, *30*(1), 79–82. https://www.int-res.com/abstracts/cr/v30/n1/p79-82
- Willmott, C. J. (2005b). Advantages of the mean absolute error (MAE) over the root mean square error (RMSE) in assessing average model performance . *Climate Research*, *30*(1), 79–82.
- Wu, Y., Miao, C., Slater, L., Fan, X., Chai, Y., & Sorooshian, S. (2024). Hydrological Projections under CMIP5 and CMIP6: Sources and Magnitudes of Uncertainty. *Bulletin of the American Meteorological Society*, *105*(1), E59–E74. https://doi.org/10.1175/BAMS-D-23-0104.1
- Yokohata, T., Annan, J. D., Collins, M., Jackson, C. S., Tobis, M., Webb, M. J., & Hargreaves, J. C. (2012). Reliability of multi-model and structurally different single-model ensembles. *Climate Dynamics*, *39*(3), 599–616. https://doi.org/10.1007/s00382-011-1203-1
- Zhang, S., & Chen, J. (2021). Uncertainty in Projection of Climate Extremes: A Comparison of CMIP5 and CMIP6. *Journal of Meteorological Research*, *35*(4), 646–662. https://doi.org/10.1007/s13351-021-1012-3
- Zhang, Y., Kong, Y., Yang, S., & Hu, X. (2023). Asymmetric Arctic and Antarctic Warming and Its Intermodel Spread in CMIP6. *Journal of Climate*, *36*(23), 8299–8310. https://doi.org/10.1175/JCLI-D-23-0118.1

- Zhu, J., Huang, B., Balmaseda, M. A., Kinter, J. L., Peng, P., Hu, Z.-Z., & Marx, L. (2013). Improved reliability of ENSO hindcasts with multi-ocean analyses ensemble initialization. *Climate Dynamics*, *41*(9), 2785–2795. https://doi.org/10.1007/s00382-013-1965-8
- Zhu, W. (2022). *Statistical parameters for assessing environmental model performance related to sample size: Case study in ocean color remote sensing*.

Annexure

In this section, all the supplementary details related to this study are presented in tables.

Table 15 Trend Analysis of PCP 585

Locations	Models	Near_Future			Far Future		
		Corrected Zc	new P-value	Sen's slope	Corrected Zc	new P-value	Sen's slope
L1	ANN	1.4547	0.1457	0.1117	3.5634	0.0004	0.0820
	LSTM	0.1730	0.8627	0.8702	1.7602	0.0784	3.6506
	Mean	3.9234	0.3536	4.9314	5.8721	4.30E-09	5.7375
	SVR	1.9397	0.0524	0.9550	1.3886	0.1650	0.2181
L2	ANN	-0.8031	0.4219	-0.0292	2.2641	0.0236	0.0520
	LSTM	-2.2482	0.0246	-7.6969	3.7198	0.0002	4.2098
	Mean	3.4385	0.0006	5.6015	7.5761	3.56E-14	4.7293
	SVR	0.4408	0.6593	0.2493	3.0546	0.0023	0.3729
L3	ANN	-0.2645	0.7914	-0.0238	2.9779	0.0029	0.0944
	LSTM	2.4940	0.0126	5.9733	4.2077	0.0422	2.2783
	Mean	1.3225	0.1860	2.0504	8.1062	5.00E-16	4.9679
	SVR	-1.2784	0.2011	-0.6593	1.5391	0.1238	0.2831
L4	ANN	0.1322	0.8948	0.0122	3.4965	0.0005	0.1025
	LSTM	-0.3527	0.7243	-1.6901	0.8820	0.3778	1.2297
	Mean	0.7359	0.4618	0.9943	4.8851	1.03E-06	6.4372
	SVR	1.5984	0.1100	0.6568	-1.5559	0.1197	-0.2990
L5	ANN	-0.1763	0.8600	-0.0125	3.3459	0.0008	0.0889
	LSTM	-0.0441	0.9648	-0.8705	2.2552	0.0241	0.9578
	Mean	0.8376	0.4023	0.9868	6.9800	2.95E-12	6.4428
	SVR	1.1902	0.2340	0.5500	0.6190	0.5359	0.1897
L6	ANN	1.2714	0.2036	0.0560	5.8053	6.43E-09	0.1808
	LSTM	-0.9257	0.3546	-5.1659	4.0069	0.2313	-0.6805
	Mean	0.4849	0.6277	0.9743	5.8219	5.82E-09	7.2236
	SVR	2.5771	0.0100	1.3193	0.3935	0.6940	0.0862
L7	ANN	0.2595	0.7952	0.0122	4.0988	4.15E-05	0.1100
	LSTM	-1.2306	0.2185	-3.6615	-5.3404	9.27E-08	-5.8944
	Mean	1.2343	0.2171	8.0185	4.9687	6.74E-07	14.7259
	SVR	2.5771	0.0100	1.3193	0.3935	0.6940	0.0862
L8	ANN	1.9837	0.0473	0.2432	3.0281	0.0025	0.1256
	LSTM	0.0000	1.0000	-0.2486	-3.2226	0.0013	-3.4013
	Mean	1.2784	0.2011	1.7098	5.6379	1.72E-08	6.1289
	SVR	0.2897	0.7721	0.1732	2.9064	0.0037	0.3904
L9	ANN	1.0671	0.2859	0.0996	4.5170	6.27E-06	0.1957
	LSTM	1.4547	0.1457	5.6363	1.0964	0.2729	1.7384
	Mean	0.3086	0.7576	0.5586	5.6045	2.09E-08	6.5938
	SVR	-0.8376	0.4023	-0.2259	0.9961	0.3192	0.1635
L10	ANN	0.4408	0.6593	0.0028	2.0217	0.0432	0.0064
	LSTM	-0.5550	0.5789	-3.2349	2.4361	0.2080	-1.9097
	Mean	2.3364	0.0195	5.3200	4.7345	2.20E-06	4.7396
	SVR	1.0139	0.3106	0.5966	0.5521	0.5809	0.1894

Table 16 Trend Analysis of TMAX 585

Location	Models	Near Future			Far Future		
		Corrected Zc	new P-value	Sen's slope	Corrected Zc	new P-value	Sen's slope
L1	ANN	5.202	0.000	0.045	8.699	0.000	0.058
	LSTM	0.661	0.508	0.006	-9.710	0.000	-0.025
	Mean	5.334	0.000	0.035	9.017	0.000	0.044
	SVR	3.522	0.000	0.027	8.649	0.000	0.043
L2	ANN	5.070	0.000	0.039	11.982	0.000	0.054
	LSTM	-1.984	0.047	-0.012	-6.475	0.000	-0.028
	Mean	5.643	0.000	0.033	11.895	0.000	0.046
	SVR	4.981	0.000	0.030	8.800	0.000	0.047
L3	ANN	5.466	0.000	0.049	8.331	0.000	0.057
	LSTM	-0.176	0.860	-0.001	-9.266	0.000	-0.069
	Mean	5.599	0.000	0.050	9.151	0.000	0.057
	SVR	5.951	0.000	0.039	8.800	0.000	0.050
L4	ANN	5.290	0.000	0.066	8.566	0.000	0.064
	LSTM	-3.350	0.001	-0.025	-20.657	0.000	-0.050
	Mean	4.826	0.000	0.050	9.051	0.000	0.056
	SVR	5.114	0.000	0.040	7.953	0.000	0.051
L5	ANN	5.334	0.000	0.066	8.716	0.000	0.065
	LSTM	2.067	0.039	0.017	1.837	0.066	0.020
	Mean	5.687	0.000	0.046	9.017	0.000	0.052
	SVR	5.510	0.000	0.041	8.766	0.000	0.050
L6	ANN	5.422	0.000	0.054	9.101	0.000	0.065
	LSTM	-5.040	0.000	-0.030	-6.697	0.000	-0.045
	Mean	5.775	0.000	0.041	9.302	0.000	0.046
	SVR	5.643	0.000	0.038	8.800	0.000	0.044
L7	ANN	4.849	0.000	0.053	9.051	0.000	0.061
	LSTM	-0.132	0.895	-0.003	3.846	0.000	0.024
	Mean	5.951	0.000	0.041	9.436	0.000	0.049
	SVR	5.158	0.000	0.036	9.084	0.000	0.049
L8	ANN	5.510	0.000	0.057	8.800	0.000	0.062
	LSTM	0.309	0.758	0.003	3.255	0.001	0.017
	Mean	5.599	0.000	0.043	9.051	0.000	0.049
	SVR	5.025	0.000	0.037	8.867	0.000	0.050
L9	ANN	5.070	0.000	0.049	9.084	0.000	0.061
	LSTM	-1.455	0.146	-0.011	-2.274	0.023	-0.068
	Mean	5.863	0.000	0.042	9.235	0.000	0.047
	SVR	5.687	0.000	0.039	8.883	0.000	0.044
L10	ANN	4.981	0.000	0.035	8.766	0.000	0.052
	LSTM	1.035	0.301	0.003	2.500	0.012	0.015
	Mean	5.731	0.000	0.034	8.326	0.004	0.041
	SVR	5.510	0.000	0.025	13.713	0.000	0.038

Table 17 Trend Analysis of TMIN 585

Location	Models	Near Future			Far Future		
		Corrected Zc	new P-value	Sen's slope	Corrected Zc	new P-value	Sen's slope
L1	ANN	5.9071	3.48E-09	0.0490	13.4634	0.0000	0.0566
	LSTM	-0.2204	0.8255	-0.0004	-6.5740	4.90E-11	-0.0145
	Mean	5.6426	1.67E-08	0.0458	9.5694	0.0000	0.0516
	SVR	5.4663	4.60E-08	0.0340	9.4021	0.0000	0.0489
L2	ANN	5.2900	1.22E-07	0.0413	10.3246	0.0000	0.0547
	LSTM	0.4408	0.6593	0.0010	-4.7847	1.71E-06	-0.0110
	Mean	6.0394	1.55E-09	0.0381	9.5192	0.0000	0.0476
	SVR	5.8631	4.54E-09	0.0299	9.4356	0.0000	0.0528
L3	ANN	6.0835	1.18E-09	0.0491	9.8641	0.0000	0.0647
	LSTM	-4.4965	6.91E-06	-0.0229	-8.1340	4.00E-16	-0.0729
	Mean	6.1276	8.92E-10	0.0520	15.9103	0.0000	0.0652
	SVR	5.8631	4.54E-09	0.0386	9.9049	0.0000	0.0640
L4	ANN	5.2900	1.22E-07	0.0466	9.4690	0.0000	0.0704
	LSTM	-2.7409	0.0061	-0.0063	-7.0724	1.52E-12	-0.0448
	Mean	5.1300	2.90E-07	0.0505	9.5025	0.0000	0.0680
	SVR	5.2459	1.56E-07	0.0367	9.3185	0.0000	0.0673
L5	ANN	5.6426	1.67E-08	0.0502	11.5259	0.0000	0.0699
	LSTM	-2.6009	0.0093	-0.0096	-7.5890	3.22E-14	-0.0579
	Mean	5.6867	1.30E-08	0.0501	10.0362	0.0000	0.0666
	SVR	5.2900	1.22E-07	0.0363	7.6386	2.19E-14	0.0619
L6	ANN	4.6892	2.74E-06	0.0416	7.8644	3.70E-15	0.0542
	LSTM	-4.0116	6.03E-05	-0.0157	-8.9169	0.0000	-0.0588
	Mean	5.6426	1.67E-08	0.0475	9.4523	0.0000	0.0587
	SVR	5.1577	2.50E-07	0.0311	9.4021	0.0000	0.0590
L7	ANN	4.7779	1.77E-06	0.0497	18.9220	0.0000	0.0624
	LSTM	1.3225	0.1860	0.0045	3.7064	0.0002	0.1202
	Mean	6.1716	6.76E-10	0.0400	9.7200	0.0000	0.0472
	SVR	4.7610	1.93E-06	0.0254	9.4584	0.0000	0.0478
L8	ANN	4.6728	2.97E-06	0.0490	12.2034	0.0000	0.0669
	LSTM	-2.2923	0.0219	-0.0087	-8.0303	9.00E-16	-0.0387
	Mean	5.3781	7.53E-08	0.0467	10.5434	0.0000	0.0658
	SVR	4.8932	9.92E-07	0.0318	10.9620	0.0000	0.0655
L9	ANN	5.2900	1.22E-07	0.0449	9.0842	0.0000	0.0554
	LSTM	-4.0556	5.00E-05	-0.0238	-8.9169	0.0000	-0.0799
	Mean	5.5986	2.16E-08	0.0482	9.4356	0.0000	0.0600
	SVR	5.0255	5.02E-07	0.0330	9.4356	0.0000	0.0598
L10	ANN	5.9071	3.48E-09	0.0414	7.2543	4.04E-13	0.0331
	LSTM	0.0371	0.9704	0.0003	-0.4892	0.6247	-0.0011
	Mean	7.0730	1.52E-12	0.0341	6.3611	2.00E-10	0.0302
	SVR	6.6097	3.85E-11	0.0253	5.6211	1.90E-08	0.0334

Table 18 Seasonal Analysis of SVI_{ME} for SSP 245

Scenario	Models		L1	L2	L3	L4	L5	L6	L7	L8	L9	L10
SSP 245	ANN	Monsoon	1.56059E-09	2.96423E-09	1.80844E-09	3.06917E-09	1.40772E-09	4.38773E-09	1.69713E-10	2.04577E-09	1.07678E-08	1.03636E-07
		Post-Monsoon Season	1.18621E-05	3.14338E-06	5.17113E-05	1.2083E-05	1.6418E-05	9.6326E-05	2.29638E-05	7.80389E-05	0.0008571 6	5.69978E-10
		Pre-Monsoon Season	2.33991E-05	1.81093E-05	0.0005025 68	2.39102E-05	1.74399E-05	0.0001034 91	0.0007578 34	0.0001427 19	0.0030985 39	1.06853E-07
		Winter	5.70299E-05	1.07231E-05	0.0005458 12	3.83852E-05	3.27445E-05	1.42156E-15	1	4.19029E-08	9.9509E-16	3.12019E-07
	LSTM	Monsoon	0.0047167 4	0.0005011 29	0.0016931 31	0.0030151 35	0.0023380 16	0.0087874 49	0.0010115 73	0.0027756 85	0.0048258 82	0.0070087 42
		Post-Monsoon Season	0.0089601 52	0.0013634 52	0.0216846 32	0.0042986 4	0.0030635 22	0.0100669 57	0.0131772 1	0.0034687 03	0.0248040 28	0.0059290 75
		Pre-Monsoon Season	0.0087248 48	0.0195135 11	0.2302969 57	0.0085143 45	0.0056889 32	0.1735082 5	0.1268708 23	0.0378251 25	0.0629206 12	0.0009276 55
		Winter	0.0286832 85	0.0153130 87	0.1546219 59	0.0031284 72	0.0080908 13	0.0366828 43	0.1872742 69	0.0303109 35	0.0073402 23	0.0069206 17
	Mean	Monsoon	0.0006866 77	0.0005722 63	0.0006681 11	0.0008191 04	0.0006311 9	0.0013132 95	0.0008449 14	0.0009536 01	0.0013388 28	0.0029525 37
		Post-Monsoon Season	0.0034137 16	0.0023418 76	0.0085239 34	0.0080811 14	0.0064607 13	0.0179480 55	0.0070321 32	0.0104720 86	0.0187508 15	0.0012169 29
		Pre-Monsoon Season	0.0028506 25	0.0076780 42	0.0118363 71	0.0105598 88	0.0115433 36	0.0755209 64	0.0176365 32	0.0284698 32	0.0622274 39	0.0064370 47
		Winter	1	0.0862698 15	0.0117280 66	0.0112911 21	0.0175917 1	1	0.0598748 73	0.4187738 14	1	0.0205763 53
	SVR	Monsoon	6.44809E-05	0.0001006 64	2.71842E-05	1.72268E-05	5.28818E-05	3.54948E-05	9.75138E-06	4.69918E-05	6.58084E-05	0.0022197 66
		Post-Monsoon Season	0.0004704 25	0.0003070 58	0.0027871 01	0.0028028 56	0.0014429 29	0.0063799 14	0.0015505 49	0.0048053 51	0.0085985 63	3.56196E-05
		Pre-Monsoon Season	0.0007230 3	0.0018769 87	0.0076054 83	0.0048237 77	0.0085046 65	0.0703730 66	0.0126394 29	0.2389169 77	0.0234167 78	0.0012226 14
		Winter	0.0030584 26	0.0112414 17	0.0076436 56	0.0043892 33	0.0089800 29	1	6.36398E-05	1.6394E-05	9.9509E-16	0.0027043 7

Table 19 Seasonal Analysis of SVI_{ME} for SSP 585

Scenario	Models		L1	L2	L3	L4	L5	L6	L7	L8	L9	L10
SSP 585	ANN	Monsoon	1.28903E-09	1.6375E-09	1.50224E-09	2.13901E-09	9.04347E-10	3.77402E-09	1.21755E-10	2.08748E-09	6.41891E-09	1.60779E-07
		Post-Monsoon Season	1.73089E-05	3.53545E-06	7.16035E-05	1.83867E-05	1.55378E-05	0.0001069	1.92477E-05	6.74067E-05	0.000976755	5.26904E-10
		Pre-Monsoon Season	3.4494E-05	2.68008E-05	0.000591302	3.45851E-05	3.08283E-05	0.0001474	0.001012455	0.000166708	0.003857185	7.91865E-08
		Winter	1.93315E-08	2.24975E-05	0.000567164	4.04228E-05	3.09451E-05	4.81051E-10	1	5.77465E-08	1.23747E-05	2.43593E-07
	LSTM	Monsoon	0.020006866	0.002293441	0.00376914	0.001985772	0.001485049	0.003919856	0.001520072	0.002153253	0.00426562	0.006707699
		Post-Monsoon Season	0.009824443	0.004593502	0.0247842	0.006588343	0.004341276	0.006971326	0.015826829	0.005408227	0.037357422	0.009147206
		Pre-Monsoon Season	0.037355847	0.044530436	0.098052408	0.007850977	0.012590697	0.28560412	0.203375922	0.027972626	0.275522429	0.001873932
		Winter	0.135880003	0.053474772	0.104485998	0.00645261	0.005750872	0.206695288	0.261538678	0.199035852	0.113339555	0.004445885
	Mean	Monsoon	0.001555643	0.001251528	0.00102259	0.001383142	0.001410731	0.002499507	0.001702598	0.001898391	0.002538262	0.005237254
		Post-Monsoon Season	0.007470925	0.00339641	0.013617523	0.012288447	0.010750764	0.020233723	0.009373665	0.01390992	0.022012942	0.002140558
		Pre-Monsoon Season	0.005160591	0.008983251	0.011698828	0.012737492	0.014962821	0.060728075	0.024158625	0.025223321	0.055967433	0.005507598
		Winter	1	0.079648249	0.012838425	0.011796991	0.016177055	1	0.051916229	0.331914791	1	0.017836228
	SVR	Monsoon	5.84782E-05	5.87409E-05	2.59519E-05	2.16929E-05	6.36774E-05	3.37604E-05	1.24938E-05	4.02572E-05	6.26924E-05	0.002735366
		Post-Monsoon Season	0.000428378	0.000294034	0.007203958	0.005544999	0.002533455	0.010197146	0.002036821	0.005097577	0.014732861	3.17636E-05
		Pre-Monsoon Season	0.000946613	0.002535326	0.009877356	0.009347518	0.008478629	0.118469482	0.024466931	0.18349728	0.047920961	0.001264701
		Winter	-9.9509E-16	0.004222375	0.011583208	0.004303562	0.006518754	1	1.86071E-05	3.42037E-05	0.000459515	0.004688921

Table 20 Monthly Analysis of SVI_{ME} under SSP 245

		L1	L2	L3	L4	L5	L6	L7	L8	L9	L10
ANN	January	0.000194919	1.3166E-07	0.00100753	5.9092E-05	5.5903E-05	1.42E-05	1	1.4134E-08	1.95E-01	3.8794E-07
	February	0.000307731	3.62266E-05	0.00102697	7.7953E-05	8.9775E-05	0.000307731	1	1.6863E-07	1.95E-01	6.36536E-07
	March	0.000212429	5.49606E-05	0.00093503	6.7166E-05	6.6183E-05	3.11423E-08	1	7.8581E-06	0.000112435	5.47204E-07
	April	0.000110847	0.000191752	0.00175039	2.0338E-05	2.607E-05	6.67106E-08	1	1.1908E-06	7.86145E-05	1.77876E-07
	May	1.06754E-05	1.08605E-05	0.00159196	9.4568E-05	7.4099E-05	0.000604221	0.000757834	0.00082283	0.004267965	2.60967E-07
	June	3.99148E-08	7.86555E-08	6.0509E-08	1.2766E-07	3.0281E-08	1.21952E-07	1.51515E-09	5.3916E-08	4.18224E-07	5.76999E-07
	July	1.50844E-10	1.12697E-10	1.4929E-11	2.402E-11	1.8591E-11	7.10963E-12	1.36469E-12	1.49E-11	1.13039E-11	4.11229E-07
	August	6.29307E-05	0.000925748	0.00010647	1.1738E-11	5.4883E-11	1.11233E-11	6.12236E-12	1.4118E-11	1.76978E-11	3.07854E-07
	September	8.69204E-05	9.66715E-05	3.3568E-09	7.0734E-09	2.3876E-09	2.36587E-08	5.05242E-09	4.06E-09	3.15853E-08	1.27332E-07
	October	3.59366E-08	1.03245E-09	4.4862E-05	2.7673E-05	5.4721E-06	0.00033655	8.90371E-06	5.6783E-05	0.001414879	2.79221E-10
	November	0.000285379	3.96192E-07	0.00020069	1.9406E-05	0.00013209	8.09423E-05	0.000558138	0.00063688	0.000995493	1.34051E-10
	December	1.6946E-06	0.000237314	0.0093507	8.236E-05	0.00011901	0.000167204	1	0.00024042	0.011716515	6.90114E-09
LSTM	January	0.040885419	0.011559364	0.20347682	0.00330361	0.00855267	0.02895458	0.162694109	0.0438896	0.006511405	0.011827812
	February	0.021668697	0.024974377	0.14368554	0.00312204	0.00799806	0.059770017	0.294278416	0.02120658	0.008991538	0.002836924
	March	0.011725935	0.029910618	0.18551877	0.00388494	0.00898216	0.135518939	0.795769554	0.02846009	0.032486949	0.001146499
	April	0.008823057	0.027734272	0.40501462	0.00971393	0.00695566	0.312638564	0.555715188	0.04881799	0.101107716	0.000756946
	May	0.007974316	0.014087594	0.40405844	0.01961984	0.00627764	0.443536214	0.122680781	0.05251205	0.130450153	0.00110703
	June	0.00760547	0.00494408	0.04389795	0.01797289	0.0382294	0.255536654	0.009291828	0.04907392	0.039367375	0.002010983
	July	0.006430154	0.000808644	0.00500623	0.01110678	0.00962277	0.031369014	0.00099269	0.01422588	0.007334764	0.004342797
	August	0.00748071	0.000495992	0.0022741	0.00356645	0.00253636	0.009796362	0.001292228	0.00336699	0.003485238	0.010428342
	September	0.008033389	0.00065552	0.0035813	0.00520703	0.00173761	0.007587964	0.002005119	0.00222513	0.01205423	0.019316061
	October	0.00883605	0.000798348	0.02691286	0.00765902	0.00298893	0.012960942	0.007507709	0.00241507	0.0383022	0.012571888
	November	0.012832821	0.001574191	0.06060089	0.00403957	0.00894151	0.014401662	0.028591337	0.02684634	0.013227239	0.005206568
	December	0.035037048	0.003829236	0.20389925	0.00378249	0.00914526	0.010462377	0.078241198	0.11379871	0.01074926	0.007181478
Mean	January	1	0.946395662	0.02555564	0.02155688	0.04446873	1	1	0.73582074	1	0.025518179
	February	1	0.085794498	0.02044267	0.02025682	0.02901859	1	0.059874873	0.47674766	1	0.044009833
	March	0.021893576	0.048976971	0.01728588	0.01868697	0.02675624	0.430137435	0.018032429	0.12664686	0.402798694	0.029649508
	April	0.006309897	0.014984103	0.04021625	0.06828223	0.08096516	1	1	0.57438754	1	0.01124088
	May	0.004810271	0.011620639	0.03385236	0.02907647	0.02172216	0.075976979	0.019516845	0.02966813	0.063164766	0.010940801
	June	0.004611344	0.004298131	0.00559262	0.00867739	0.00612395	0.006665907	0.005073552	0.0061908	0.006951885	0.011853043
	July	0.001482344	0.001226834	0.00144849	0.00183836	0.00150718	0.001709912	0.001689153	0.00160969	0.001823709	0.006398153
	August	0.002057175	0.001598522	0.00075101	0.00108858	0.00095156	0.00246483	0.001424319	0.00135823	0.002491106	0.006959325
	September	0.00189787	0.001494552	0.00199771	0.00324962	0.00258345	0.006887415	0.00333484	0.0042998	0.006983551	0.006659805
	October	0.004096998	0.003219314	0.00957863	0.01277317	0.00922841	0.022655367	0.009153237	0.01562034	0.022591954	0.002561585
	November	0.011572238	0.005403549	0.20342519	0.07807696	0.03149171	0.065603136	0.028736329	0.03120503	0.112236479	0.001867664
	December	0.004709735	0.024631593	0.05107461	0.02470359	0.04200192	0.164166055	0.167073294	0.10393866	0.136327706	0.006461978
SVR	January	0.003058426	1	0.01292796	0.00500279	0.00636912	1	0.000843114	1.5186E-06	0.843113713	0.003224064
	February	1	0.011241417	0.01923775	0.02146108	0.02782903	1	0.333716722	0.53465861	1	0.007439727
	March	0.001673312	0.033709073	0.00746198	0.00733469	0.0090315	1	0.002389293	0.71764503	0.000571285	0.005181956
	April	0.001532037	0.024156158	0.0045511	1	0.03178836	1	0.52934114	1	0.0014852	0.001850009
	May	0.001486747	0.002079885	0.05273981	0.03328121	0.04016103	0.070373066	0.038985625	0.24108564	0.035172302	0.002573318
	June	0.00045941	0.000839135	0.00034582	0.00055327	0.00033953	0.001442327	9.73671E-05	0.00057459	0.002382046	0.019732213
	July	0.000246246	0.000285822	4.8425E-05	4.5404E-05	0.00014749	4.14481E-05	3.22178E-06	8.605E-05	5.82115E-05	0.008523321
	August	0.000232236	0.000292718	4.5193E-05	2.7089E-05	0.00019944	5.00647E-05	1.46271E-05	6.5401E-05	6.52888E-05	0.004397931
	September	0.000129039	0.000330646	0.00020432	0.000176	0.00035082	0.000421041	0.000308725	0.00027109	0.00074078	0.003527391
	October	0.000476189	0.000252158	0.00299341	0.00378796	0.00118314	0.019197854	0.002580011	0.00621336	0.025409365	0.000140531
	November	0.007256424	0.002069559	0.00016398	0.00163864	0.02859388	0.001577928	0.006793656	0.02460302	0.003964954	0.000419431
	December	1.29405E-05	0.014185184	0.06121403	0.03355447	0.11439266	0.001233134	2.24262E-05	0.0144735	0.047045554	0.000223302

Table 21 Monthly analysis SVI_{ME} under SSP 585

		L1	L2	L3	L4	L5	L6	L7	L8	L9	L10
ANN	January	0.111220558	2.08E-10	0.000883	4.88E-05	3.16E-05	1.85952E-09	1	2.83E-08	2.07671E-05	3.65E-07
	February	8.61455E-08	7.68E-05	0.001	8.28E-05	7.8E-05	0.000247556	1	2.11E-07	0.125185693	6.7E-07
	March	0.000263747	8.1E-05	0.001048	9.32E-05	8.47E-05	5.65875E-08	1	8.78E-06	0.000205852	4.54E-07
	April	0.000147882	0.000263	0.001728	1.49E-05	1.52E-05	2.30705E-07	1	1.79E-07	0.000140235	1.19E-07
	May	1.10782E-05	5.87E-06	0.001392	0.000113	0.00011	0.000833003	0.001012455	0.000939	0.005248005	1.97E-07
	June	3.64754E-08	4.29E-08	4.55E-08	9.25E-08	2.25E-08	1.14621E-07	1.41618E-09	6.52E-08	2.51602E-07	5.69E-07
	July	1.31121E-10	2.45E-10	1.66E-11	4.55E-11	2.83E-11	6.15435E-12	1.42838E-12	1.7E-11	9.28362E-12	3.93E-07
	August	6.53581E-11	1.57E-10	1.16E-11	6.28E-12	1.65E-11	7.0097E-12	3.57479E-12	7.58E-12	9.75614E-12	3.5E-07
	September	5.35607E-11	1.31E-10	4.46E-09	1.1E-08	1.45E-09	1.28008E-08	3.22691E-09	1.66E-09	1.49031E-08	1.37E-07
	October	8.72035E-09	3.98E-10	6.09E-05	3.55E-05	3.97E-06	0.000388667	6.18856E-06	4.26E-05	0.001683866	4.29E-10
	November	0.000424646	2.73E-07	0.000405	2.55E-05	0.000121	7.73923E-05	0.000400463	0.000532	0.00179577	1.96E-10
	December	2.36821E-06	0.000263	0.007368	9.61E-05	0.000139	0.000143147	1	0.000142	0.009571157	4.99E-09
LSTM	January	0.183434537	0.045023	0.113343	0.007321	0.00608	0.20673796	0.250655621	0.223471	0.094549148	0.008349
	February	0.141565134	0.217402	0.102305	0.006184	0.006426	0.210175491	0.675192397	0.199907	0.188139619	0.003988
	March	0.102711442	0.18355	0.103557	0.007725	0.005071	0.268069942	1	0.092476	0.387759658	0.004081
	April	0.052419568	0.079913	0.089375	0.009003	0.015308	0.377985638	1	0.024434	0.491504204	0.001293
	May	0.022012602	0.020341	0.129308	0.010065	0.1202	0.287678417	0.20180354	0.019634	0.257330111	0.001303
	June	0.024955336	0.004836	0.024251	0.012399	0.063647	0.113265199	0.013493885	0.013802	0.055678371	0.002042
	July	0.041389427	0.002932	0.008322	0.008867	0.003295	0.011159984	0.00139713	0.011907	0.004040665	0.004423
	August	0.035271351	0.003671	0.00401	0.003381	0.001604	0.003775235	0.001740292	0.001944	0.003687363	0.00941
	September	0.022038996	0.005084	0.005962	0.002627	0.001857	0.003487112	0.003149593	0.001619	0.012858883	0.018837
	October	0.014863478	0.004099	0.036336	0.009494	0.005527	0.007029105	0.008345409	0.005021	0.050537935	0.016364
	November	0.042143239	0.005609	0.028577	0.00662	0.009835	0.014495891	0.054541627	0.009014	0.048536526	0.008405
	December	0.417387024	0.008471	0.112236	0.011309	0.009844	0.072450745	0.108421516	0.040654	0.055130647	0.009418
Mean	January	1	0.753519	0.023364	0.017669	0.038249	1	1	0.475805	1	0.021369
	February	1	0.079783	0.019145	0.018775	0.024652	1	0.051916229	0.44672	1	0.049494
	March	0.017979688	0.052569	0.018843	0.024456	0.029376	0.290758279	0.021172384	0.132409	0.2746385	0.0237
	April	0.007883865	0.022444	0.034769	0.058809	0.055483	1	1	0.621911	1	0.010412
	May	0.00768688	0.011447	0.025501	0.027636	0.026322	0.061178159	0.026518695	0.025977	0.05666387	0.008013
	June	0.005179106	0.005184	0.006914	0.008724	0.006223	0.007662496	0.006209873	0.006978	0.007845871	0.012704
	July	0.002241555	0.001863	0.001278	0.001862	0.001887	0.002806847	0.001985608	0.002168	0.002881406	0.009505
	August	0.002469214	0.001801	0.001091	0.001483	0.001484	0.003112488	0.002304146	0.002118	0.003225215	0.009451
	September	0.004295379	0.002463	0.00397	0.005596	0.004149	0.007696266	0.005303308	0.00517	0.007759872	0.006865
	October	0.007378836	0.003308	0.015349	0.019724	0.014403	0.023225305	0.010540841	0.017908	0.026769999	0.002811
	November	0.019434498	0.008798	0.177445	0.095154	0.029583	0.06624017	0.019286217	0.026267	0.10745009	0.002786
	December	0.367083983	0.030476	0.03857	0.02863	0.048083	0.163154431	0.1214416	0.112245	0.123593546	0.006472
SVR	January	0.25452639	1	0.0204	0.004415	0.005695	1	0.257627801	2.83E-06	0.000459515	0.005238
	February	1	0.004222	0.025065	0.017911	0.022036	1	0.413544064	0.475007	1	0.015018
	March	0.002133728	0.03149	0.015553	0.01332	0.010547	1	0.00455191	0.725914	0.001722105	0.009791
	April	0.002023503	0.039391	0.00429	1	0.011122	1	0.257724669	1	0.003058426	0.001911
	May	0.001580348	0.002621	0.071677	0.039452	0.062131	0.118469482	0.094456766	0.184527	0.077000471	0.002352
	June	0.000409124	0.000552	0.000282	0.000418	0.000382	0.001041324	0.000154068	0.000467	0.001934815	0.036399
	July	0.000274358	0.000243	4.13E-05	4.37E-05	0.000176	3.37588E-05	1.38232E-06	5.82E-05	4.94485E-05	0.008631
	August	0.000128858	0.000225	5.88E-05	2.85E-05	0.000131	3.1121E-05	1.66855E-05	5.47E-05	4.81829E-05	0.007616
	September	8.00378E-05	0.000217	0.000186	0.000239	0.000341	0.000248854	0.000204148	0.000233	0.000892068	0.003094
	October	0.000531957	0.000184	0.008036	0.008922	0.002765	0.033142151	0.003057988	0.005827	0.046764509	0.000111
	November	0.010907878	0.001964	8.62E-05	0.007854	0.025776	0.002563953	0.004512817	0.032186	0.004753188	3.97E-05
	December	1.13307E-05	0.016376	0.105064	0.03245	0.12147	0.15996208	4.24822E-05	0.016686	0.081050869	0.000214